186138

NASA Contractor Report 4538

P-101

Three-Stage Linear, Split-Stirling Cryocooler for 1 to 2K Magnetic Cold Stage

R. C. Longsworth

(NASA-CR-4538) THREE-STAGE LINEAR, SPLIT-STIRLING CRYOCOOLER FOR 1 TO 2K MAGNETIC COLD STAGE (APD Cryogenics) 101 p

N94-13897

Unclas

H1/70 0186138

CONTRACT NAS2-13180
August 1993

National Aeronautics and Space Administration

NASA Contractor Report 4538

ORIGINAL CONTAINS
COLOR ILLUSTRATIONS

Three-Stage Linear, Split-Stirling Cryocooler for 1 to 2K Magnetic Cold Stage

R. C. Longsworth

APD Cryogenics
1833 Vultee Street
Allentown, PA 18103

Prepared for
Ames Research Center
CONTRACT NAS2-13180
August 1993

National Aeronautics and
Space Administration

Ames Research Center
Moffett Field, California 94035-1000

Table of Contents

PRECEDING PAGE BLANK NOT FILMED

1.0 Summary

1.1 Goals

The goal of this program was to design, build and test a long-life, three-stage, linear, split, Stirling cycle cryocooler with a high efficiency in producing refrigeration at 8 K that is needed to produce the refrigeration required for a 50 mW, 1.5 K magnetic cold stage. The original cryocooler conceptual design is shown in Figure 1. Dual opposed piston compressors are driven by moving-coil linear motors. The three stage expander is also driven by a linear motor and is designed to produce 15 W at 60 K, 4 W at 16 K, and 1.2 W at 8 K. The cold regenerator employs a parallel gap construction for high efficiency. The magnetic stage operates between 8 K and 1.5 K, and consists of two AC superconducting magnets conductively cooled, two gadolinium gallium garnate (GGG) cylinders of magnetic refrigerant, and gas gap thermal control switches.

The scope of the Phase 2 program was established by the time and funding available. The Phase 2 program was to demonstrate several of the critical technologies while building a cryocooler to produce the refrigeration required for a 50 mW 1.5 K magnetic cold stage. These key technology areas are: 1) warm and cold flexible suspension bearings, 2) performance of a three stage expander with a cold flexure bearing, and 3) a new cold regenerator geometry for high efficiency at 8 K.

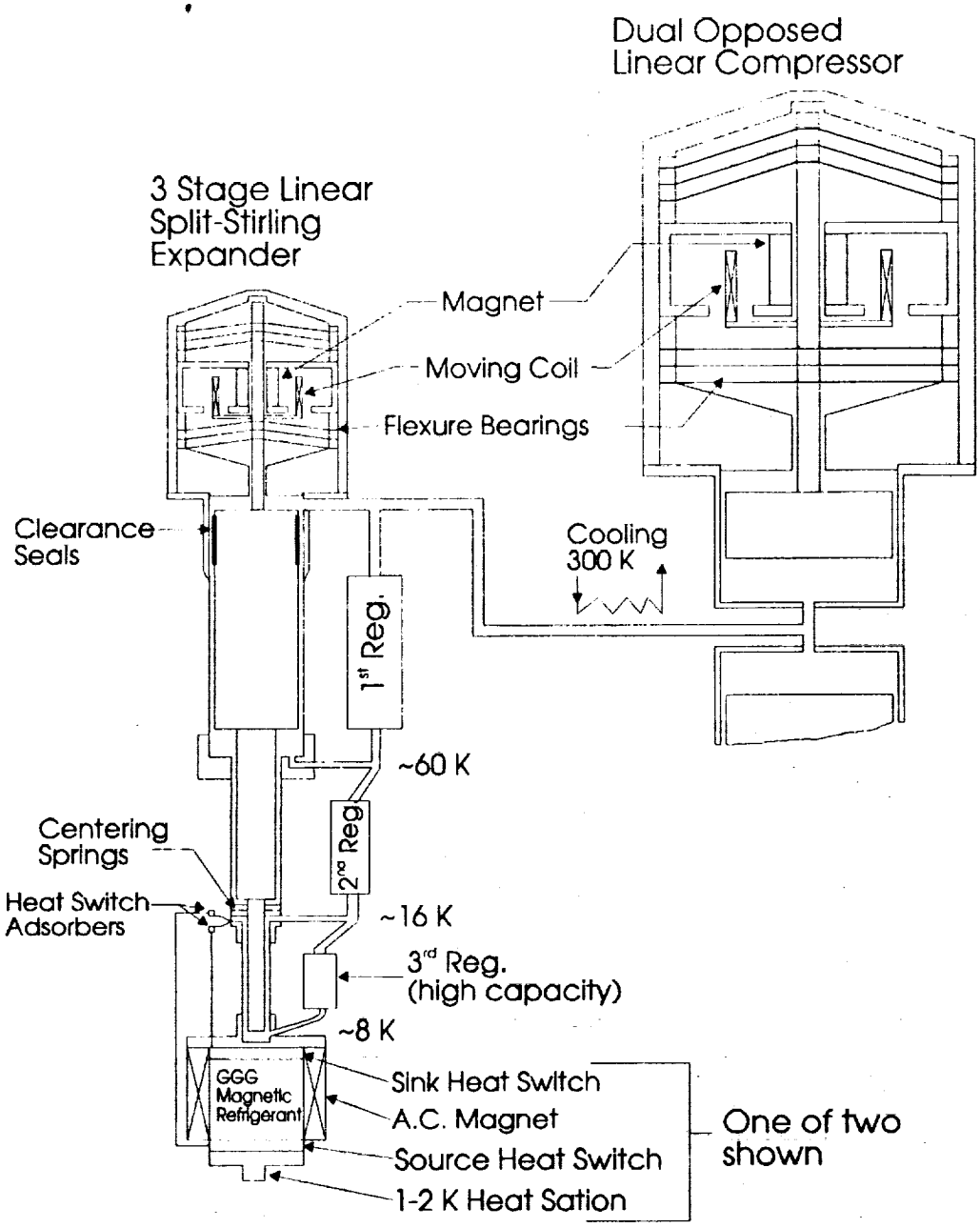

Figure 1. Three stage linear split-Stirling cryocooler with magnetic cold stage for 50 mW at 1 - 2 K.

1.2 Accomplishments

A 3-stage, linear, split Stirling cryocooler has been designed and partially constructed. A pair of dual opposed linear compressors were designed built and tested. A 3-stage expander was designed and the parts were manufactured. Final assembly was not done because problems in assembling the compressor resulted in a shortage of funds to complete the expander. Figure 2 shows the unit final design and key design features.

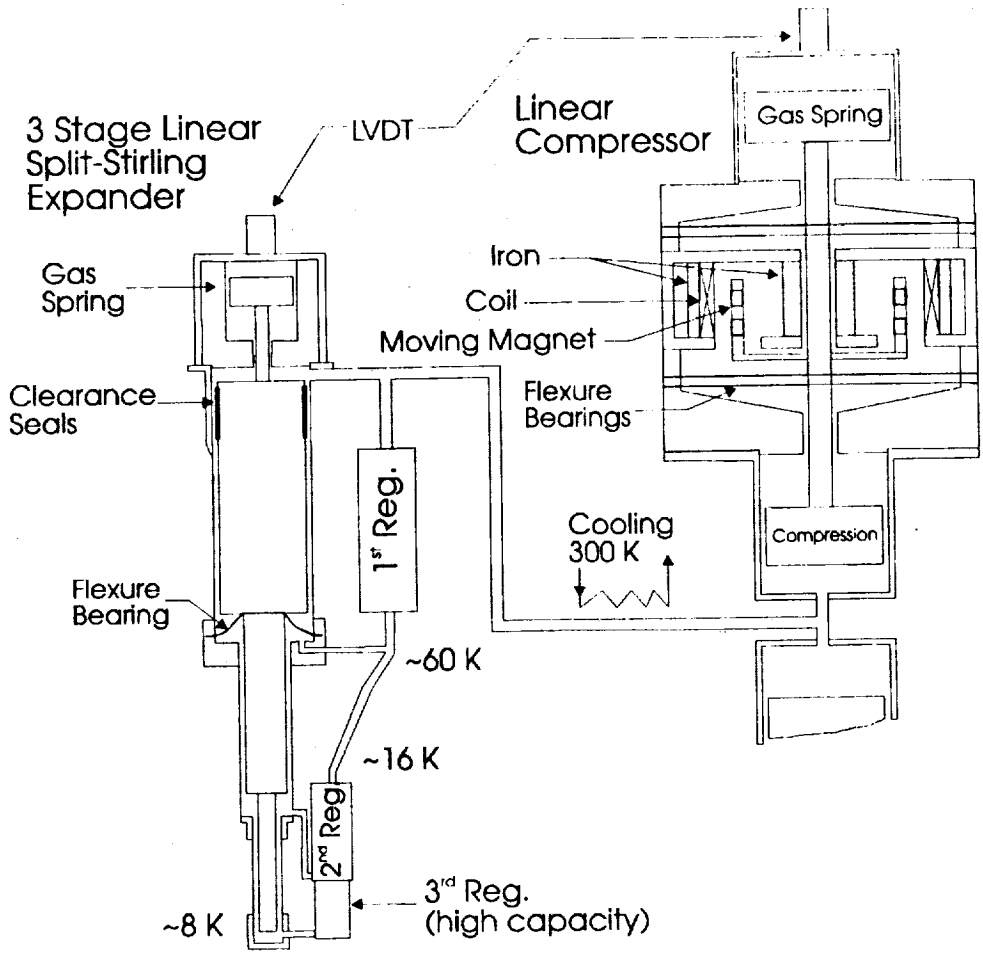

Figure 2. Split Stirling Cycle System Schematic.

1.2.1 Compressor

The compressors are dual opposed linear motor units. The units being 180° out of phase cancel most of the vibrations. Four spiral-cut flexure bearings provide for the centering of the compressor shaft and partial restoring force. Additional restoring force is provided by a gas spring which also is the means of adjusting the natural frequency of the compressor. Rulon sleeves were used on the piston surfaces for seals to hold down machining costs.

The final motor design is of a moving magnet, stationary coil design. The Phase I studies indicated the motor would operate more efficiently with a high reciprocating mass, so the change was made to the moving magnet design. It operates at a resonance frequency of 40 Hz. This frequency was chosen based on system efficiency and weight. A moving magnet design was chosen based on the assumption that the flexure bearings could provide the spring constant needed for 40 Hz operation. However, the spiral flexure spring has a non-uniform stress pattern so that the reciprocating mass is large relative to its spring constant, thus it would require a large number of springs to achieve the desired

stiffness. A gas spring was added to the compressor to give the necessary spring rate for 40 Hz operation.

1.2.2 Expander

The expander has three stages with shell type displacers and stationary, external regenerators to minimize the reciprocating mass. The displacer pistons have sliding clearance Rulon sleeves for gas sealing. A cold flexure bearing, similar to the compressor flexure bearings, is located between the first and second stage displacers to provide radial centering of the displacers. The displacer is driven pneumatically by a gas spring, which is tuned to provide a leading phase angle of 60°.

During the thermal analysis phase the refrigeration rates were changed slightly from the Phase I proposal. This was due to a more accurate program predicting more of the losses. The expander was designed to produce 1, 2, and 10 watts of cooling at 8, 16, and 60 K.

The first stage regenerator operates between 300 and 60 K, and is packed with fine mesh wire screen in a large diameter to length ratio housing to reduce pressure drop losses. The second stage regenerator operates between 60 and 16 K and is packed with extremely fine lead shot. The third stage or cold regenerator spans the 16 to 8 K region and is a novel design. The cold regenerator is a parallel plate heat exchanger. The plates are made of a composite material that maximizes the radial heat storage and minimizes the axial conduction losses.

All the components for the expander and regenerators have been fabricated. The first stage regenerator has been assembled and used in the compressor tests. Final assembly of the expander was not done due to lack of funds and time. However, all parts except for the second and third stage regenerators were test assembled to assure proper fit-up.

1.3 Performance, Design and Actual

The compressor is designed to produce 500 W of P-V work with 900 W of power at a gas pressure ratio of 1.5/.7 MPa with a stroke of 20 mm. The expander is designed to produce 1, 2, and 10 watts of cooling at 8, 16, and 60 K, and operate at a frequency of 40 Hz.

The compressors have been successfully built and tested. The compressors operate at their design point of 900 W input power and a pressure ratio of 1.6/.6 MPa. The stroke is about 75% of the 20 mm design. The stroke is not centered due to the motor design. The off-centered stroke and the size of the power supply contribute to the reduced stroke of the compressors.

2.0 Introduction

2.1 Results of Phase I Analysis

The Phase I Study started with the design of a magnetic cold stage which resulted in a specification of the cooling that is required by the three-stage Stirling Expander. A computer model of a three-stage expander was generated and used to size components and predict efficiency as a function of phase angle and speed. Operating pressures of 1.5 / .7 MPa were selected based on helium properties that are most favorable for good performance at 8 K. A computer model of the linear compressor was then developed and used to calculate the system weight and power input over a range of speeds.

Table 1 lists the expander cooling requirements that were calculated as being needed to produce 50 mW at 1.5 K.

TABLE 1. EXPANDER COOLING REQUIREMENTS

Stage Temperature	K	60	16	8
Magnet Leads	W	7.0	1.4	.17
Instrument Leads	W	.5	.2	--
Radiation Shield	W	3.5	.3	--
Thermal Switch	W	--	.8	.03
Cold-Stage Heat	W	--	--	.55
TOTAL	W	11.0	2.7	.75
Design	W	15.0	4.0	1.2

The expander program was used initially to study the effect of the phase angle relationship with the compressor. 65° was found to give the best efficiency and was used for all subsequent analysis. Operating speeds of 20, 30, and 40 Hz were studied. As the operating speed is increased, the size of the components decreases, machining becomes more difficult, and the regenerator L/D ratio gets smaller. Operation at 40 Hz appears to be the upper limit based on the availability of fine wire mesh for the first-stage regenerator and manufacturing tolerances in general. An efficiency of 44% was calculated for operation at 40 Hz compared with 48% at 20 Hz. Key to good performance at 8 K is the design of the novel third-stage regenerator which has high thermal storage capacity and low void volume and pressure drop losses relative to lead spheres. The expander program calculates the P-V work required from the compressor as being 450 W. A value of 250 W was used for the design of each of the two opposed compressors.

The analytical model for the compressor is based on an energy approach. Piston motion is more nearly sinusoidal and efficiency highest if the energy stored in the resonant reciprocating system is large relative to the work output per cycle. Energy is stored in the form of kinetic energy at mid-stroke when the piston velocity is maximum and in the form

of potential energy at the end of stroke in the flexure bearing spring and the gas spring which results from the pressure difference between the compression volume and the housing. The relationship for the reciprocating mass vs. stroke for speeds of 30, 40, and 60 Hz, and 250 W of kinetic energy times frequency is shown in Figure 3. Operation at 40 Hz with a stroke of 20 mm requires a reciprocating mass of 2.0 kg for a 1:1 energy ratio. The preliminary design was based on an energy ratio of 3:1 and a reciprocating mass of 6.2 kg. It was assumed that the reciprocating mass of the flexure bearings would be small so it was decided to design the motor with reciprocating magnets.

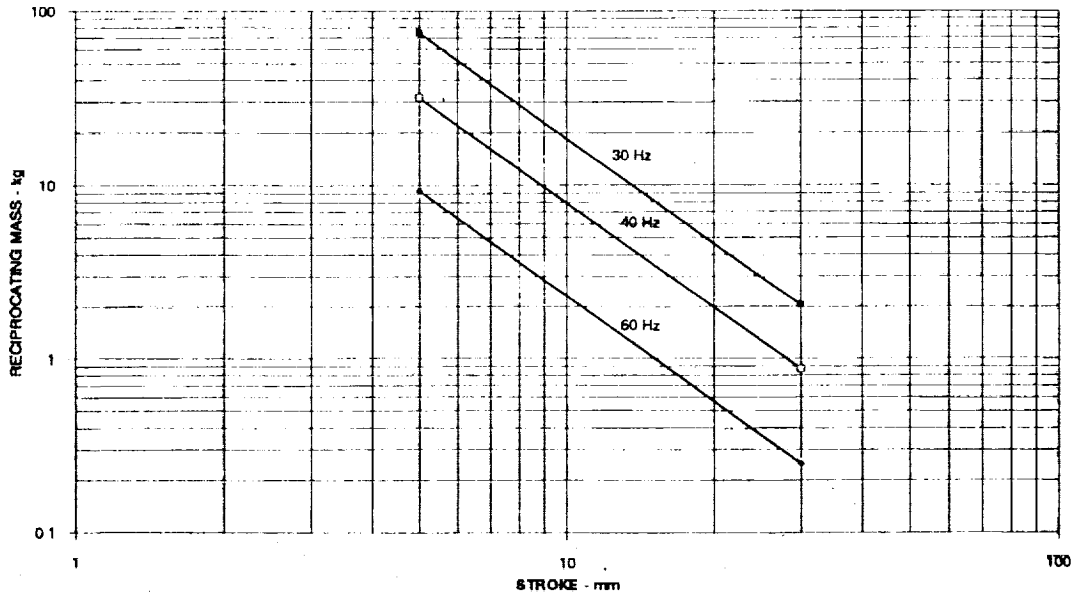

Figure 3. Reciprocating mass vs. Stroke, 1/2 MV^2 = 250 W.

The program for designing the linear motor assumed the geometry of a sumarium cobalt magnet, the piston stroke and diameters, speed of 40 Hz, P-V work of 250 W, and an energy ratio of 3:1. From this the motors and spring were sized and efficiency and weight were calculated. Results of these calculations are shown in Figure 4.

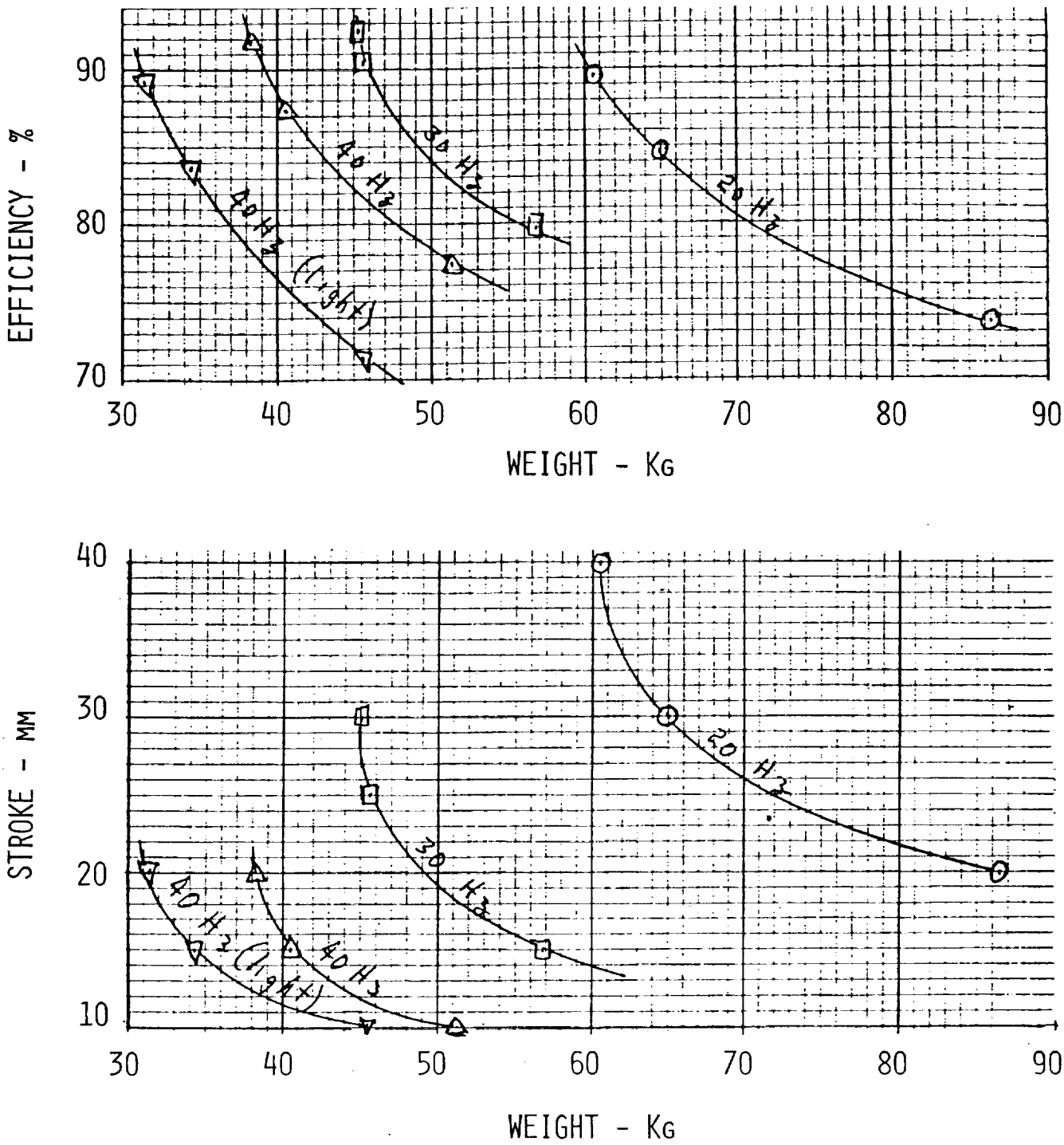

Figure 4. Compressor weight, stroke, efficiency relations for one compressor delivering 250 W of output power to gas and stored energy ratio of 3:1.

Conclusions from the Phase I Study were as follows:

1. Dual-magnetic cold stages are needed to provide 50 mW continuously at 1.5 K. Conductively cooled AC superconducting magnets using Nb3 Sn operating at 5 T and 8 K are practical. Lead losses can be nominal.

2. A cold regenerator consisting of nested cylinders of Pb/Sn layers provides high efficiency with low void volume and pressure drop losses in the 16 K to 8 K region.

3. Flexure suspension at the first stage (60 K) of a three-stage expander can be used to provide non-contacting clearance seals in the expander.

4. Flexure suspension can be used in a dual-piston linear drive compressor to center the piston and store enough energy to provide stable resonant operation.

Operation at 40 Hz has been found to provide the best trade-off between size, weight and efficiency. The recommended design has the following approximate characteristics:

	Size -- L	Weight -- kg	Power -- W
Cold Stage	5.1	17	20
3-Stage Expander	.6	5	50
Dual Compressor	20	64	650
TOTAL	25.7	86	720

2.2 Design Concepts and Phase II Changes

The design concepts that are incorporated in the compressor and expander are summarized in Table 2. The design which resulted from the "Phase I" studies was modified as a result of early Phase II studies to "preliminary."

Table 2. Three Stage Stirling Cooler Design Concepts

COMPRESSOR DESIGN	Phase I	Preliminary	AS BUILT
MOTOR TYPE	Linear	Linear	Linear
BALANCE	Opposed Piston	Opposed Piston	Opposed Piston
FLEXURE BEARINGS	Non-reversing	Reversing	Reversing
RECIP. MASS	Large	Moderate	Moderate
RECIP. COMPONENT	Magnet	Magnet	Magnet
CLEARANCE SEAL TYPE	Non-contacting	Sliding	Sliding
SPRING	Flex Bearing	Flex Bearing	F-B + Gas
EXPANDER DESIGN			
SPEED	40 Hz	40 Hz	40 Hz
NUMBER OF STAGES	3	3	3
DRIVE	Linear Motor	Gas Spring	Gas Spring
WARM BEARING	Flexure	Sliding	Sliding
COLD BEARING	Flexure	Flexure & Sliding	Flexure & Sliding
CLEARANCE SEAL TYPE	Non-contacting	Sliding	Sliding
FIRST REGENERATOR	SS Wire Screen	SS Wire Screen	SS Wire Screen
SECOND REGENERATOR	Pb Shot	Pb Shot	Pb Shot
THIRD REGENERATOR	Parallel Plate	Parallel Plate	Parallel Plate
REGENERATOR POSITION	Stationary	Stationary	Stationary

Further studies resulted in the final "as built" design. The reasons for these changes are as follows:

2.2.1 Compressor

Flexure Bearings -- The Phase I Concept was to have flexure in only one direction because the fatigue stress limit is much higher. Radial stiffness, however, drops as the spring is stretched so it is best to have the spring flex around the neutral position.

Reciprocating Mass -- It was found that it is hard to design the spiral spring to be as stiff and light as needed for a high energy ratio. The reciprocating mass was thus reduced.

Clearance Seal -- Non-contacting seals are envisioned for a final system, but sliding seals were used here to reduce cost.

Spring -- We were unable to design the spiral spring to be stiff enough so gas springs were added.

2.2.2 Expander

Drive -- After some thought and analysis, it was decided that a pneumatic drive could be built for the expander that would be cheaper than a linear motor and still be able to control the stroke and phase angle.

Warm Bearing -- While a final system would have a warm flexure bearing, it was decided to use a simpler sliding bearing in this unit.

Cold Bearing -- Rather than cantilever the cold stages of the first stage rigidly, it was decided to use flexible couplings and sliding bearings.

Clearance Seal -- A non-contacting clearance seal could be used in a final unit, but sliding seals were used here to reduce cost.

3.0 Analysis

The cryocooler was separated into major functional groups for analysis. The results of the analyses were used to design the components.

3.1 Compressor Analysis

3.1.1 System Studies

Motor Size

The computer program "LMC1" developed in Phase I was used to provide the basic dimensions of the linear motor. A copy of the program and a sample of the output are included as Appendix A. These basic design requirements were given to Field Effects, a division of Intermagnetics General Inc., for further study and design as described in Section §3.1.3. The motor was designed for operation at 40 Hz with a stroke of 20 mm; P-V work of 250 W, an energy ratio of 3:1, and 6.0 kg reciprocating mass.

Reciprocating Mass vs. Efficiency

Program "SCD3" was developed in order to analyze the effect of reducing the energy ratio on efficiency. A copy of this program is included in Appendix B.

The model assumes that the expander displacer motion is sinusoidal and that the voltage applied to the compressor is sinusoidal and lags the expander by 65°. Displacer volumes, pressures, stroke, and speed are the same as the preliminary design except that the expander is treated as a single-stage unit. Regenerator pressure drop is neglected.

The following parameters are calculated and plotted vs. "crank" angle:

Vc - Volume displaced in compressor
Vd - Volume displaced in expander
NP - Velocity of compressor piston
Ml -- Mass flow rate of gas at cold end of the regenerator
Ef - Emf providing driving force for compressor piston
(applied voltage - back Emf).

Plots are also generated of pressure vs. Vc and Vd and Ef vs. Vc. Key plots are included in Appendix B.

We looked at the effect of reducing the reciprocating mass while adjusting the spring constant to maintain resonance at 40 Hz and also the effect of operating at off-resonant speeds above and below 40 Hz. Applied voltage was adjusted to obtain full stroke of the compressor without hitting either end. Results of the analysis are summarized in Table 3.

Table 3. Effect of Energy Ratio and Off-Resonance Operation on Efficiency.

Ur	Mp - kg	N - Hz	I^2R Loss - %
0.7	1.39	35	15.5
0.7	1.39	40	9.4
0.7	1.39	45	17.0
1.0	1.98	40	9.1
1.5	2.97	40	8.5
3.0	5.94	38	30.9
3.0	5.94	40	7.7
3.0	5.94	42	29.1

It was found that the reciprocating mass can be reduced to about 30% of the Phase I design without reducing efficiency significantly. The plots in Appendix B show the results for Run #1 which has an energy ratio Ur of 0.7 and a reciprocating mass of 1.39 kg. The I^2R loss is 9.4% of the power input compared with a loss of 7.7% for an energy ratio of 3.0 which required a reciprocating mass of 5.94 kg (each piston). The lighter piston allows the speed to be changed with a smaller penalty in I^2R losses.

One disadvantage of the lighter piston is that the gas spring forces dominate over the mechanical spring force so that changes in gas pressure will have more of an effect on performance. For an energy ratio of .7:1 the mechanical spring stores only 15% of the required energy.

Design of the reciprocating magnet / piston / spring assembly showed a weight of 2.84 kg without the springs and a reciprocating weight of 0.13 kg per spring with a spring rate of 4.789 kN/m. It would take 16 springs and a reciprocating weight of 11.0 kg for 40 Hz resonance.

It was then decided to use only 4 springs and add gas spring pistons in order to keep the reciprocating weight down. Reciprocating mass for unit as designed is thus about 3.5 kg and the energy ratio is about 1.7:1.

Current, Voltage, Power Supply

Program "SCD3" was refined to include actual wire diameter and coil winding details to find out what wire diameter should be used in the coils to select a power supply that could be purchased at a reasonable cost. The result of this analysis was to specify 16 gauge square wire which results in coils having a resistant of 0.9 Ω and requiring a power supply with a 64 V AC output.

3.1.2 Flexure Bearings

The flexure bearings are essentially spiral leaf springs with low axial stiffness and very high radial stiffness. They are based on the early Oxford design, being a circular plate with three narrow 360° Archimedes spiral slits positioned 120° apart and cut through the plate. The reciprocating shaft is clamped at the inside radius (**Ri**). The outside radius of the spring (**Ro**) is anchored stationary. The Archimedes spiral, shown in Figure 5, is linear and defined as $\mathbf{R} = \mathbf{a}\theta$, where **a** is a constant and **R** varies from **Rsi** to **Rso** as θ varies, in this case, from 0 to 360°.

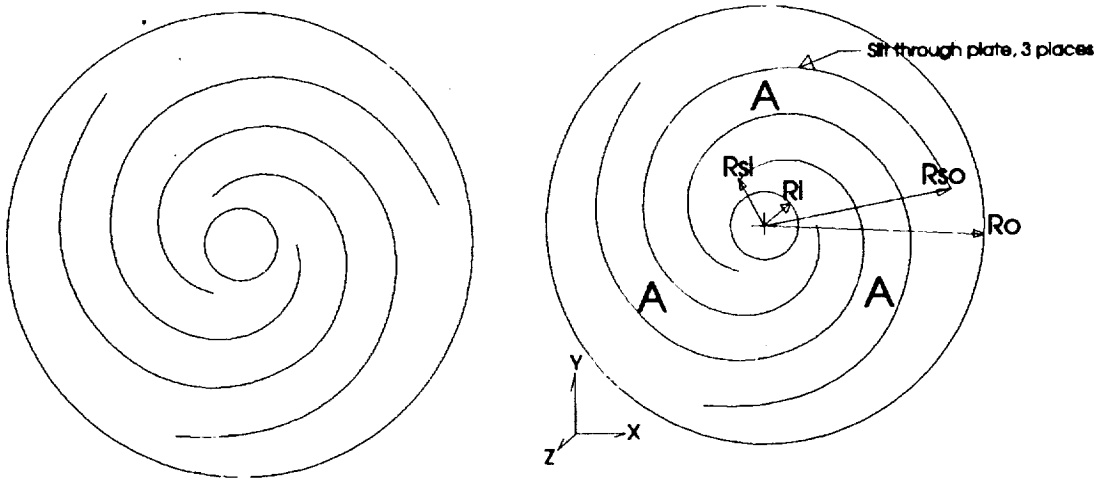

Figure 5. Typical spiral flexure bearing (left), with geometric notation (right).

In general, the i.d. and o.d. of the flexure bearing are chosen to contain the spirals. The spiral inner or outer radius is chosen based on the estimated spring rate using the scaling functions shown in the Empirical Relations section that follows. The other radius is then determined from the spiral equation. The thickness of the material and other details are finalized as part of the iterative material selection and finite element analysis (FEA). The operating frequency and stress limitations further refine the final design choices.

The flexure bearings could have been used in either a uni-directional bending mode (referred to as R = 0 mode for cyclical bending fatigue tests) or in a bi-directional, reverse bending mode (a.k.a. R = -1 mode). The uni-directional bending mode affords a higher material endurance strength. This means that the same or more deflection in one direction can be achieved as for the case of reverse bending for which the fatigue limit is 248 MPa. The radial stiffness however is much less for deflection in one direction, so for these reasons a reverse bending mode was chosen with the flexure bearings undeflected at rest in the centered, null-stroke position.

Empirical Relations

The leaf springs that are formed by the three narrow slits comprise a complicated geometry that cannot be properly analyzed without the aid of modern FEA computer software. However, early in the program a beryllium-copper Oxford spiral flexure bearing, like that shown, was tested for axial stiffness and the following scaling functions were developed:

$$F \cong 10^{-4} E\left[\left(\frac{0.0438 t^{2.69}\delta}{(2\,Rso)^{1.62}}\right)+\left(\frac{0.00118 t^{0.91}\delta^{2.33}}{(2\,Rso)^{1.47}}\right)\right]$$

$$W = \int F d\delta$$

$$\cong 10^{-6} E\left[\left(\frac{0.0219 t^{2.69}\delta^{2}}{(2\,Rso)^{1.62}}\right)+\left(\frac{0.000354 t^{0.91}\delta^{3.33}}{(2\,Rso)^{1.47}}\right)\right]$$

$$\sigma_A \cong \frac{0.1404 E\delta^{1.33}}{t^{0.093}(2\,Rso)^{1.47}}$$

where:

F ≡ applied axial force @ Ri, N
E ≡ elastic modulus, Pa
t ≡ plate thickness, cm
W ≡ spring energy, J
δ ≡ z-axis deflection of spring @ Ri, cm
Rso ≡ outer radius of spring slit, cm
σ_A ≡ stress @ locations A @ max. δ deflection, Pa

The initial operating conditions for the flexure bearings were based on the following:

a.) Compressor output power = 250 W @ 40 Hz.

b.) Energy ratio = 0.70

c.) Piston stroke = 20 mm.

d.) Required spring energy = (250 W) (0.70) / 40 Hz = 4.375 J.

Analysis of Archimedes Spiral

A FEA program, COSMOS/M (version 1.61 from Structural Research & Analysis Corporation, Santa Monica, CA), was used to accurately evaluate the axial, radial, and

dynamic behavior of these spiral flexure bearings. The displacements, tensile and shear stresses, axial and radial stiffness, and natural frequency harmonics were determined. Initially, a single spiral spring leaf finite element model (FEM) was created and analyzed. It was designated SPR1. Figure 6 displays a representative z-axis displacement plot of SPR1. Color photocopies of the original Poloraid print are given (pages 23 and 24) at the end of this section. This model was not used for further analysis because the interactions with the other two spiral leaf springs were missing and the boundary nodal displacements were therefor inaccurate. However, from this preliminary model the following were determined:

a.) The majority of the spring deflection occurs from the center to ~ 1/3 of the length of the spiral leaf.

b.) Peak tensile stress risers occur at the ends of the spiral slits @ Rsi and Rso. These stress risers are highest when the clamped edges of the spring are on Rsi and Rso.

c.) The spiral leaf twists slightly in the vicinity of location A, as previously noticed during the preliminary hardware tests, causing an increased tensile stress along the inner spiral slit of the leaf. However, this stress is much less than the stress risers at the slit ends.

d.) The preceding scaling functions were found to be accurate only for a narrow range of thicknesses with beryllium copper.

e.) The average tensile stress along the spiral spring leaf was estimated as $\sigma_{ave} \cong (\sigma_{max} + 3\ \sigma_{min}) / 4$.

f.) Translational and rotational degrees-of-freedom (DOF) at the center (Ri) were constrained in the x and y axes for the analysis. Only z-axis translation and rotation were allowed. This was based on the fact that close-tolerance clearance seals are used on the piston and thus guide the reciprocating shaft and flexure bearing. Unconstrained analyses were also conducted and the results did of course indicate x and y axes rotations.

Next, a complete three-leaf spiral flexure bearing FEM was created and analyzed. It was designated SPR2. Figure 7 displays a representative z-axis deflection plot of this model. SPR2 was used to evaluate the effects of different finite element types, element counts, model bandwidths, plate thicknesses, slit widths, radii ratios (Ro/Ri and Rso/Rsi), clamping locations, F vs. δ, and σ_{ave} vs. δ, and materials. The following summarizes the results of those analyses:

a.) A linear triangular thick-shell element having six DOF (three translational and three rotational) was determined as the most appropriate; COSMOS/M designates this element as SHELL3T.

b.) The number of elements, N, in the meshed model effects the stress results. Convergence toward the truest result (i.e. toward unity safety factor) with the least error

distribution was achieved with ~ 5700 elements. The safety factor, Fs, was estimated to decrease ~ 10 % for each doubling of the element count (e.g. if Fs ≅ 1 @ N ≅ 5700, then Fs ≅ 1.1 @ N ≅ 2850). This allows one to perform analyses faster with coarse mesh models. The lesser element count causes an over-prediction of the stress and a larger error distribution, hence the interpretation of a larger safety factor.

c.) The bandwidth of the FEM matrix was minimized by using the automated meshing algorithms within COSMOS/M such as MA_RG, followed by node compression (NMERGE), node renumbering (NCOMPRESS), and element aspect ratio checks (ECHECK).

d.) Plate thickness, t, was varied from 0.5-2.3 mm (0.02-0.09 in). The resultant spring rate and stresses varied proportionately with the thickness. For example, with t = 1.59 mm (0.0625 in), then k = 4.7 kN/m (27 lbf/in) and σ_{max} = 427 MPa (62 kpsi) @ Rsi; with t = 2.29 mm (0.09 in), then k = 14 kN/m (81 lbf/in) and σ_{max} = 869 MPa (126 kpsi) @ Rsi.

e.) The slit width was varied from 250-500 μm (0.01-0.02 in). This range had no effect.

f.) Radii scaling ratios were determined as follows: Ro/Ri ≅ 7, and Rso/Rsi ≅ 3.66. The latter, Rs, ratio is determined by the Archimedes spiral function, whereas the former, R, ratio is appropriate only to this application.

g.) The clamping location on the flexure bearing i.d. and o.d. was confirmed to increase the stress risers at the slit ends when the clamped edges are on Rsi and Rso.

h.) The flexure bearing spring rate, k ($\equiv dF/d\delta$), was linear over the intended half-stroke of 10 mm (0.394 in) and varied proportionately with plate thickness.

i.) The analyses exhibited linear σ_{ave} changes proportional to F, δ and t.

j.) Two material classes were considered, corrosion-resistant steels and beryllium-coppers. For a given spring rate, the resultant stresses varied proportionately with the elastic modulus.

Modifications to Improve Stress Distribution

The SPR2 model was revised for the final design FEM, designated SPR3. Reducing the peak stresses at the slit ends became the focus of the efforts with SPR3. The FEA code changes were now stabilized. The geometry of the flexure bearing was fixed at Ri = 15.9 mm (0.625 in), Ro = 102 mm (4.00 in), Rsi = 23.8 mm (0.937 in), Rso = 89.8 mm (3.53 in), and t = 1.59 mm (0.0625 in).

The material for the flexure bearing was chosen for its high corrosion resistance, low magnet permeability, high fatigue strength, and hardenability. Initially, both precipitation-hardenable corrosion-resistant steels (e.g. 17-7 or 17-4) and precipitation-hardenable beryllium-coppers (e.g. Brush-Wellman alloy 25) were considered. Be-Cu was finally chosen for its availability in sheet form. Alloy UNS C17200 was chosen in temper A, having a non-directional grain structure to reduce the promotion of crack growth along the spiral slits. Elastic modulus E = 127.5 GPa (18.5 Mpsi). Available endurance strength data for this material was limited to 10^7 cycles. Extrapolations were made from that data for a 10 yr. life, > 10^{10} cycles @ 40 Hz. The reverse-bending endurance strength limit was conservatively established as Se = 248 MPa (36 kpsi).

Figure 8 displays a representative z-axis displacement plot of SPR3 at 10 mm deflection. This data was used to validate the analytical determination of the reciprocating mass contribution from the spiral flexure bearing. This plot also contrasts with the inaccurate single leaf model SPR1 displacement plot shown in Figure 6.

Figure 9 displays a representative stress plot of SPR3 at 10 mm deflection. The von Mises stress result (based on his Maximum Distortion Energy theory) was used throughout the FEA. The stress risers at the slit ends are noticeable as the lightest colors in the black & white photocopy of the original color Polaroid print. The stress on the inside spiral of each leaf is also noticeable and is due to the slight twisting as previously noted. Figure 10 is a close-up of the stress concentration at the slit end at Rsi for that same plot. The i.d. of the flexure bearing was clamped away from Rsi. The peak stress was 425 MPa (61.7 kpsi).

In order to reduce the stress risers at the slit ends, it was decided that increasing the length over which the stress is concentrated would re-distribute that stress and reduce its intensity at any given point. The first implementation of this concept was a ∅ 1.5 mm hole placed at the end of the 375 μm wide slit, which had terminated with a 188 μm radius. The resultant peak stress concentration at that slit end was reduced ~ 20 % (@ 10 mm stroke). A larger hole, ∅ 3 mm, was placed there and the result was a further reduction in the stress concentration of ~ 20 %. Figure 11 displays the stress concentration plot of an even larger hole, ∅ 6 mm. The resultant peak stress at this condition was 223 MPa (32.4 kpsi). Although this stress was less than the chosen endurance strength limit for the intended Be-Cu, it presented two new problems:

a.) the large diameter end relief hole restricted the space available for clamping the flexure bearing; and,

b.) a stress riser began to form at the intersection of the large diameter hole and the much narrower slit.

The next implementation of the increased stress concentration concept was to curl the end of the slit, away from the center at Rso and toward the center at Rsi. The slit ends were first curled at a 4.3 mm (0.17 in) radius at Rsi and Rso. The curl increases the effective spring length, thereby softening the spring. Placement of the start of the curl was adjusted

to recover the same spring rate. The resultant peak stress concentration along the radiused ends was reduced to 199 MPa (28.8 kpsi) @ Rsi. Figures 12 and 13 display the stress concentration plots of this arrangement at Rsi and Rso respectively. Other curl radii were tested. A parabolic curvature curl was conjectured to be the optimum, but the complexity that it added to the FEM precluded any complete FEA results. The final design incorporated 5.8 mm (0.23 in) radiused ends. The radiused ends are obviously the better implementation of the concept because it eliminated the two problems which resulted with the end relief holes:

a.) the radiused end could be placed inward along the spiral slit to reduce the loss of clamping space without losing cantilevered spring length; and,

b.) there was no secondary stress riser formation.

After the stress concentration problem was resolved at the slit ends, the other attributes of the final design were analyzed as follows:

a.) The axial spring rate was determined as 4.78 kN/m (27.3 lbf/in). This equates to a spring energy of 0.239 J (2.12 lbf-in) @ 10 mm (0.394 in) stroke for each spiral flexure bearing. An actual flexure bearing was later measured for spring rate and found to be 4.69 kN/m (26.8 lbf/in), or < 2 % difference.

b.) The radial stiffness was determined as 1.22 MN/m (6980 lbf/in) @ 10 mm full deflection. Under the final sprung mass load of 3.2 kg (6.9 lbm) the four flexure bearings deflect 7.6 μm (0.0003 in).

c.) The first six natural frequency modes were determined by COSMOS/M as 30.6, 75, 79.5, 97.7, 192 and 205 Hz. There were no anticipated problems from this result. Based on the effective reciprocating mass of the spring as derived in the following section, and the preceding spring rate, the calculated natural frequency of the spring, $\omega_{ns} \equiv (k/m_{eff})^{0.5} = 32.0$ Hz.

d.) In-plane and cross-plane shear stresses were checked, but all were very low for the Be-Cu material and thus would not influence the life of the flexure bearing.

Refer to drawing 259508D for the final design details.

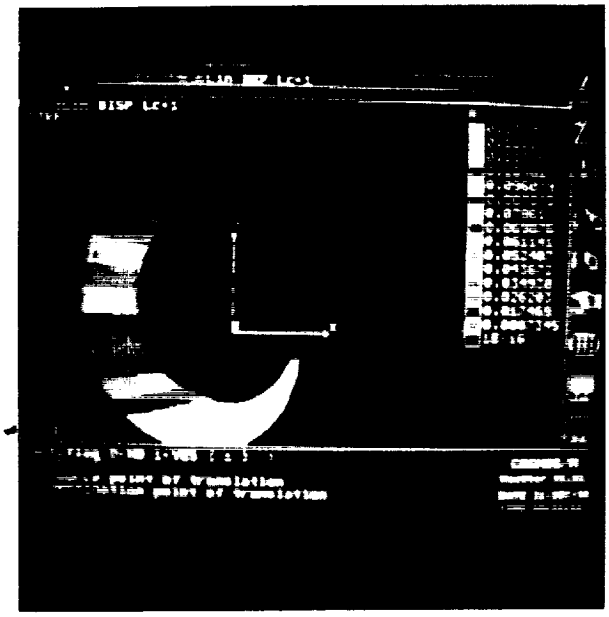

Figure 6. Single spiral leaf spring FEM: Z-axis displacement plot of SPR1.

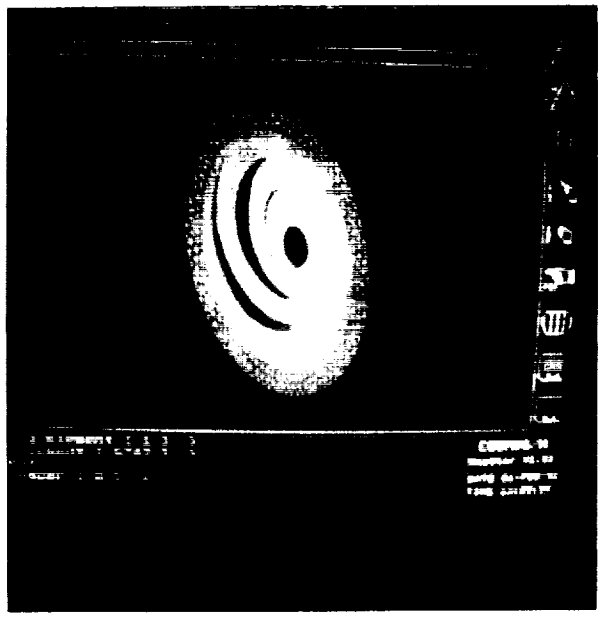

Figure 7. Full three-leaf spiral flexure bearing FEM: Z-axis deflection plot of SPR2.

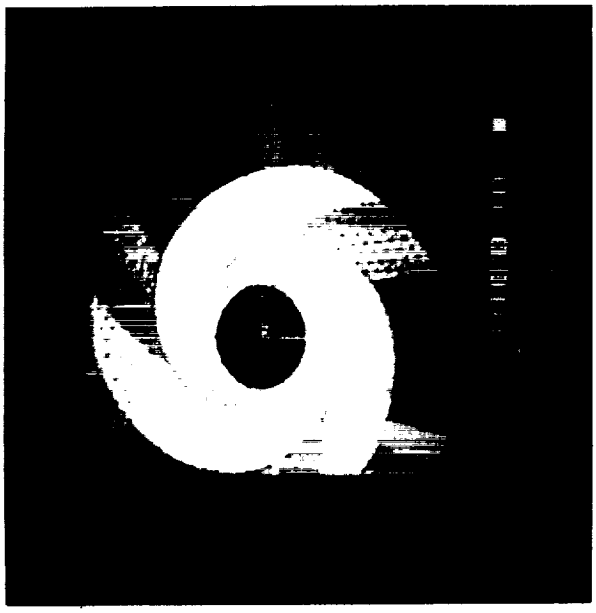

Figure 8. Z-axis displacement plot of SPR3 with 10 mm stroke @ i.d..

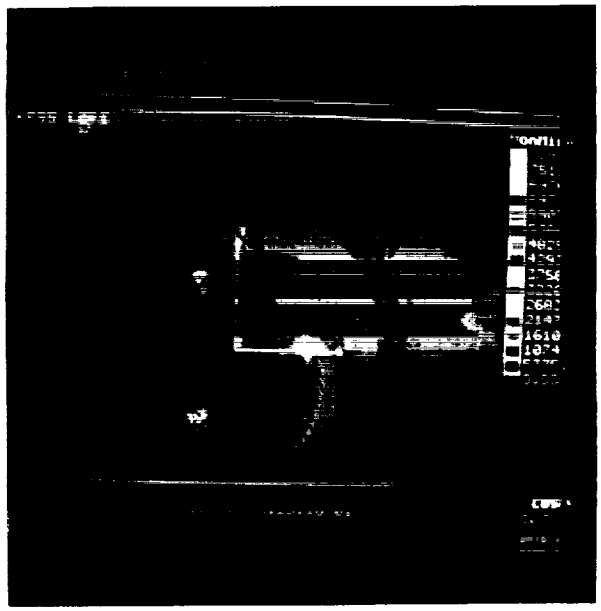

Figure 9. Von Mises stress plot of SPR3 with 10 mm stroke @ i.d..

ORIGINAL PAGE
COLOR PHOTOGRAPH

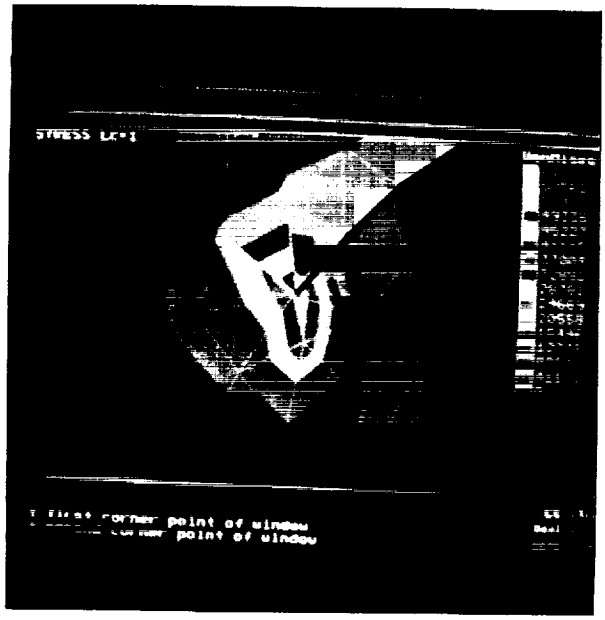

Figure 10. SPR3 FEM: Stress concentration @ slit end @ Rsi with 10 mm stroke @ i.d. and flexure bearing clamped away from Rsi.

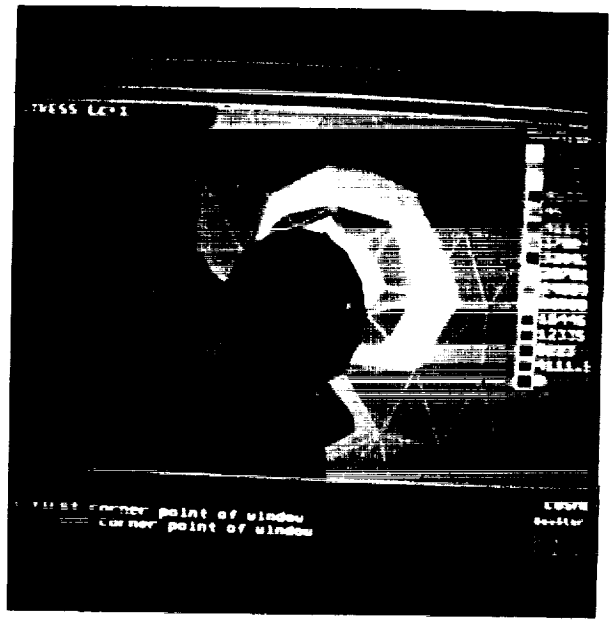

Figure 11. SPR3 FEM: Stress concentration plot of slit end relief hole, ∅ 6 mm, 223 MPa (32.4 kpsi) peak stress here, @ 10 mm stroke.

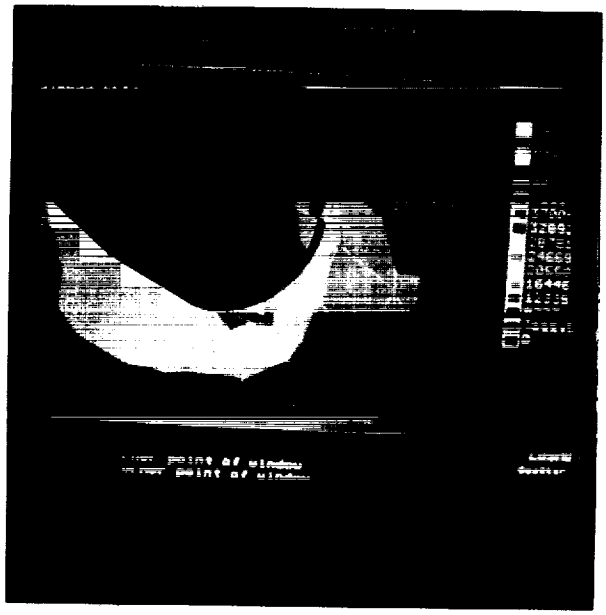

Figure 12. SPR3 FEM: Stress concentration plot of 4.3 mm radiused slit end @ Rsi. 199 MPa (28.8 kpsi) peak stress here, @ 10 mm stroke.

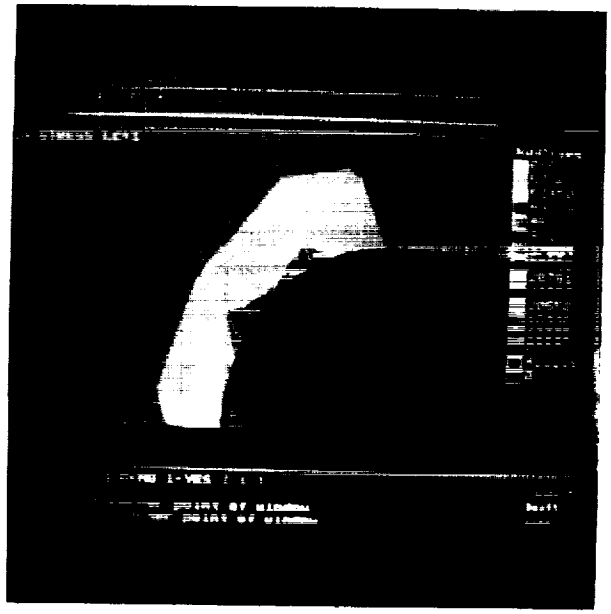

Figure 13. SPR3 FEM: Stress concentration plot of 7.1 mm radiused slit end @ Rso. 170 MPa (24.7 kpsi) peak stress here, @ 10 mm stroke.

ORIGINAL PAGE
COLOR PHOTOGRAPH

Reciprocating Mass Reduction

To check the validity of the original assumption that the springs contributed very little to the reciprocating mass, an analysis was done. Figure 14 shows a schematic representation of the spring being deflected by a force, F, some distance, δ. The spring at rest is shown as a heavy line and its nonlinear deflection by the dashed line.

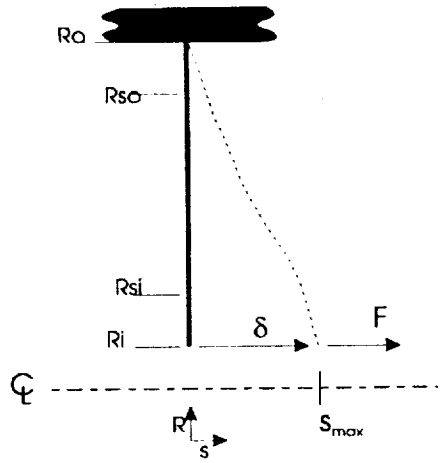

Figure 14. Schematic representation of spiral flexure bearing deflection.

Displacement in the axial direction is represented by s, and s_{max} is the maximum displacement along the centerline equal to the half stroke of 10 mm. At all other points on the spring, the displacement is a nonlinear function of the radius, $s(r)$. In the radial direction r_i is the inner radius of the spring, r_{si} is the inner radius of the spiral groove, r_{so} is the outer radius of the spiral groove, and r_o is the outer radius of the spring.

The natural frequency, ω_n of the system is determined from

$$\omega_n = \sqrt{\frac{k}{m}}$$

where k is the spring constant, and m is the reciprocating mass. Equating the kinetic energy of the reciprocating system with the potential energy of the spring gives

$$W = \frac{1}{2}mv^2 = \frac{1}{2}ks^2$$

$$\frac{k}{m} = \frac{v^2}{s^2}$$

where v is the velocity. Therefore, $m \alpha s^2$ and $k \alpha v^2$, if the other variables are fixed, and

$$\frac{m(r)}{m_{total}} = \frac{s^2(r)}{s^2_{max}}.$$

The effective spring mass, m_{eff}, is the contribution of the spring to the reciprocating mass of the system and is given by

$$m_{eff} = \sum m(r) = \int_0^m dm = \frac{m_{total}}{s_{\max}^2}\left(\int_{r_i}^{r_o} s dr\right)^2$$

The functional relationship of the displacement of the spring with radial position was determined by numerically integrating results of the finite element analysis using the following relationship

$$\int_{r_i}^{r_o} s dr = \frac{\sum s\Delta r}{r_o - r_i} = 5.41\text{mm}$$

This was then used to find the effective mass

$$m_{eff} = 0.293 m_{total}$$

and the total mass of the Be-Cu alloy spring is given by

$$m_{total} = \rho t \int_0^{2\pi r_o}\int_{r_i} r dr d\theta = 0.4\text{kg}$$

Since the effective mass of the spring is ~ 29 % of its total mass, the contribution of the springs to the reciprocating mass of the system can not be neglected. An increase of the reciprocating mass requires an increase in the spring rate to maintain a natural frequency of 40 Hz. However, the additional springs needed to increase the spring rate also increase the mass, which in turn creates a need for more springs. The initial reciprocating mass of the compressor, not including flexure bearings, was estimated to be 2.8 kg. Thirty-eight springs were thus required to achieve 40 Hz with this mass. However, these springs increased the reciprocating mass to 7.2 kg! Thus, there was no convergent solution to this problem with this spiral design, and the number of springs was already becoming impractical. At this point we had a choice of a) persuing an alternate spring geometry, b) changing the motor design to a moving coil, c) adding a gas spring. After considering time and cost, it was decided to provide the additional restoring force by a gas spring. The functions of the flexure bearings were thus reduced to providing the shaft support and radial guidance. Four flexure bearing springs were used for this purpose. The actual final design reciprocating mass with the gas spring and four flexure bearings became 4.82 kg.

3.1.3 Linear Motor

The linear motor design was conceived originally as a moving-coil design with stationary magnets, operating in a resonant mode and driven by a sinusoidal voltage source. The motors of the two compressor halves were to be connected in parallel to the same voltage source. The moving-magnet concept was selected instead, because it provided more reciprocating mass which was thought to be needed to achieve high efficiency. The magnets are located between the inside diameter of the coil assembly and the outside diameter of the inner iron. An outer iron piece is located on the outside diameter of the coil assembly to close the magnet circuit.

Iron Path, Field Plots

Based on the motor size study (see section 3.1.1), the magnets were chosen as IG Technologies, Inc. Incor 26HE, a 2:17 SmCoFe material with a maximum energy product capability of 26 MGOe. The intended field in the motor gap was to be 0.5 T, and 1.1 T in the iron pieces.

A FEM was created of the initial motor magnetic circuit and analyzed using Pandira FEA. Flux plots were generated. The field in the gap was found to be an excellent 0.6-0.7 T, the maximum cross-section average (MCA) field in the inner core iron was 1.24 T, but the MCA field in the outer shell iron was 2.1 T. The design was changed by shifting material from the core to the shell iron in order to get a more uniform flux density distribution. Inactive material on the corners of the iron pieces was also removed. Figures 15 and 16 depict the flux plots of the original and revised (final) design, respectively, with the magnets at mid-stroke and an assumed peak current of 9.6 A in the coils.

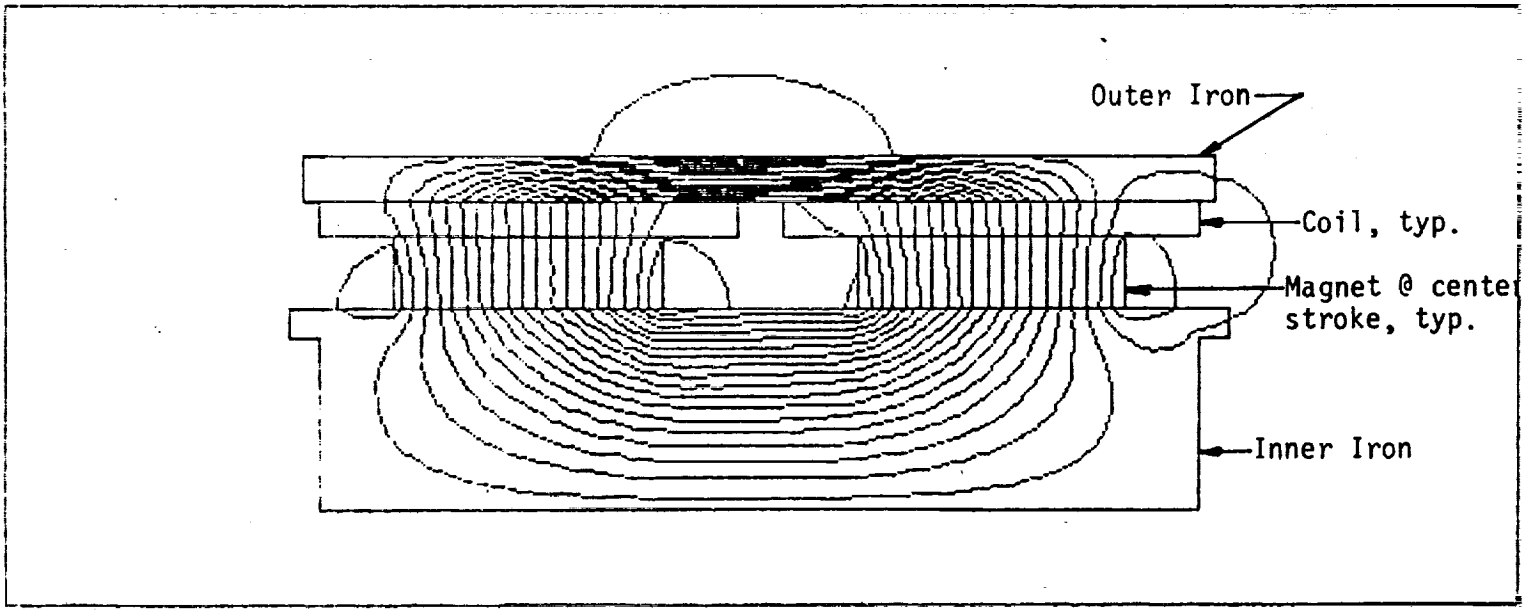

Figure 15. Flux plot.

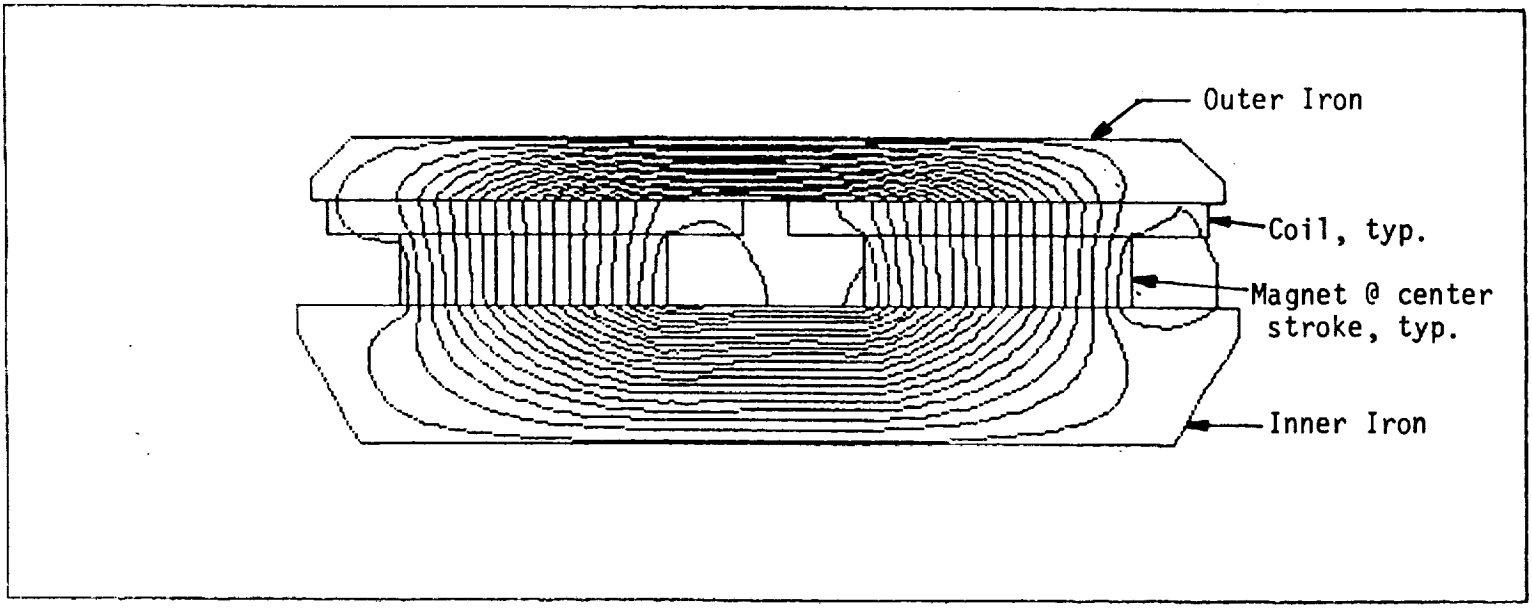

Figure 16. Flux plot

Hysteresis Loss, Laminations

The inner (core) and outer (shell) iron for the return paths of the magnetic circuit were initially intended to be solid cylindrical machined parts carrying a field of 1.1 T. However, the eddy-current loss and time constant were erroneously calculated. After these errors were discovered, the design was changed to a segmented or laminated assembly.

The magnetic field hysteresis loss in the shell and core iron was not initially estimated. After the shell and core were laminated, the hysteresis loss was calculated from the data provided by the lamination material manufacturer. The material for the laminations was chosen as 635 μm thick (0.025 in) Tempel Steel Co. 24N208, a non-oriented annealed 3 % silicon steel ($\approx$ AISI M19) designed for low hysteresis loss (rated as 2.08 W/lbm @ 15 kG, 60 Hz, 50 % w/ the grain). The core contains 208 laminations, each with a thickness:width aspect ratio $\alpha = 0.025/0.74 = 0.034$ and a weight m = 10.4 grams. The shell contains 534 laminations, each with $\alpha = 0.073$ and m = 5 grams. Each lamination is separated from the next by two $\varnothing$ 3 mm plastic shims and electrically insulated with epoxy. From the FEA, the final design maximum field cross-section averages were 1.74 T in the core and 1.88 T in the shell. Using the Tempel data, the estimated peak hysteresis loss @ 40 Hz is 8 W in the core and 10 W in the shell.

Depending on the assumptions, the eddy-current power loss in the laminated shell and core iron assemblies could still be significant. For example, a 170 W loss was calculated for the laminated cylindrical shell iron (ref. drawings 259364C and 259366D) based on the following: @ 40 Hz with B = 0.7 T, $\alpha = 0.073$, n = 534 and $\rho = 40$ $\mu\Omega$-cm, (Kittel, P.)

$$P = 0.03125\,(dB/dt)^2\,\Gamma AV\,\rho^{-1}\,(\alpha^2 + n^{-2})\,(\alpha^2 + 1)^{-1}$$

Magnet Carrier Analysis

The magnet carrier was designed with the aid of FEA. The magnet carrier has to firmly hold the segmented magnet rings in place under the reciprocating loads without deflecting more than the radial clearance gap in the magnetic circuit. The radial clearance gap is 343 μm (0.0135 in) to allow for magnet carrier deflection, axial angular misalignment and assembly mis-concentricity. The magnet carrier must also be as low in weight as possible to reduce the reciprocating mass. The magnetic circuit dimensions limited the radial thickness of the carrier in the area of the magnets to a very slim 229 μm (0.009 in). Simple beam and buckling equations would not suffice.

Figure 17 shows the force balance on the magnet carrier and piston/shaft assembly.

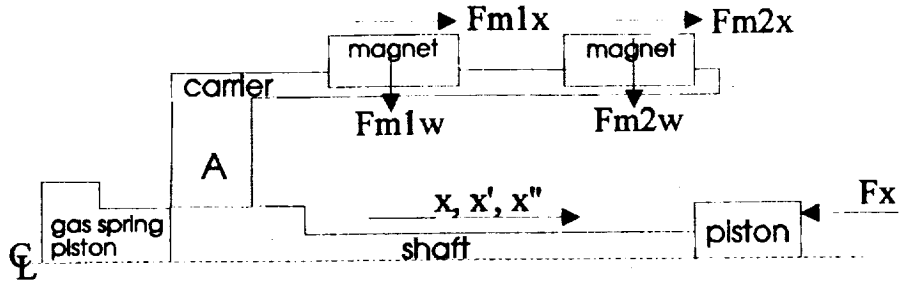

Figure 17. Force balance on the magnet carrier in the forward, compression direction.

Fx ≡ peak axial load = Σ peak forces due to gas compression, flexure bearings, gas spring inertia ($m\delta\omega^2$) and housing gas pressure.
Fm1x = Fm2x = Fx/2 ≡ peak axial load per magnet ring
Fm1w = Fm2w ≡ magnet ring and carrier weight
x, x', x" ≡ displacement, velocity, acceleration

The peak axial load was conservatively calculated to be 6.84 kN (1537 lbf) in the forward, compression direction, and 6.16 kN (1385 lbf) in the reverse, suction direction. The magnet carrier material was chosen as austenitic stainless steel due to its availability and low magnetic permeability. The magnet ring and carrier weight contribution were calculated to be 6.9 N.

The FEM was designated MAGCAR. It was an axisymmetric model of the cross-section of one half of the total carrier, and was meshed using triangular elements. The initial design included a wide rectangular cross-section at the vertical upright (location A) and thin horizontal sections at the magnets. Sresses in the upright were low, but vertical deflections were excessive. The horizontal sections were increased in thickness and the upright cross-section mass was reduced. Mass that was added to the horizontal sections was subtracted from the vertical upright. Eventually, the vertical upright became webbed with holes drilled through it to maintain this compromise of mass vs. stiffness. Fillets were also added where necessary to either add stiffness or remove mass. See final design drawing 259460C.

Figures 18, 19, 20 and 21 display the stress and deflection plots of the final design magnet carrier in the deformed (exaggerated) condition for both forward and reverse directions. The maximum vertical deflection of 19 μm (0.0074 in) was found to be at the far right-hand cantilevered end of the carrier in the forward direction. This was well within the allowable air gap in the magnetic circuit. The stress levels are also very low for the stainless steel, 58.6 MPa (8.5 kpsi).

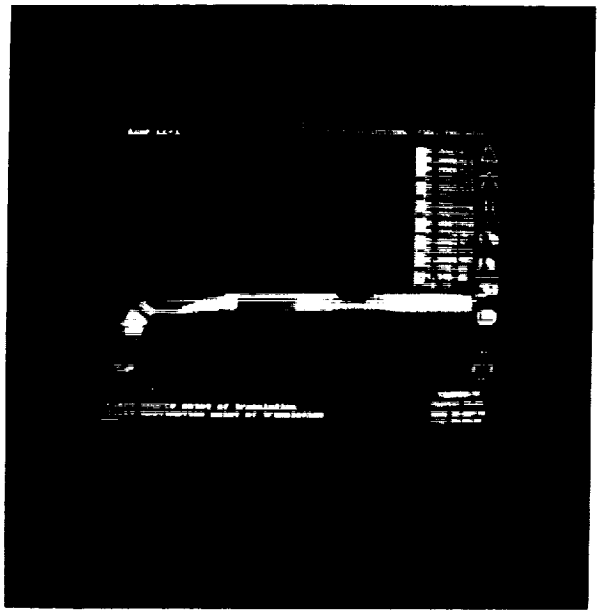

Figure 18. MAGCAR FEM: Deflection plot @ peak load in forward, compression direction.

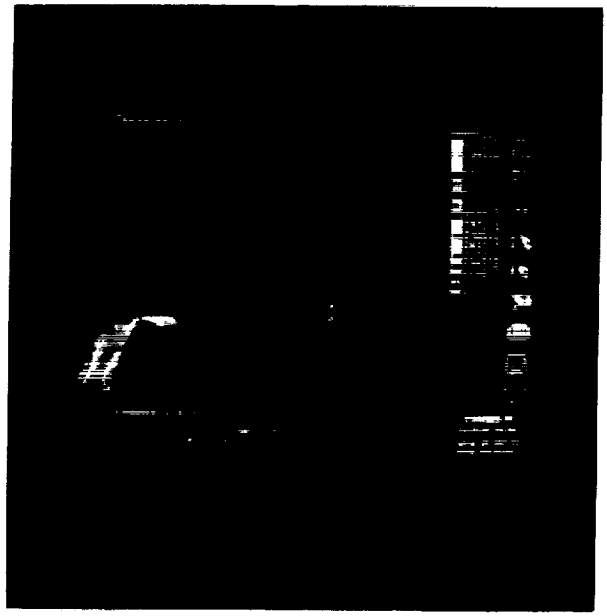

Figure 19. MAGCAR FEM: Stress plot @ peak load in forward, compression direction.

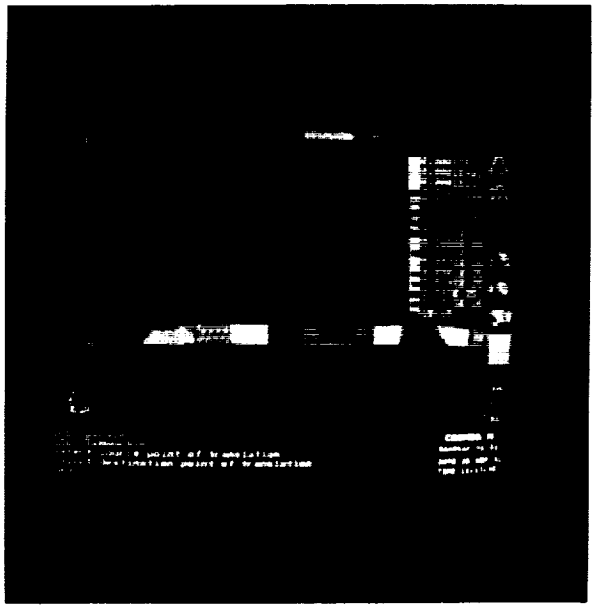

Figure 20. MAGCAR FEM: Deflection plot @ peak load in reverse, suction direction.

Figure 21. MAGCAR FEM: Stress plot @ peak load in reverse, suction direction.

ORIGINAL PAGE
COLOR PHOTOGRAPH

Windings

Based on the motor size study (see §3.1.1), the coil assembly is configured as two coils wound in opposition, each with 100 turns in a space 55 mm long X 4.65 mm radial thickness X 103.5 mm mean diameter. This arrangement affords adequate surface area for heat dissipation. The coil assembly was estimated to carry 300 W input power, 9.6 A peak current @ 40 Hz with a 0.5 T field gap.

Coil density is maximized by using 16 AWG (1.29 mm) square cross-section copper wire, having a resistivity $\rho = 3.57\ \Omega/1000$ feet. Resistance of the coil assembly was calculated to be 0.89 Ω. The FEA indicated that the gap field along the coils had a gradient of ~ 150 gauss/cm with 9.6 A peak current assumed. The coil/iron motor assembly inductance was calculated to be 7.8 mH.

The number of turns/coil was later increased to the final design of 117 turns (3 rows X 39 turns per row) by adding more turns at the center area in order to reduce some power loss at the ends of the stroke. 75 turns/coil are coincident with the magnet. This could still be an additional loss in the motor, whereby the coil does not extend beyond the magnet enough at the ends of the stroke to minimize the end-stroke stray field depicted in the preceding FEA field plots.

3.1.4 Gas Spring

Program "SCD3" was modified to add a gas spring piston to the back end of the drive shaft. The compressor housing was assumed to remain at an average pressure while the gas spring volume changed pressure opposite to the pressure change in the compressor piston. A gas spring rate of 74 N/m was calculated as being needed which is provided by a gas piston having a diameter of 89 mm and a cylinder length of 79 +/- 20 mm. The volume was designed so that it can be adjusted +/- 20 mm to adjust for resonance at 40 Hz. Pressure in the gas spring is established by leakage past the piston, but an external bypass line with a needle valve and check valve was added so the pressure can be biased to center the stroke.

3.1.5 Pressure Analysis

During normal operation the compressor is charged to 125 - 170 psig (0.86 - 1.2 MPa), which is felt in all spaces. During operation the compression space is subjected to a cyclic pressure ranging from 80 - 250 psig (.55 - 1.7 MPa). The gas spring / LVDT volumes experiences a cyclic pressure ranging from 100 - 195 psig (.7 - 1.3 MPa). The motor housing experiences a cyclic pressure that is approximately ± 10 psig (69 kPa) from the nominal charge pressure.

A simple stress analysis was done on the housings and end plates to insure that they would withstand these pressures. A static analysis of the bolts was done using the catalog yield strength. These calculations were done based on the Phase II proposal drawing.

3.2 Expander

3.2.1 Thermal Analysis of Displacer/Regenerator

The computer program used in Phase I for the expander analysis was modified to include conduction, seal leakage, piping, and void volume losses. The program was used to size the regenerators, the displacers. A listing of the program is given in Appendix C. A modified version of this program was used to size the pneumatic drive, and is listed in Appendix D.

Assumptions

The computer code assumed a single compressor with the output capabilities of the dual opposed compressors. The compressor and displacer motion is assumed to be sinusoidal, and the phase relationship is variable. The expansion and compression processes are treated isothermally. Gas properties are assumed to be ideal, except at the cold end where non-ideal corrections are used. The cycle is divided into 24 steps of 15° increments. The void volume at each stage is a variable percentage of displacement, currently assumed to be 10%. The regenerator analysis assumes that the first stage regenerator is made of stainless steel wire screens, the second stage regenerator is made of lead shot, and the third stage is a parallel plate regenerator.

Design Optimization

The overall system is highly inter-related, and changing one parameter, such as regenerator length will effect the regenerator, and overall system performance. Thus the system was difficult to optimize using a trial and error approach. Final optimization was achieved by designing a statistical factorial experiment. The following independent variables were used: first, second, and third stage regenerator diameters (DR1, DR2, DR3) and lengths (LDR1, LDR2, LDR3); diameter of the second stage regenerator spheres (DS); and the spacing of the third stage regenerator plates (DT). The effects of changing the independent variables was examined on the following dependent variables, system efficiency, the first, second, and third stage refrigeration, and the work of the compressor. Each parameter was given reasonable high/low values, and a factorial experiment was developed. The program was then run 256 times. The data generated was then reduced using multiple linear regression to yield a relationship between the variables.

Design Summary

Table 4 shows the results of the multiple regression. The three largest factors effecting the dependent variables are based on the t-values of the regression analysis. Though the actual relations between the variables is very complex, the R^2 values show that a linear model is a good predictor over the range studied.

Table 4. Regression analysis results.

Dependent Variable	Equation	Largest Factors	Adj. R^2
Cycle Efficiency	50.9 - .07*DR1 +.11*DR2 - .53*DR3 + 6.4*LDR1 - 4.7*LDR2 - 3.1*LDR3 - 145*DS - 153*DT	DR3, LDR2, LDR3	.8855
1st stage Refrigeration	59.9 + .16*DR1 - 2.2*DR2 - .63*DR3 + 22.7*LDR1 - 23.6*LDR2 - 3.7*LDR3 + 124*DS - 255*DT	DR2, LDR2, LDR1	.9971
2nd stage Refrigeration	8.9 - .15*DR1 + .41*DR2 -.2*DR3 - 3.9*LDR1 + 4.7*LDR2 - 1.67*LDR3 - 90.1*DS - 17.8*DT	DR2, DS, LDR3	.9921
3rd stage Refrigeration	4.2 - .09*DR1 - .04*DR2 + .06*DR3 - 1.9*LDR1 - 1.1*LDR2 +.6*LDR3 + 11.4*DS + 1.5*DT	LDR1, LDR3, DR3	.9897
Compressor Power	1618 - 16.8*DR1 - 11.6*DR2 - 4.9*DR3 - 282*LDR1 - 110*LDR2 - 28*LDR3 - 1970*DT	DR1, LDR1, DR2	.9988

The coefficients in the equations indicate the direction of change, and the magnitude indicates the size of the change needed to change the dependent variable. For example, to increase the 2nd stage refrigeration, the diameter of the second stage regenerator would be increased or the size of the lead shot decreased. Since the absolute value of the coefficient of the shot is much larger than that of the regenerator diameter (90.1 vs. 0.41), it takes a larger change in the regenerator size to affect the same change in refrigeration as a change in the sphere size.

These variables were then used to gain insight in the optimization of that particular dependent variable. As an example, suppose that we try to maximize the refrigeration of both the first and second stages. The diameter of the second stage regenerator is the key factor in both parameters and the direction and magnitude of the change is seen from the coefficients in the equations. However, the effect of increasing the diameter of the second stage regenerator decreases first stage refrigeration and raises second stage refrigeration. The decrease in 1st stage refrigeration is greater than the increase in second stage refrigeration as seen by the coefficients (-2.2 vs. 0.41). Utilizing information such as this, a series of trade studies was done to get to the final design.

Key design results obtained from the computer program are given in Table 5. The operating speed of 40 Hz was chosen previously in the compressor analysis study. It was found that the expander operates more efficiently at lower speeds, with a peak efficiency at 33 Hz. However, operation at 33 Hz would result in a much heavier system, and the compressor design was finalized at 40 Hz. Increasing the charge pressure increases the efficiency of the expander, but also increases compressor work. The charge pressure was raised to the point where compressor power approached 500 W. The best operating frequency and charge pressure can be determined from tests.

Table 5. Design specifications from computer program.

Displacer Stroke 5 mm	Operating Speed 40 Hz	Pressure Ratio 1.64/0.69 MPa	Efficiency 23.4%
Compressor P-V 488 W	Helium Mass 0.143 g	Phase Angle 60° leading	Charge Pressure 0.85 MPa
Specification	**1st Stage**	**2nd Stage**	**3rd Stage**
Displacer Diameter	28 mm	12 mm	6 mm
Displacer Length	126 mm	48 mm	36 mm
Regenerator Diameter	31.5 mm	17.0 mm	16.0 mm
Regenerator Length	19.53 mm	11.14 mm	20.8 mm
Hydraulic Diameter of Regenerator Matrix	25 μm	44.5 μm	20 μm
Porosity of Regenerator Matrix	68.6%	41%	4.25%
Shuttle Loss	.55 W	.056 W	.003 W
Conduction Loss	8.1 W	.51 W	.33 W
Seal Leakage Loss	.91 W	.54 W	.05 W
Piping Flow Losses	1.53 W	.56 W	.24 W
Temperature	60 K	16 K	8 K
Refrigeration	10.6 W	1.48 W	.91 W

Shown in Figure 22 is the compressor outlet pressure and the individual stage pressures over the operational cycle in the expander. Also plotted is the displacer position which shows the relationship between the displacer and pressure pulse. As expected, the pressures in the system decrease at each stage due to the pressure drops in the piping and regenerators.

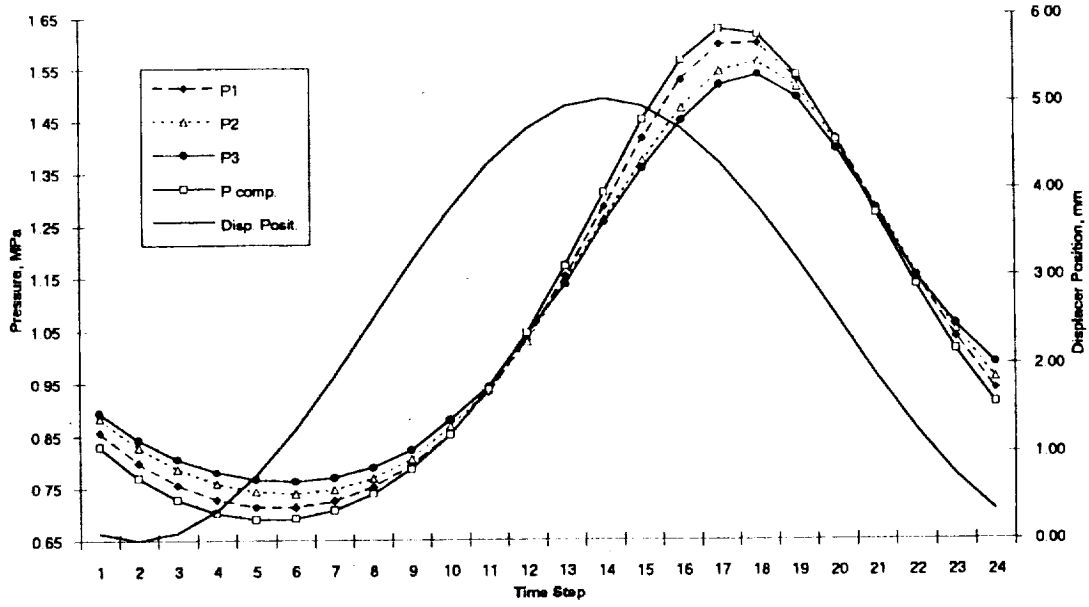

Figure 22. Expander pressures versus time step for one cycle shown in 15° increments.

The mass flow rates through the regenerators are shown in Figure 23 along with displacer position for comparison. The mass flow rates for the regenerators decrease from first through third stage. The mass flow rate through the first stage regenerator is considerably higher than the rest of the flows. This demonstrates the necessity of having a low pressure drop in the first stage regenerator. Low pressure drops are also desirable to minimize the losses in the displacer clearance seals. A low pressure drop was achieved by using a short, large-diameter regenerator.

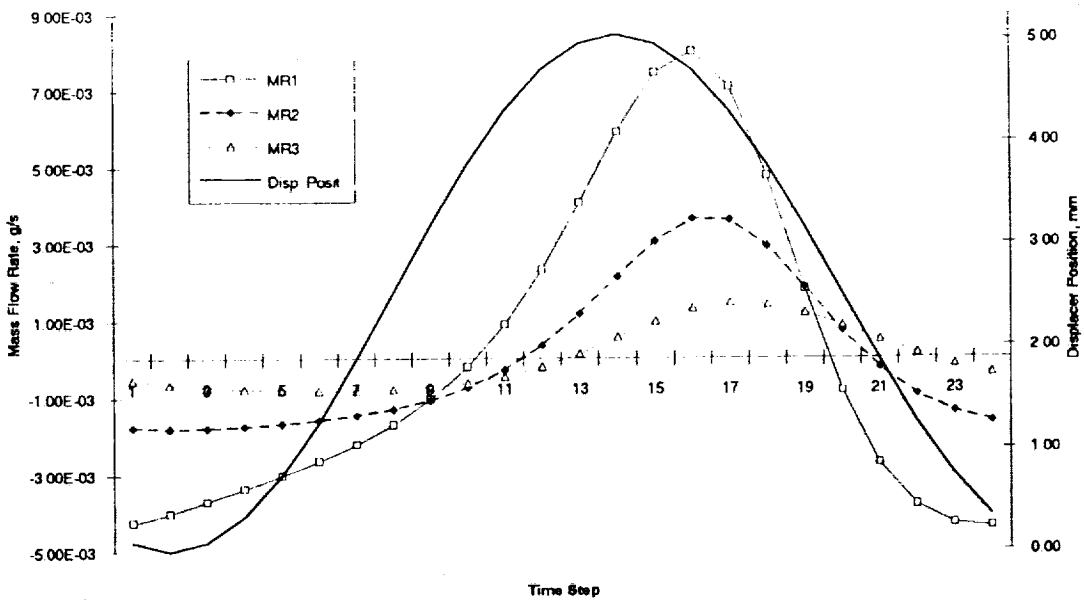

Figure 23. Regenerator mass flow rates versus time step for one cycle shown in 15° increments.

3.2.2 Gas Spring Driver

Analysis of the pneumatic expander drive was completed based on the model shown in Figure 24, using the code in Appendix D. The analytical model assumes a single-stage expander operating at 38 K to represent the actual three-stage unit. Displacer weight, stroke and operating pressures and pressure drop are the same. This model was used to size the drive stem, the gas spring piston diameter and the gas spring volume. It was also used to analyze the sensitivity of the stroke and phase angle on the spring volumes and pressures. The unit is built with variable volumes to control the phase angle and centering of the displacer and a bleed valve to control the stroke.

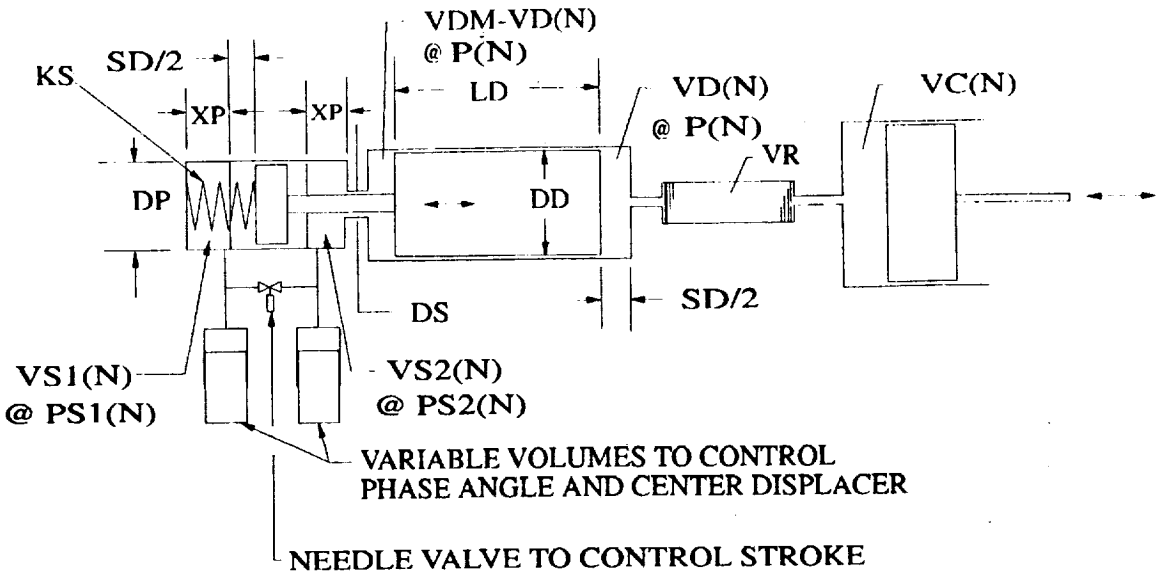

Figure 24. Dynamic model of the expander.

3.2.3 Mechanical Analysis

A simple stress analysis was done on the expander cylinders and displacer piston assemblies. This insured the cylinders would hold the system pressures, and the displacer assemblies would not collapse.

4.0 Design

Detailed design studies led to the production of a set of drawings for the compressor, expander and test stations. A complete set of drawings are enclosed. Fabrication methods and assembly procedures were studied and finalized.

4.1 Compressor

The compressor is constructed with three modular units; the compression end, the motor section, and the gas spring end. The compression end consists of a compression piston attached to the main shaft, and a water cooled cylinder. The motor section consists of the stationary inner iron, the magnet carrier assembly which is attached to the main shaft, the coil form assembly, a housing and water jacket. The gas spring end consists of the gas spring piston which is attached to the main shaft, a water cooled cylinder and a position indicator.

In a long-life compressor with sliding clearance seals the alignment of the component parts is critical. Though sliding interference seals made of Rulon were used, the compressor was designed with close attention paid to the stack up of tolerances and insuring the fit of key alignments. Appropriate assembly fixtures and procedures were developed to insure the proper fit of the compressor parts.

4.1.1 Pistons

The compression piston and gas spring piston were machined from 6061-T6 aluminum to minimize the reciprocating mass. The size of the compression piston was determined from the stroke of 20 mm and the required swept volume of 29.5 cm^3. The design of the gas spring piston is discussed in a following section.

The sides of the pistons were covered with a Rulon sleeve. Rulon is the trade name of a carbon filled Teflon. Rulon was chosen to give a complete gas seal while minimizing the amount of sliding friction. The use of Rulon seals makes the design more tolerant to slight misalignments as Rulon wear particles will not cause catastrophic failure of the motor like metal wear products do.

A 0.020" Rulon tape was epoxied to the sides of the pistons with HB Fuller #7004 flexible epoxy. The stresses imposed on the epoxy by the thermal mismatch of the Rulon and aluminum was studied.

$$\Delta\varepsilon_{epoxy} = \varepsilon_{Rulon} - \varepsilon_{Al} = 112 * 10^{-6} C^{-1}$$

$$\tau_{epoxy} = G\Delta\varepsilon = 56 psi / C$$

The allowable stress on the epoxy is 5000 psi which translates into a temperature difference of 90 C. However, the Rulon is limited to a temperature of 40 C to prevent

possible thermal decomposition. Therefore, the pistons are limited to a maximum temperature of 40 C. This information is used later in the cooling requirements.

4.1.2 Shaft

The main compressor shaft was made from 6061-T6 aluminum to minimize the reciprocating mass. The shaft was designed such that it would not buckle under the compressive loads nor twist in torsion during assembly. The shaft has a length of 6" and a diameter of 3/8".

The critical force needed to produce failure of the shaft due to elastic instability, buckling, is given by the Euler equation

$$\frac{P}{A} = \frac{C\pi^2 E}{\left(\frac{L}{k}\right)^2} \quad \text{(Euler)}$$

where P is the total load, A is the section area, E is the modulus of elasticity, L/k is the slenderness ratio, L is the shaft length, k is the radius of gyration, and C is the coefficient of constraint (Young, 1989). The constraint coefficient can range from 1 to 4 depending on the end conditions. A value of 1 was chosen to keep the design conservative. The slenderness ratio is very important in determining whether the shaft is long (Euler) and fails by buckling or is short (Johnson) and fails by yielding. The change-over ratio is given by

$$\left(\frac{L}{k}\right)_{change} = \sqrt{\frac{2\pi^2 CE}{S_{sy}}} = 69$$

where S_{sy} is the static yield strength (Shigley and Mitchell, 1983). The compressor shaft's L/k is 64 < 69, which means the shaft is a Johnson shaft, but is still close to the dividing point. The critical force for a Johnson shaft is given by the following

$$\frac{P}{A} = S_{sy}\left(1 - \frac{S_{sy}}{4\pi^2 CE}\left(\frac{L}{k}\right)^2\right) \quad \text{(Johnson)}$$

Since the shaft's L/k was close to the dividing point the critical force was calculated both ways and is presented Table 6.

Table 6. Critical force comparison for compressor shaft.

Method	Force, lbf	Safety Factor
Euler	2,660	1.72
Johnson	3,440	2.23
Actual Force	1,540	N/A

The shaft is adequately designed to withstand the force of compression as shown by the factor of safety of at least 1.7.

During assembly, the compression piston and gas spring piston are threaded onto the shaft. The maximum torque was determined so that the shaft would not twist in torsion. The maximum shear stress, τ_{max}, at the diameter of the threads is given by

$$\tau_{max} = S_{sy} = \frac{16T}{\pi d^3}$$

where T is the torque, and d is the diameter. This equation was used to find the maximum torque which was used in the assembly procedure.

$$T_{max} = 360 \text{ in} - \text{lb} = 30 \text{ ft} - \text{lb}$$

4.1.3 Motor

Iron Laminations

The inner (core) and outer (shell) iron for the return paths of the magnetic circuit were initially intended to be solid cylindrical machined parts. However, the eddy current loss would have been too large. The design then became a segmented iron or laminated assembly. The exact configuration of the laminations and assemblies are as shown on drawings 259363C, 259364C, 259365D and 259366D.

Magnet Carrier

The FEA resulted in the final design of the magnet carrier as shown on drawing 259460C. The machined magnet carrier was then assembled with the magnet arcs, drawing 259355C, in proper magnetic alignment, epoxied and clamped in place on the carrier as shown on drawing 259356D.

Coil Form Assembly

An assembly was designed to contain the windings, and outer iron laminations (see APD drawing 256366D-P). This assembly also provided a means for inserting the windings into the housing and maintaining the proper alignments. The coil form is a metal can upon which the wire is wound. The laminations are placed over the windings, and the assembly is potted with an epoxy. The coil form was made of 316 annealed stainless steel instead of BeCu to save money. The necessary air gap (0.014", .36 mm) between the windings and the magnets dictates a very thin-walled can (0.016", .41 mm).

The narrow gap between the magnets and the coil form requires very tight dimensional control of the coil form, and proper alignment during assembly. The coil form assembly is designed to be press fit into the motor housing to insure it is concentric with the shaft and

magnet carrier. A stress analysis was performed on the coil form assembly to insure it would not collapse under the pressure of the press fit.

Electrical Feed Through

A method to transfer power from the power supply to the compressor motor was needed. This was accomplished by use of a hermetic receptacle. A cord from the power supply was attached to the female end of the military-style twist-on connector. The motor housing had the flange mount receptacle mounted on it. A Detoronics DTOH-8 was chosen based on initial calculations and availability. This receptacle is rated for a maximum of 5 amps continuous duty. It was found during testing, that typically, the compressors each draw 15 amps RMS. Though this is not constant duty, it is doubtful that the plug is adequate and it should be replaced before sustained operation of the compressor.

4.1.4 Flexure Bearing Holder

The flexure bearings are grouped in pairs at both ends of the shaft. The total spring rate is the summation of each. Each flexure bearing is placed with the direction of the spiral slits opposite that of the adjacent flexure bearing in each pair. This arrangement cancels the x and y axes rotations during the stroke that are caused by the spirals twisting. The i.d. and o.d. of the flexure bearings are close-fitted to the shaft and housing diameters to maintain radial position and perpendicularity. Spacers are placed between each flexure bearing to minimize any metal-metal contact during operation. The contact would be caused by the non-planar deflections of the spiral leaf springs due to their slight twisting or harmonic resonances during reciprocation. The stack of flexure bearings is solidly clamped on the i.d. between the shaft and piston shoulders as the piston screws onto the shaft, and at the o.d. to the housing by a clamping ring and cap-screws.

4.1.5 Gas Spring Assembly

Refer to drawing 259399D, sheet 1 of 2, and to drawing 259410C. The gas spring assembly, on the left-hand side of sheet 1 of 2 of drawing 259399D, was designed to be adjustable over a 20 mm range. It was therefore necessary to have the end cap, item 2 on drawing 259410C, fitted with inner and outer sliding gas seals and a threaded stem in order have it moveable while maintaining the centrally-located LVDT transducer stationary. A gas pressure control valve was also located between the gas spring working volume and the main compressor housing. After assembly, it was found that under pressure the friction between the threads of the adjusting nut and end cap stem were too great to allow for easy adjustment. During testing, it was found that the gas spring had little effect regardless of its adjsutment, and was left in the full out position.

4.1.6 Cooling Requirements

The heat from the motor and the compression spaces must be removed in order to prevent temperature increases that could lead to equipment damage. It was assumed that 10% of the compression work goes into frictional heating, and that 100% of the i^2R, eddy current and windage losses of the motor also go into heat. The total heat removed by the water cooling is

$$\begin{aligned}\dot{Q}_{water} &= \sum \dot{Q} \\ &= \dot{Q}_{comp} + \dot{Q}_{gas\ spring} + \dot{Q}_{motor} \\ &= 250\,W\end{aligned}$$

Each compressor requires 250 W of cooling and a total of 500 W. Additional heat loads are removed by the cylinder heads and the after-cooler on the compressor gas outlet line. The required water flow rate was found by

$$\dot{Q}_{water} = \dot{m} C \Delta T$$

assuming a temperature rise of 10 C. The required flow rate is 1/4 gpm. The connections to the cooling jacket are 3/8" lines and the water is supplied from local municipal services. Thus the flow rate easily exceeds this requirement and the temperature rise of the water is indiscernible.

4.1.7 Instrumentation

To tune and evaluate the compressor performance, several pressures, the displacement, current, and voltage must be monitored. On each compressor the stroke was measured with a LVDT, the pressure with transducers, the current with current sensors, and the voltage with a voltage sensor. The output of each of these instruments was recorded with a computerized data acquisition system. The general compressor instrumentation scheme is shown in Figure 25.

The output pressure and the stroke of the compressor were measured, and used to generate a Pressure - Volume diagram. The pressures on either side of the gas spring were measured to evaluate the behavior of the gas spring. The compressors were powered in parallel by the power supply. The voltage is identical for both units and is measured at the power supply output. The current in each unit is ideally identical, but in reality varies, and is measured independently for each compressor. The measurements of the voltage and current are used to evaluate the power required by the compressors.

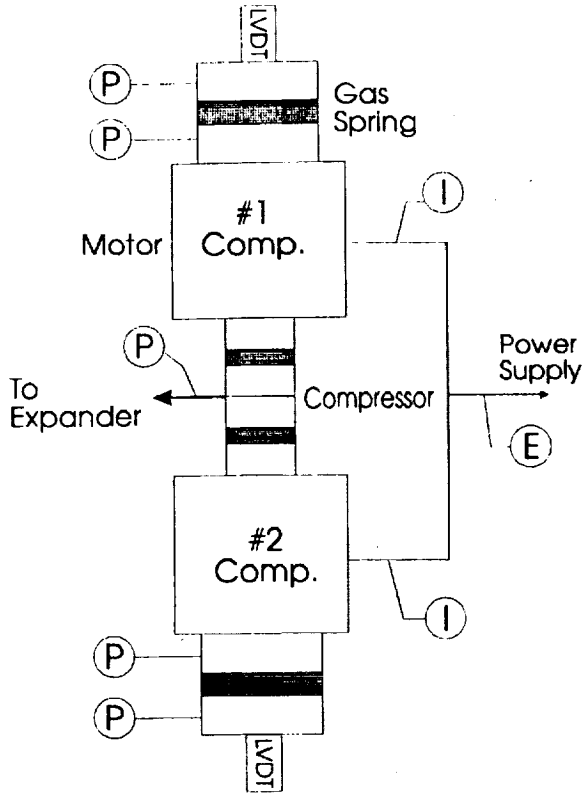

Figure 25. Compressor instrumentation scheme.

The pressure transducers are all made by Barksdale and require a 10 V DC input. Each pressure transducer was wired using a DB-9 pin connector. The pins are wired as follows:

Pin 1	+ power in
Pin 2	- power in
Pin 3	+ signal out
Pin 4	- signal out

A specification sheet for the pressure transducer is enclosed. The output of the pressure transducers was sent to a signal conditioning unit and then to the data acquisition system. This system was then used in the calibration of the sensors. Thus the calibration curves for the transducers are unique to the system.

The linear displacement was measured using a Schaevitz LVDT. These were connected to a power supply / signal conditioning module (ATA-101). The LVDT's were calibrated using the procedure described in the power supply's technical manual. The result of this procedure is that a full scale deflection of the LVDT (0.5") corresponds to a 10 V output. The LVDT specification sheet is enclosed.

The current and voltage sensors are made by LEM and their specifications are attached. These sensors require a ±15 V DC input power. The output of these devices is a current.

Since the data acquisition system measured voltages, this current was converted to a voltage by passing it through a resistor to ground. The voltage drop across the resistor was then measured. The two current sensors have a red and black wire for power input and the output is connected to a banana plug. There is a pin connector that connects the wires to the sensor as shown in the specifications. The voltage sensor operates, and is wired in a similar fashion. These sensors were calibrated and their equations are given below.

Voltage Sensor	E (volts) = 13.24 * reading
#1 Current Sensor	I1 (amps) = 4.862 * reading
#2 Current Sensor	I2 (amps) = 4.483 * reading

4.1.8 Assembly

Alignment

To maintain the critical alignments of the compressor a combination of press fits, shims and dowel pins was used. The coil form assembly was press fit into the motor housing as were the end flanges. These press fits insured the proper geometric alignments.

The compressor and gas spring pistons were individually machined with their mating cylinders to achieve a light interference fit. This fit gives a good seal without too much friction.

The flexure bearings were pinned in place to insure exact alignment and positioning of the shaft. This also allows for disassembling the unit, and subsequent reassembly while keeping the proper alignment.

The final step in maintaining alignment is the shimming of the compressor cylinder and gas spring cylinder. A shim is placed between the seating surface of the cylinder and the motor housing. This shim is then ground at an angle so that the piston runs true within the cylinder.

Cleaning

Cleanliness is vital to the prolonged operation of the compressors. All parts were cleaned prior to assembly. The assembly was done inside of a bench-top clean air hood. The clean air hood is a vertical flow model with a 99.99% efficient HEPA filter at 0.3 μm particles. Special care was taken at all times to avoid any metal particles from entering the system.

Fixtures

Special fixtures were designed to aid in the proper assembly of the compressors. These included fixtures to hold Rulon seals on pistons, to insert and support the coil form assembly into the motor housing, to hold the motor housing while assembling additional

components, to grind the shims, and to insert the shaft / magnet carrier assembly into the motor.

4.2 Expander

The results from section 2.4 were used to design the expander components. The expander is composed of four subassemblies. The first is the displacer assembly including the gas spring, the second is the cylinder assembly, the third includes the three external regenerators, and the fourth is the gas spring / driver.

The top assembly drawing of the expander assembly is shown in Figure 26. The expander assembly consists of three displacer assemblies coupled together inside of cylinders. They are connected to the pneumatic drive, or gas spring. An LVDT (Linear Velocity Displacement Transducer) is attached to measure the displacement of the expander so that its phase relation to the compressor and stroke may be determined. Rulon seals were also used in the expander to minimize machining costs. A cold flexure bearing was inserted between the first and second stages to center the displacers. The location was moved from between the second and third stage displacers to reduce void volume losses.

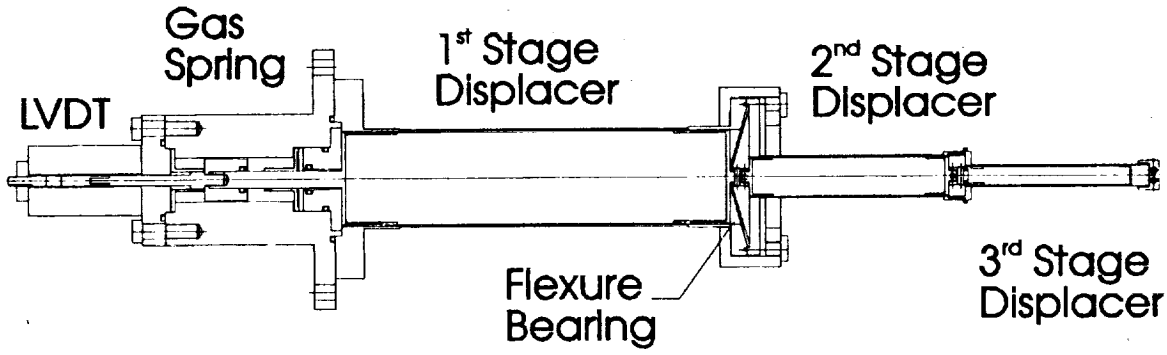

Figure 26. Expander Assembly from APD Drawing 259949B-P.

4.2.1 Displacers

The displacers were composed of four major parts. The thin cylindrical shell, the end-caps, the couplings and Rulon seals.

Shells

The design of the three displacer assemblies was the same except for the actual dimensions which varied from stage to stage. Figure 27 shows the second stage displacer assembly. The shells and end-caps were made of 304 stainless steel. The wall thickness of the shells and end-caps was very thin (~0.010") to minimize axial conduction losses, and the reciprocating mass. The walls could not be made much thinner because of difficulties in machining and welding such thin sections, and also the possibility of collapsing under pressure. The lip on the end-cap was designed to maintain the concentricity of the

assembly to within 0.0005". The closure weld traps air inside the displacer. Radiation and convection losses in the body of the displacer are minimized by packing glass inside the cavity.

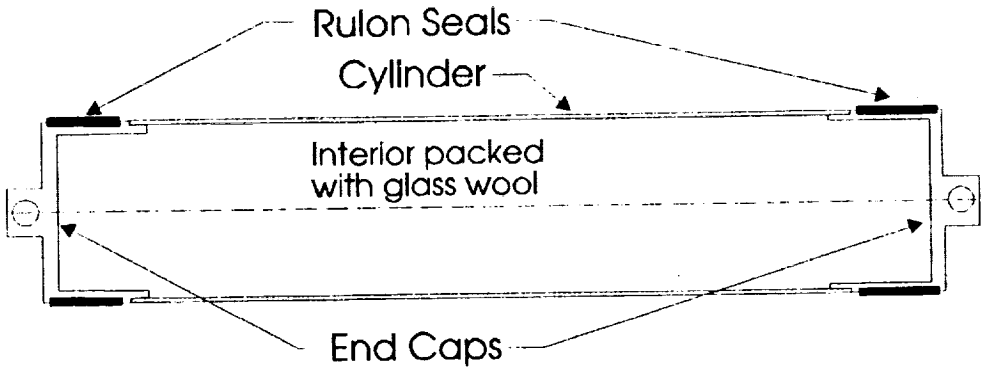

Figure 27. Second Stage Displacer Assembly from APD Drawing 259955A-P.

Seals

The Rulon seals were fabricated as thin cylinders. The seals were designed to have a slight interference fit with the end-caps. This shrink fit along with lips on the end cap locked the seal in place without the need for adhesives.

Couplings

The top of the first stage displacer piston is directly connected to the gas spring piston and the LVDT by means of a stainless steel shaft. The LVDT shaft is threaded directly into the first stage displacer assembly. The first stage displacer is connected to the second stage displacer by a Delrin coupler. A similar coupler is used to connect the second stage to the third stage as shown in Figure 28. Two roll pins, 90° apart, are driven through a holes in the coupler and end-cap. These couplers are flexible and compensate for slight misalignments between the displacers.

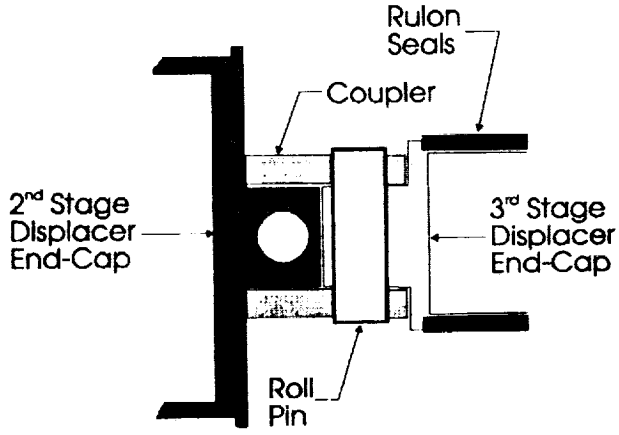

Figure 28. Coupler for second and third stage displacers.

4.2.2 Cylinder Assembly

The cylinders are thin walled 304 stainless steel tubes to minimize the axial conduction losses. Wall thickness is established by machining limitatations and exceeds that needed for a working pressure of 2.0 MPa. Each cylinder had ports to let the working fluid in and out. The second and third stage cylinders were welded together. The first stage cylinder was connected to the second and third stage assembly by means of a clamp and indium gasket seal. This was done so that there is easy access to the flexure bearing located between the first and second stages.

4.2.3 Cold Flexure Bearing

A flexure bearing to center the displacers and provide some restoring force was designed by the same method used on the compressor flexure bearings as described in §4.1.5. The bearing was made from a thin sheet of BeCu and had three radial spirals cut on it. The bearing was placed between the first and second stages to minimize the thermal and void volume penalties.

4.2.4 Regenerators

The Stirling cryocooler used three external regenerators to reduce the reciprocating mass of the displacer. The Stirling cycle is operated at a relatively high speed of 40 Hz to achieve a high efficiency. This also requires the regenerators be designed for high speed operation. The higher temperatures of the first two regenerators allowed conventional construction with fine stainless steel wire and lead shot. The cold regenerator, spanning 8 - 16 K, used a novel gap design to achieve acceptable results at high speeds. The basic parameters for the regenerators, such as length, diameter, and matrix size, were determined by the computer program.

Uniform distribution of flow is important in all the regenerator designs. This is accomplished by flow inlet headers in the bases of the regenerators as shown in Figure 29. Concentric slots are cut into the base plate with chamfered tops to promote flow distribution. The inlet/outlet tubing then intersects each of these rings.

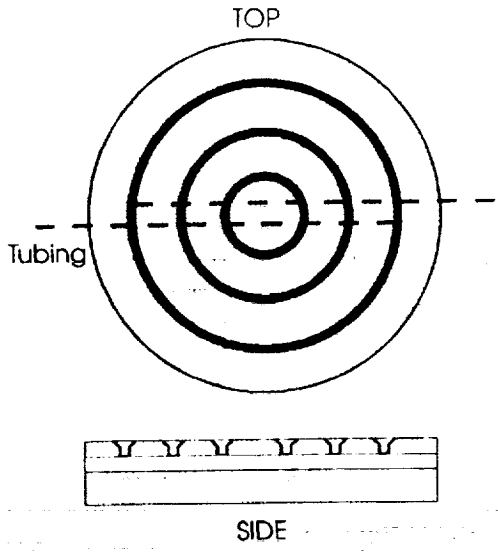

Figure 29. Typical flow distribution header.

The flow is further distributed by a sintered metal plate. This is a 316 stainless steel matrix of a random distribution of 10 μm holes. The plates are 0.031" (0.79 mm) thick and are sized to fit in their respective regenerators. Each regenerator has the generic configuration shown in Figure 30.

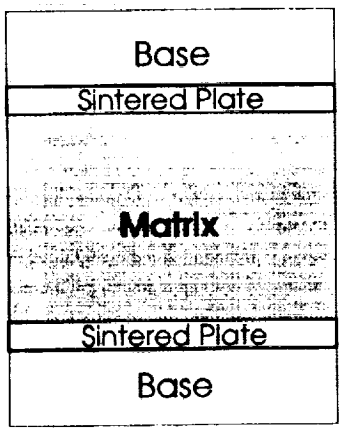

Figure 30. Typical regenerator construction.

First Stage Regenerator

The first stage regenerator spans the temperature region from 300 K to 60 K, and has the highest flow rates through it. It is important to minimize the pressure drop through the regenerator to minimize P-V and seal leakage losses. The pressure drop is reduced by designing the regenerator with a large diameter to length ratio, 31.5/19.5. The regenerator is tightly packed with the finest stainless steel wire available. The screen is stainless steel 400 X 400 wires per inch mesh with a wire diameter of 0.001".

Second Stage Regenerator

The second stage regenerator spans the temperature region from 60 to 16 K. This regenerator is filled with the finest lead shot available. The 16 grams of shot ranged in size from 0.001" to 0.0025" and is composed of 99.99% Pb. The second and third stage regenerators are designed as an integral unit to minimize the void volume and flow distribution losses in the system. The bottom of the second stage regenerator is also the top of the third stage regenerator.

Third Stage Regenerator

The third stage regenerator spans the temperature range of 16 - 8 K. Efficient heat transfer with low pressure drop and void volume losses at 40 Hz in this temperature region is extremely difficult using spherical materials. A parallel plate heat exchanger design was chosen because it offers the best ratio of heat transfer to pressure drop and can be built with the lowest void volume fraction, about 15%. The plates are made of a composite material chosen so as to have high radial heat storage and low axial heat conduction.

Gap geometry heat exchangers can be made using parallel plates, concentric cylinders or spiral rolls as shown in Figure 31. A parallel plate design was adopted because this geometry is the easiest to manufacture and get close tolerances between the plates.

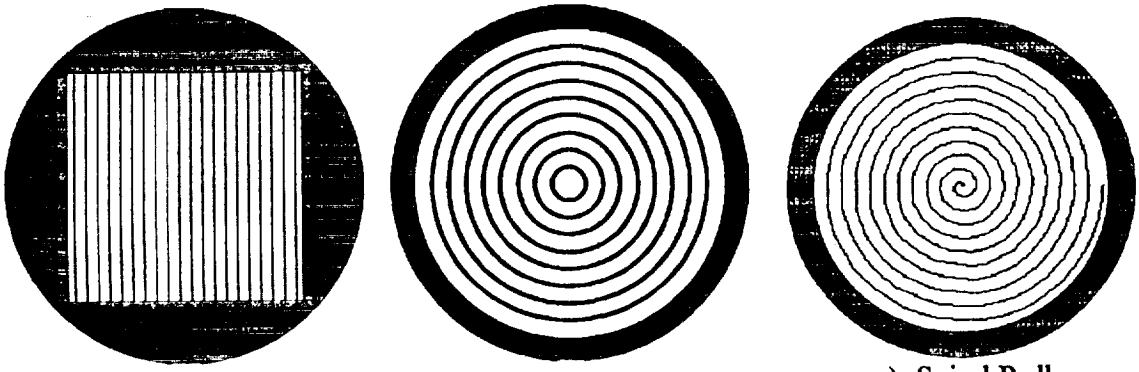

a.) Parallel Plates b.) Concentric Cylinders c.) Spiral Rolls

Figure 31. Schematic end views of gap regenerators.

The plates are made of a composite material to achieve the desired properties. The bulk material in the plate is lead which has a high thermal conductivity to conduct heat to the interior of the plate, and thus maximize heat storage relative to free volume. The lead is separated by thin layers of an insulating material to minimize axial conduction losses.

The final regenerator design is shown in Figure 32. The design of the regenerator considered the ease of manufacture of the plates and pressure vessel. The best shape for the pressure vessel is cylindrical. This would require all the plates to have different lengths

which drives up manufacturing costs. An insert was designed to adapt a cylindrical pressure vessel to a rectangular shape as shown below. The insert is made of Macor, a machinable ceramic which is an excellent insulator.

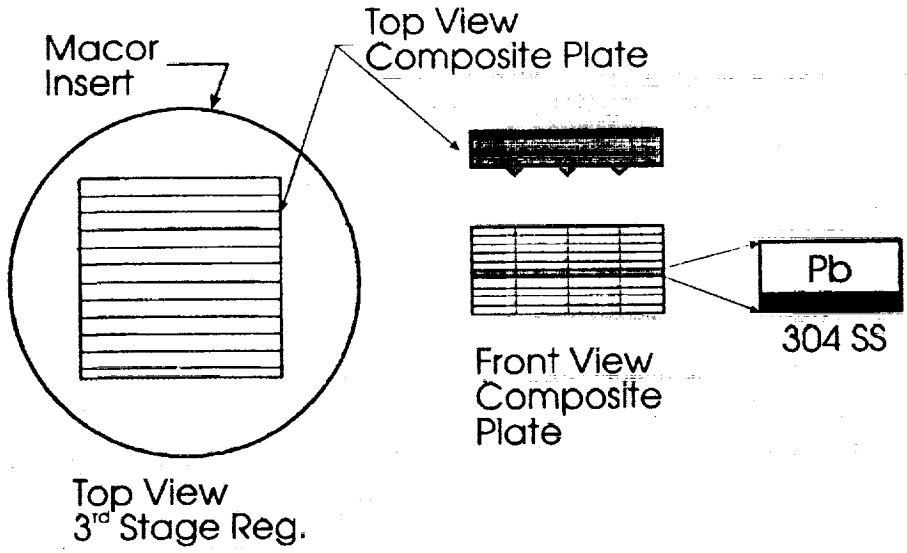

Figure 32. Schematic of third stage regenerator and composite plates.

The composite plates are EDM cut from a composite block. The small tips are greatly exaggerated so that they are visible in the drawing. These tips serve as the plate's spacers and are ~0.0002" (5 μm) high. The composite block is made from alternating layers of lead and stainless steel. The ratio of lead to stainless steel is approximately 9:1. The two materials must be bonded together prior to machining. Several different methods such as soldering and diffusion bonding were tried. It was not possible to achieve a satisfactory bond with the stainless steel, necessitating a change in materials. Additional insulating materials were investigated for their insulating properties at low temperatures and their ability to form a bond with lead. The final design uses a 50/50, lead / indium alloy.

4.2.5 Gas Spring Driver

The gas spring is used to control the motion of the displacer. The gas spring consists of a Rulon coated piston attached to the displacer assemblies inside of a specially designed housing. The expander should operate at a leading phase angle of 60° from the compressor. By adjusting the stiffness of the gas spring this angle can be changed to find the optimum phase relation. The stiffness is controlled by adjusting control volumes, V, on either side of the gas spring piston, see Figure 33. The needle valve provides variable dampening.

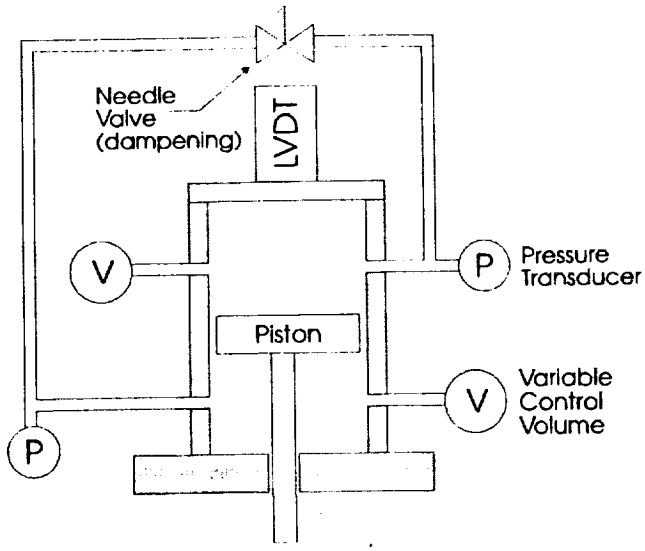

Figure 33. Schematic diagram of the expander gas spring.

4.2.6 Instrumentation

The instrumentation scheme for the expander is best seen on APD drawing number 259948D-P (see enclosed drawing package). The instrumentation measures displacement, pressure, and temperature along with heat input.

A Schaevitz LVDT was attached to the top of expander via a connecting rod to the gas spring piston. This allowed the displacement of the expander to be measured and the phase angle relative to the compressors to be calculated.

The expander requires a heater and a temperature sensor for each stage. The temperature sensors are Lakeshore silicon diodes, and the heaters are manganin wire resistance heaters wrapped around a conductive heat station.

The pressure is measured at the first stage displacer to monitor both the pressure drop across the first stage regenerator and the phase relationship to the compressor output.

Additional instrumentation could be added to study the pressure drop across other components, and temperature differences throughout the system.

4.3 Compressor Test Station

The Phase 2 plan of work called for the compressors to be built one at time, with the first unit tested before the second unit is built. This requires a test station for use with the compressors. A pulse tube refrigerator was designed for testing the compressors. The pulse tube has a variable volume so that it can be used with a single compressor and with dual compressors.

The test housing for the pulse tube was designed such that it would also work with the expander. A complete description of the test housing is found in §4.4.1.

4.3.1 Compressor Power Supply

The power source used to drive the compressors must have an adjustable voltage and frequency. The voltage is adjusted to control the stroke of the compressor, and the frequency is adjusted to find the resonant frequency of the unit. The output of the power supply must be sinusoidal, with a frequency range of 40 $\pm$ 10 Hz, a voltage range of 60 $\pm$ 20 V RMS, and a minimum power of 1000 W. An important requirement is that the voltage and frequency must be independently adjustable. This requirement eliminates many less expensive solutions.

A variety of potential power sources were considered. A DC power supply and a wave generator could be combined to give the desired results. But to achieve the necessary power drives the cost of the option up. Solid-state micro-processor controlled power supplies would work but were eliminated because of cost. A motor-generator set was also considered and eliminated due to expense. Finally, a frequency converter from Abacus Controls was chosen because it would produce the desired power at an affordable price. The frequency converter/power supply produces 2000 VA over a frequency range of 29 - 60 Hz, and a voltage of 27 - 90 V.

The power supply is attached to the compressor by a heavy duty wire cable. There is a military style plug on the compressor end. There is also a current sensor located at this end. The other end of the cable is attached to the power supply. The green wire is the ground, and the black and white wires are the $\pm$ power wires.

4.3.2 Test Volume, (Pulse Tube)

A pulse tube was designed for use as a test volume for the compressors. Program "SPT-1" listed in Appendix E was used to size the pulse tube. The design incorporates control valves to shift the phase of the flow. The design in shown in Figure 34. The test volume has needle valves and check valves between the pulse tube cavity and surge volume to explore the consequences of shifting the phase of the gas flow.

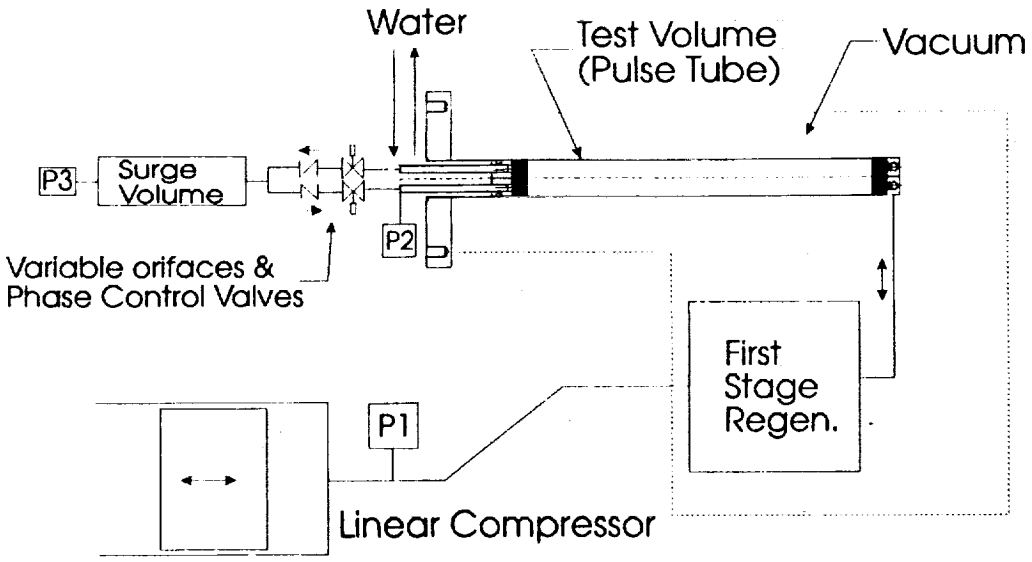

Figure 34. Compressor test volume (pulse tube).

4.3.3 Data Acquisition System and Software

The instrumentation devices used on the compressor and expander were all selected and designed to work with a data acquisition system. Two IEEE 488 analog/digital conversion (ADC) boxes were used to read the data signals from the instrumentation. One of the boxes used sample-and-hold technology so that 8 channels were read simultaneously. This technique was used with rapidly fluctuating quantities such as current, voltage, displacement and output pressure, to insure that these readings were exactly in phase. The remaining channels were read sequentially, and could be a maximum of 3° out of phase.

The output from the ADC boxes was transferred to a personal computer were it was recorded. The whole process was controlled with a simple basic program that stored the data as comma separated values in a file. This file was then opened with a spreadsheet program and the data analysis was performed.

4.4 Expander Test Cryostat

4.4.1 Test Housing

A vacuum housing was designed to hold the expander or pulse tube, the regenerator, and instrumentation. A cryopump is used to maintain the vacuum required for insulating the pulse tube. To minimize duplication of equipment, the test cryostat was designed to be used for both the pulse tube and expander. The regenerator used with the pulse tube is the first stage regenerator for the expander. A simplified sketch of the test cryostat is shown below in Figure 35. The vacuum housing was designed in conjunction with the pulse tube and expander so that both refrigerators would fit in the cryostat.

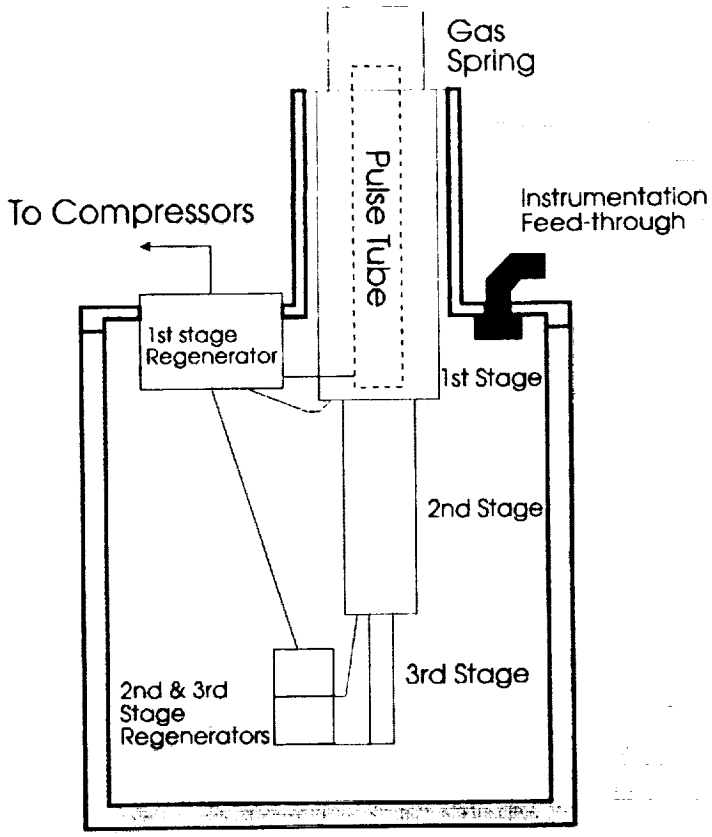

Figure 35. Schematic view of the test cryostat.

4.4.2 Instrumentation

The test cryostat was designed so that the instrumentation connections could be easily made through a 19 pin hermetic receptacle in the housing. An additional pressure tap was added to measure the gas pressure of the expander first stage. The cryopump station used to evacuate the test housing contained its own valving and pressure measurement devices.

4.4.3 Cooling

Additional cooling was added to the first stage regenerator line, and the top cap of the regenerator. This was to remove the heat of compression from gas flowing in the connecting line from the compressor.

5.0 Fabrication

The fabrication of the compressor components was begun while the expander was being designed. Then as the compressor was assembled the expander parts were manufactured. The expander was to be assembled during the compressor test phase.

5.1 Compressor

To control the alignment of the compressor, many of the parts had tight tolerances and numerous critical dimensions. This increased the complexity of getting the parts made. Most of the compressor parts were sourced from different outside vendors to obtain competitive costs. This caused some delays in assembly because of coordination problems with arrival of mating pieces and difficulties with rejected parts.

5.1.1 #1 Unit

Motor Assembly

The linear motor was made by Field Effects, and consisted of the spool / laminate assembly, magnet carrier assembly, and coil form assembly (259365D-P, 259355D-P, 259366D-P). They were late in beginning manufacture of the parts, and encountered many difficulties in their fabrication. Since the motor elements were the pacing items of the entire compressor assembly this contributed significantly to the overall delay of the project.

Field Effects realized late that they did not have the capability to machine the inside diameter of the coil form assembly to the proper dimensions. This step is critical, because the inside diameter must be exact. If it is too small, the magnet carrier will contact the coil form, and if it is too big the wall of the coil form will be pierced and the windings compromised. Field Effects shipped the unfinished parts to APD for final machining. APD then found a vendor with the skill required to successfully complete this task, but it added to the delay in assembly.

Assembly

Some assembly work was able to be done prior to the arrival of the motor parts. The compressor cylinder assembly (259516B-P), gas spring cylinder assembly (259520B-P), compressor motor housing assembly. (259503C-P), and gas spring volume / LVDT assembly (259410C-P) were assembled for both compressors.

Once the motor parts arrived the assembly procedure could be continued. At this point only the #1 unit was assembled. The compressor flange assembly (259497C-P) was made by attaching the spool / laminate assembly to the compressor flange.

The compressor shaft / magnet carrier assembly (259557C-P) was made by shrinking the magnet carrier onto the compressor shaft. Great care was taken with the magnet carrier, as the magnets were very powerful and would attract tools and debris.

The compressor motor housing sub-assembly (259499C-P) was made by inserting the coil form assembly into the motor housing. The inside of the motor housing had a light coating of epoxy to insure good thermal contact. The coil form assembly was press fit into the motor housing using special fixtures.

The compressor motor and shaft installation (259574D-P) was made by inserting the shaft / magnet assembly into the motor housing. A special fixture was used to control this operation. The insertion of the magnet into the motor housing completed the magnetic circuit developing very strong forces. A fixture was used to control the insertion to avoid damage to the internal components.

The remainder of the compressor assembly followed a detailed assembly procedure (270413A-P). This procedure describes the step by step assembly of the remaining components with emphasis on pinning and shimming requirements to achieve the required alignments. The flexure bearings are installed and pinned in place. The compressor and gas spring cylinders are installed and then shimmed into proper position.

Pressure Failure

The NASA Linear Compressor consists of three main sections, the gas spring end, the motor mid-section, and the compression end. A simplified schematic is shown in Figure 36. There are seven bolted pressure boundaries (1 - 7). The discharge of the compressor goes directly to the pulse tube / expander.

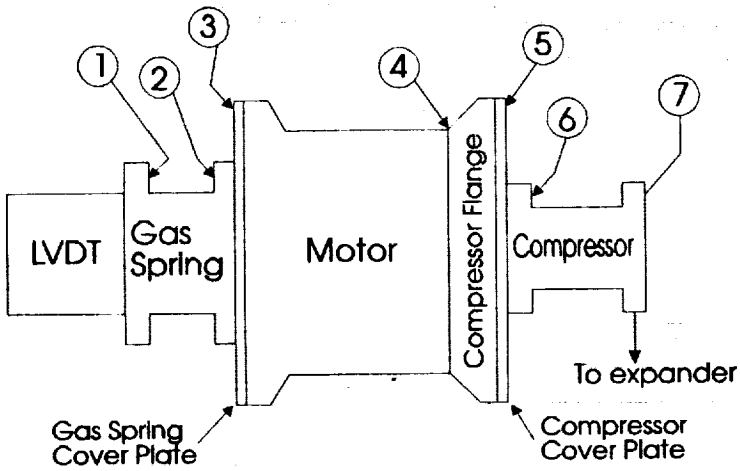

Figure 36. Schematic of the linear compressor pressure boundaries.

While calibrating the pressure transducers at a system pressure of 285 psig (1.96 MPa), There was a failure at the #5 joint which released gas at a rate that caused the coil form to be deformed and bent the drive shaft.

The dimples in the coil form would interfere with the motion of the magnet carrier. The magnets could not be machined because it would reduce motor efficiency. So the dimples in the coil form assembly were removed by carefully honing the coil form. This honing process completely removed the inner wall of the coil form, which completely exposed the windings. During this operation a short to ground occurred in the windings. Several very intricate machining operations were performed in order to remove the short and save the coil form assembly. All the windings were coated with a layer of varnish and epoxy for protection.

Joint #5 was designed on the assumption that the pressure inside the system would not exceed 170 psig, and under these conditions the fasteners had a factor of safety of 2.

Redesign

The threaded fasteners on the two end cover plates (3 and 5) were redesigned. The number of fasteners was doubled to 16. The #10 SS cap screws have been replaced by 1/4" grade 8 alloy steel cap screws. The heli-coils have been replaced with a through-hole, and a nut.

The joint has a very conservative design, assuming a cyclic stress of 0 to 300 psig, and a maximum pressure of 300 psig. The necessary pre-load requires the cap screws to be torqued to 123 in-lbf. The joints now have a safety factor of 3 for fatigue and of 8 for static failure.

The material of the remaining fasteners was changed from 18-8 SS to grade 8 alloy steel. The size and number remained the same.

The maximum rated pressure of the system is 300 psig. A relief valve set at 240 psig is located between the charging connection and the compressor.

5.1.2 #2 Unit

Motor

After the coil form assembly had been inserted into the motor housing, it was found that the coil form assembly had a short to ground. This was unacceptable and an attempt was made to repair the coil form. A slot was cut through the motor housing to expose the wires and find the short. This did not work, the coil form was removed from the housing, and the slot in the housing was repaired. A new coil form assembly was ordered from Field Effects.

Field Effects modified the coil form design because some features required the wire to bend too much. When the new coil form assembly arrived, it was also found to have a short to ground. A fourth coil form assembly was ordered from Field Effects. Further modifications were made to the coil form. An underlying design problem is that the dimensions of the coil form require bending the wire in some locations to a tighter bend radii than the wire manufacturer recommends. The wire is of square copper cross section and has a thin poly-amide coating for insulation. This coating is easily scratched and electrical shorts are possible. To prevent shorts due to small cracks or scratches in the coating, an insulating tape was used on the fourth assembly. Kapton, a 2 mil thick insulating tape was used to wrap the coil form in the areas where the wire contacted it, and especially in areas where the wire was bent. With these improvements the fourth coil form assembly was acceptable.

Assembly

The #2 unit was assembled similar to the #1 unit. There were some small dimples on the inner surface of the coil form assembly. These were removed without incident. No further difficulties were encountered in the assembly of the #2 unit.

5.2 Compressor Test Station

While the compressors were being assembled the compressor test station was fabricated. The pulse tube was fabricated, assembled, inserted into the test housing and connected to the first stage regenerator. These parts were relatively easy to machine and assemble. The power supply, instrumentation and data acquisition system were all collected, tested, and debugged.

5.3 Expander

The expander components were even more difficult to make than the compressor components due to their small size, close tolerances and precise fits. To have the greatest chance for success all the work was contracted to the best machine shop in the area, ARC Manufacturing. A series of meetings took place between ARC Manufacturing and APD Cryogenics to settle all the details of fabrication. This cooperative arrangement worked very well and the expander was completed on-time.

5.3.1 Displacers

The end caps and cylinders were machined by ARC Manufacturing, and shipped to APD Cryogenics for assembly. Centering points were left on end caps for future operations. A welding fixture was made and practice welds were done on similarly sized material until a satisfactory weld was achieved. The shell was then lightly packed with glass wool, and the end caps were welded in place.

The Rulon seals were heated with a hot air gun, and slipped over the retaining lip on the end-caps. Once the seals had cooled they were firmly in place. The displacers were then shipped back to ARC Manufacturing for final machining. The end caps were final machined and the length of the displacers carefully measured. This measurement was used to get the proper length of the matching cylinder. The Rulon seals were honed to achieve the proper sliding fit with the cylinders.

The couplings to connect the displacers were machined from Delrin. The placement of the holes for the dowel pins was determined from measurements of the distance between the displacers. The second hole was drilled to maintain a distance of .197/.198" between the displacers.

5.3.2 Cylinder Assembly

The three cylinders were machined by ARC and welded by APD. The cylinders had the necessary tubing for the gas inlet/out welded in place. The second and third stage cylinders were welded together, paying particular attention to keeping the alignment straight.

5.3.3 Regenerators

First Stage

The components for the first stage regenerator were fabricated and assembled. The first stage regenerator is firmly packed with stainless steel wire screens. It is fully assembled and has been used with the pulse tube to test the compressors.

Second Stage

The components for the second stage regenerator have been fabricated. The regenerator has not been assembled.

Third Stage

The parts for the third stage regenerator have been fabricated. The regenerator has not been assembled. The housing and base plate were easily machined. The Macor insert, used to adapt a cylinder for rectangular plates, was also easily manufactured.

The laminated plates to form the regenerator matrix were a major challenge to fabricate. Before the regenerator plates could be cut, a composite block of material had to be bonded together. This block was originally made by alternating 0.018" layers of lead with 0.002" layers of stainless steel. The lead has a high thermal conductivity to transport the heat to the interior of the plate. The stainless steel has a very low thermal conductivity and it is used to minimize the axial heat conduction. The problem encountered with this combination of materials was getting an effective bond between the lead and the stainless

steel. Stainless steel forms a thin layer of chromium oxide which is difficult to completely remove, and will not allow bonding with other materials. Though a flux would remove the oxide, it was not possible to use one because of the difficulty of the residual flux escaping from between the layers during bonding. Brazing of the materials was attempted in a standard oven, an oven with small vacuum drawn, an oven with an inert atmosphere, and a hydrogen furnace. Different combinations of time, temperature and fixturing were tried without success.

A new material was selected as the insulating layer. A 50/50 alloy of lead/indium was selected because its thermal conductivity was similar to that of stainless steel at low temperatures, and since it was a lead alloy it should bond with the lead. Oxide layers remained a problem. A special cleaning solution was used, before assembling the stack of thin sheets, to remove the oxides. The brazing was done in the hydrogen furnace, since the hydrogen gas acts as a flux to further inhibit the growth of oxides. Several attempts yielded a successful block of material from which the plates could be cut. The composite block was then sent to a wire EDM machine shop to cut the individual regenerator plates.

5.3.4 Gas Spring

The components for the gas spring have been fabricated. The gas spring was assembled to check for clearances and proper fits. The retainer seal and bumpers have been final machined to obtain the proper fits as described in 259949B-P. The control volumes have been assembled and attached to the gas spring housing along with the necessary plumbing.

5.3.5 Final Status

All the components for the compressor have been fabricated. The expander assembly (259949B-P) was assembled to check for fits. All parts fit together satisfactorily. The unit was left assembled for shipment purposes only. Prior to use the unit should be completely disassembled, thoroughly cleaned, and then reassembled.

The first stage regenerator was fabricated, assembled and used with the compressor test volume. All the components for the second and third stage regenerators have been fabricated, but not assembled.

6.0 Test

6.1 Compressor

The #1 unit was tested by itself while the second compressor was being built. Then both units were run together. All test results were using the pulse tube.

6.1.1 Test Set Up

During the test of the single compressor, a mounting system was devised to minimize the vibrations. The unit was suspended in the air by cables during operation. Since it was running singly and not as an opposed pair there were some vibrations. When both units were run as a pair they were mounted on a vibration damping pad which in turn rested on a wooden base on a workbench. As a pair they produced very little vibration. The compressors were somewhat noisy during operation. This is believed to be due to the flexure bearings touching each other because they are arranged in opposition. If this is the case, the problem can be corrected by orienting all of the spirals in the same direction or increasing the thickness of the spacers between the springs. Having the spirals all oriented in the same direction will result in the piston rotating as it reciprocates, but conceptually it should not effect its concentricity. Calculations show that the spring stiffness does not change significantly.

6.1.2 Instrumentation

The appropriate instrumentation described in previous sections was used in the compressor tests.

6.1.3 Data Acquisition Program

A basic computer program was used to collect the readings using a data acquisition system.

6.2 Single Compressor

The main focus of the single compressor tests was to measure the compressor stroke, and adjust the length of the stroke and its centering. During this phase, the #1 unit was run for approximately 105 minutes.

The gas spring was adjusted in and out to see the effect on compressor operation. As the gas spring is made stiffer the stroke gets shorter, and as it is made less stiff the stroke gets longer.

The best results occurred with the gas spring in its softest position and these were as follows: 60 Volts, 16.3 Amps, 978 W, 40 Hz, 0.63" (16 mm) stroke, minimum pulse tube temperature of 230° K. The stroke is only 75% of the intended design stroke.

6.3 Dual Compressor

The tests with the dual compressors were much more extensive. The focus of this testing was to achieve the design stroke and obtain an understanding of the system operation. The compressors were connected to the test station and pressure measurements taken as shown in Figure 37

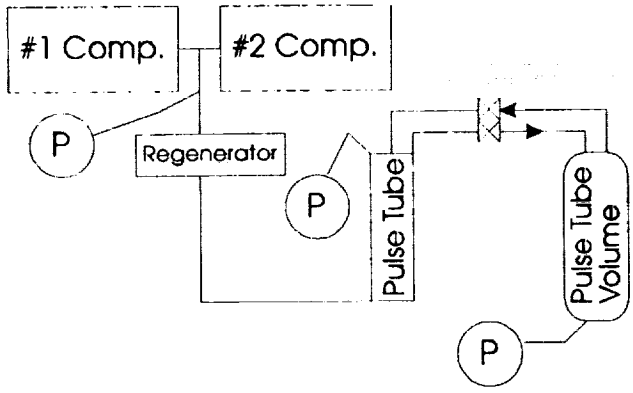

Figure 37. Schematic of dual compressor test set up.

The following series of figures show typical data obtained from the compressor operation. Figure 38 is a voltage and current diagram for an input of 50 V RMS at 40 Hz. The general shape of the curves are as predicted. The compressor currents are not quite identical and are slightly out of phase. Figure 39 shows the stroke of the compressors. Again it is seen that the compressors are slightly out of phase and that the #2 unit draws less current and has a shorter stroke. Figure 40 is a P - V diagram and its general shape is as anticipated. Figure 41 is the compressor outlet pressure, pulse tube pressure and pulse tube volume pressure. Figures 42 and 43 show the effect of closing the pulse tube valves. This results in the pulse tube acting as a gas spring and causes a slight increase in the P - V diagram. The effectiveness of the pulse tube is severely diminished with the lowest temperature in this configuration being only 190° K. Figures 44, 45, 46, and 47 show the effect of throttling the inlet and outlet valves of the pulse tube volume. In both cases, the pulse tube temperature rises and the P - V diagram slightly increases. Thus it was found that the most effective setting of the pulse tube valves was full open.

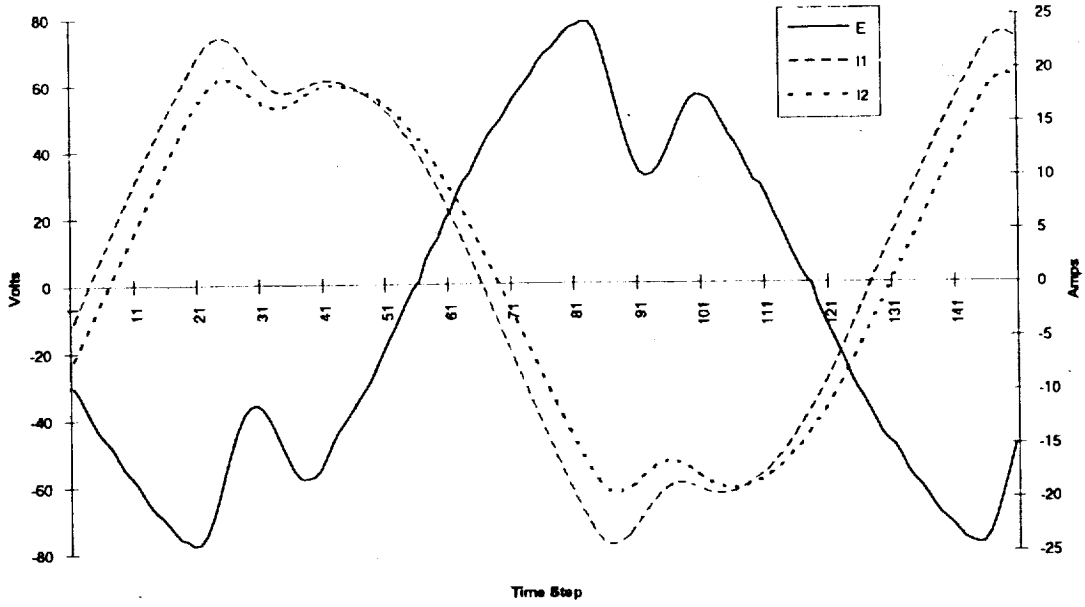

Figure 38. Voltage and current diagram versus cycle time. The input conditions were 50 Volts RMS at 40 Hz and these conditions were maintained for Figures 38 - 47. Total power of 1527 Watts. Pulse tube valves open.

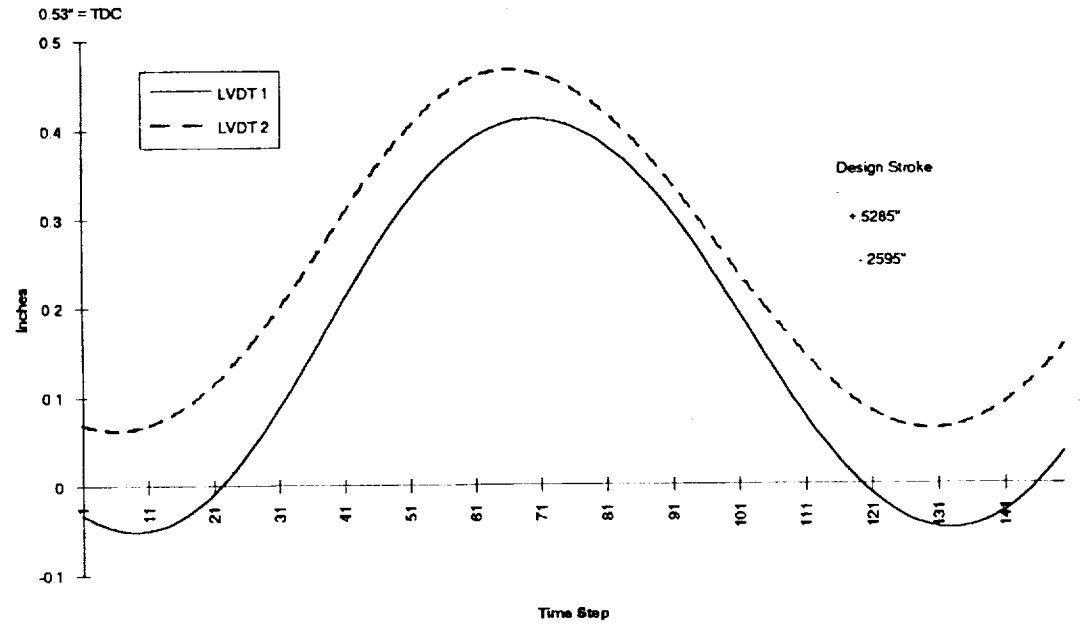

Figure 39. Compressor stroke versus cycle time for the same conditions as Figure 38. Average stroke of the compressors is 0.433", and the compression ratio is 2.12.

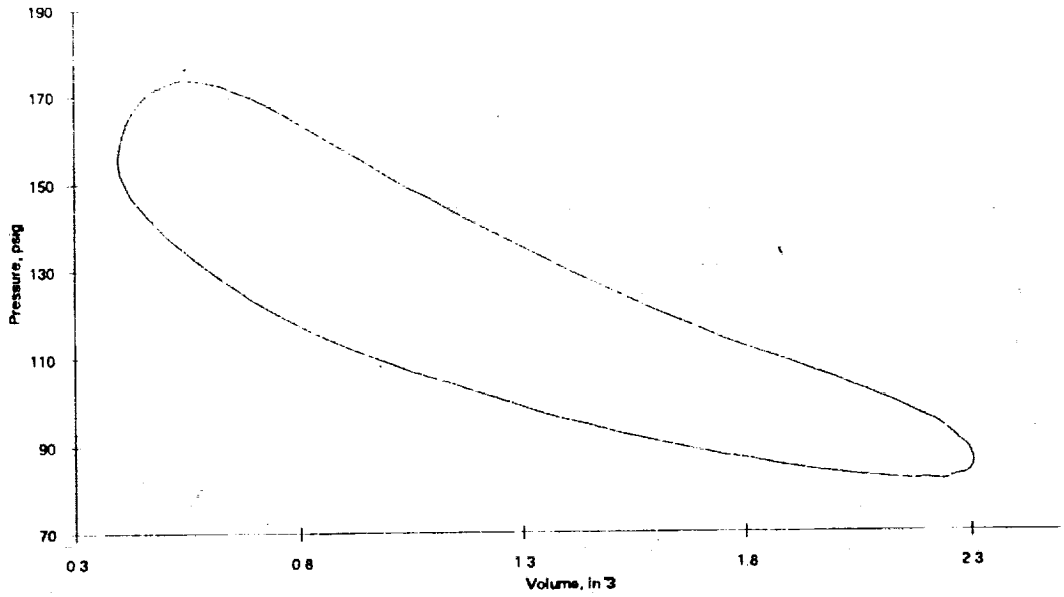

Figure 40. P-V diagram for the same conditions as of Figure 38.

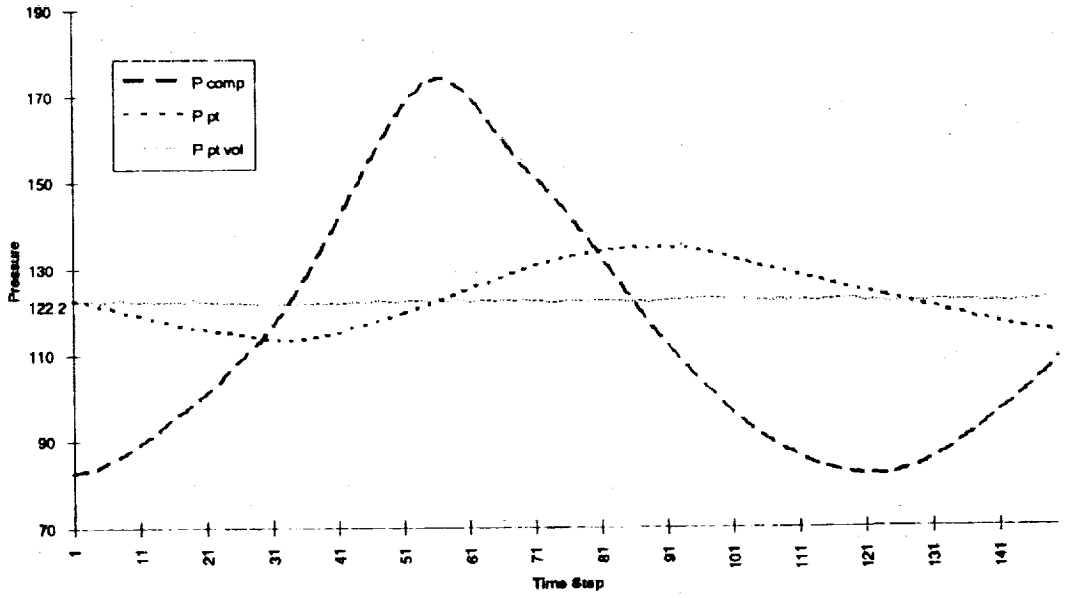

Figure 41. Pressure diagram for the same conditions as of Figure 38.

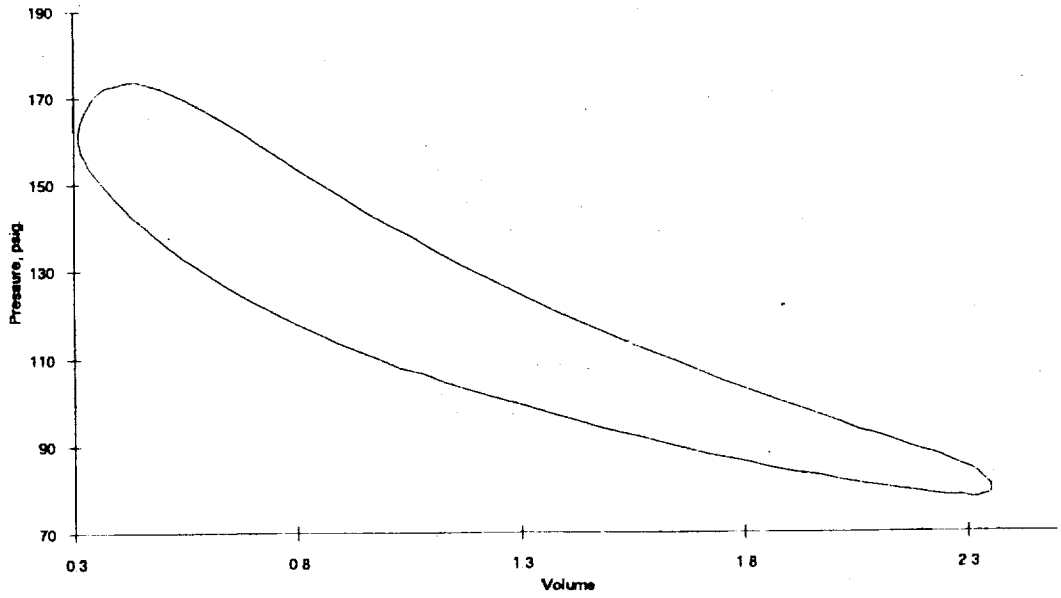

Figure 42. P-V diagram with the pulse tube valves closed.

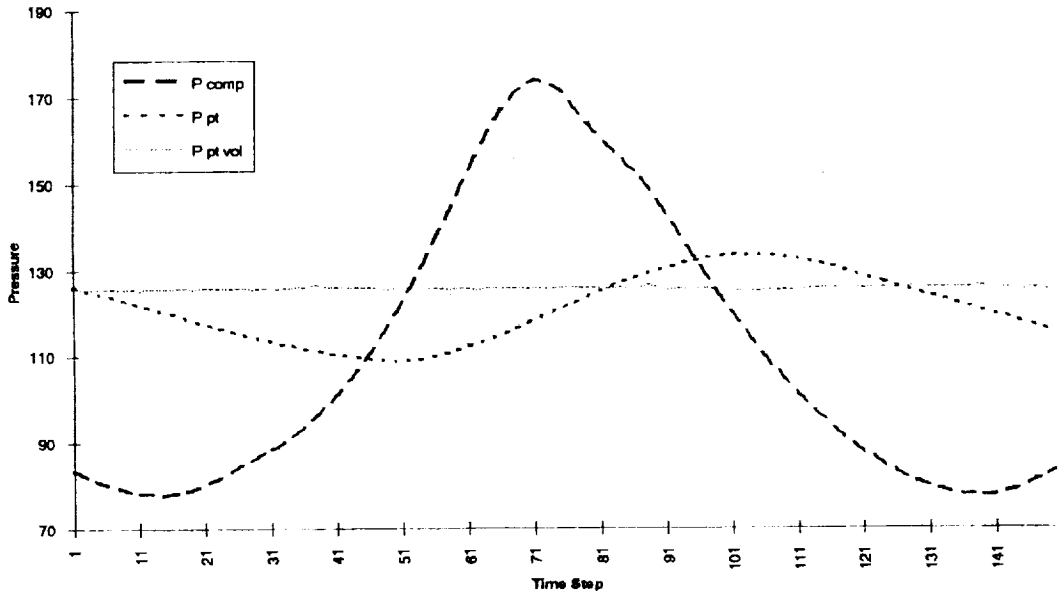

Figure 43. Pressure diagram with pulse tube valves closed.

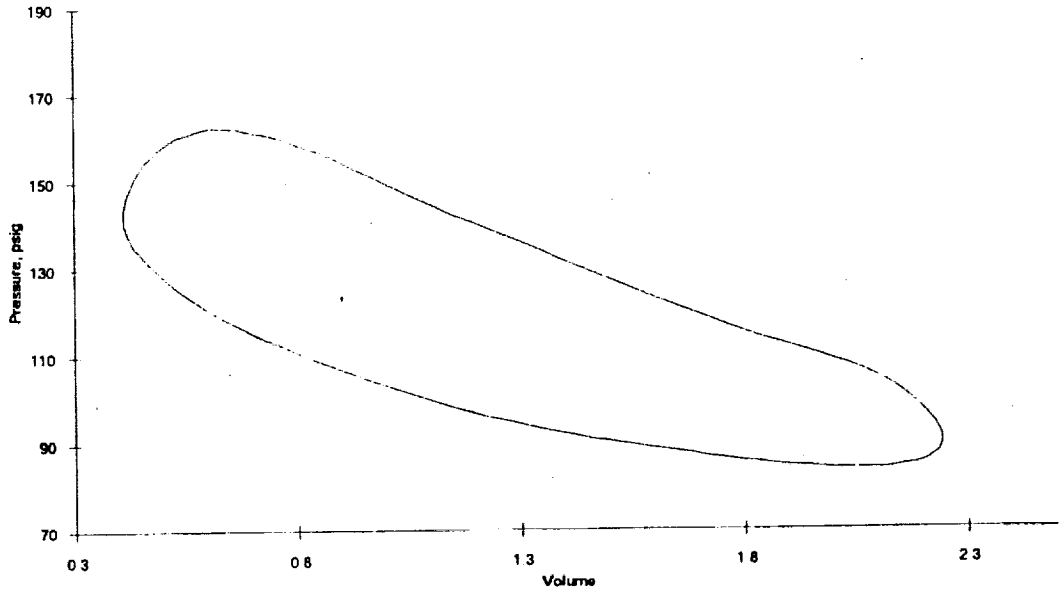

Figure 44. P-V diagram versus cycle time. The pulse tube volume outlet valve was throttled until the pulse tube temperature began to rise. The inlet valve was fully open.

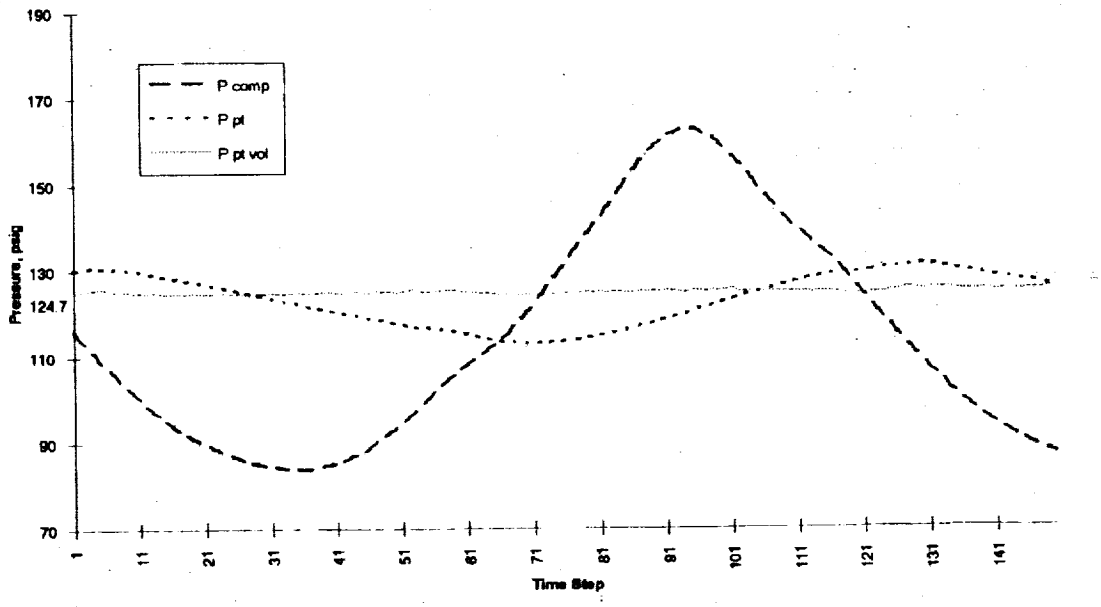

Figure 45. Pressure diagram for the same conditions as of Figure 44.

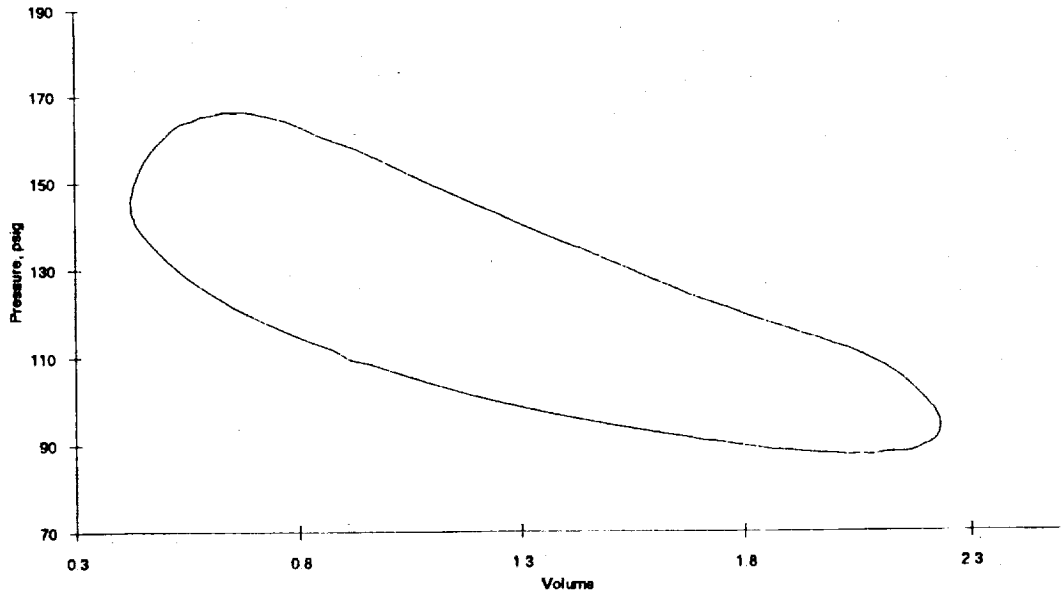

Figure 46. P-V diagram versus cycle time. The pulse tube volume inlet valve was throttled until the pulse tube temperature began to rise. The outlet valve was fully open.

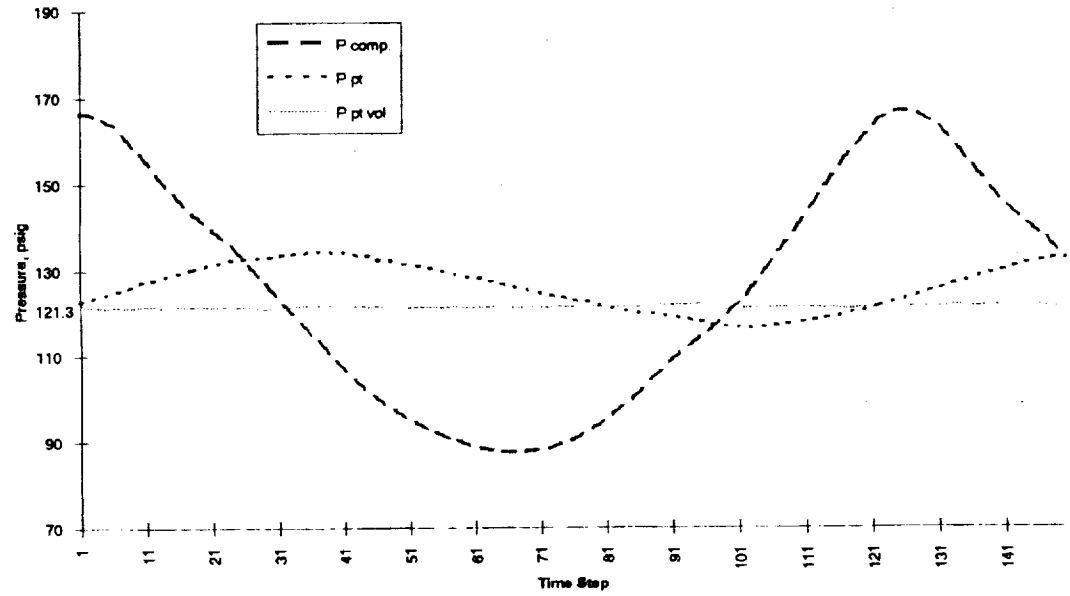

Figure 47. Pressure diagram for the same conditions as Figure 46.

Testing of the dual compressors continued with some slight modifications to the test set up. The pulse tube control valves appeared to be ineffective. Therefore, they were changed from needle valves to globe valves. In an attempt to equalize the stroke and power draw of the two compressors an equalization line between the two compressor's gas springs was added. This brought the strokes in phase, as shown in Figure 48. Figure

49 shows similar structure of the P - V diagrams for the two gas springs. Figure 50 shows the instantaneous power of the two compressors along with the numerically integrated average power.

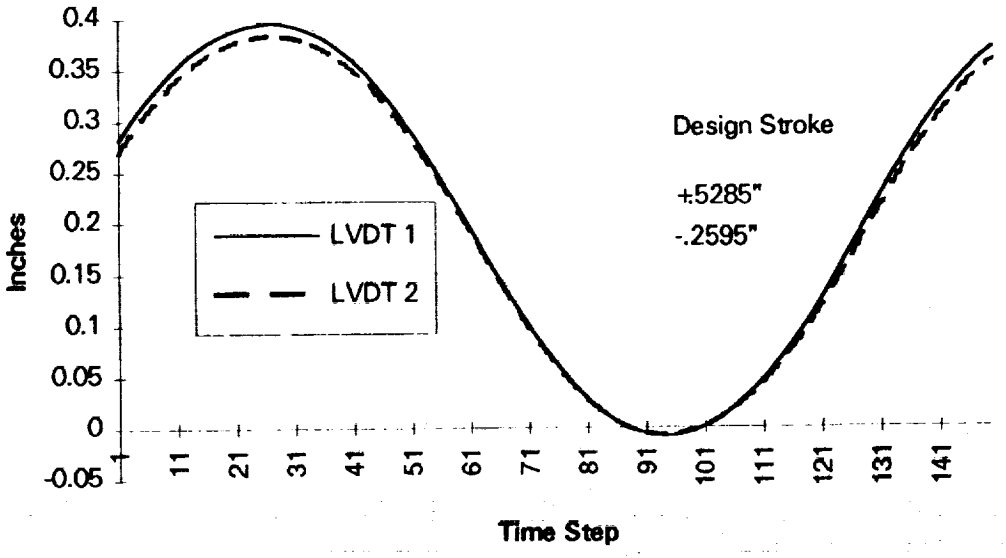

Figure 48. Compressor position versus time.

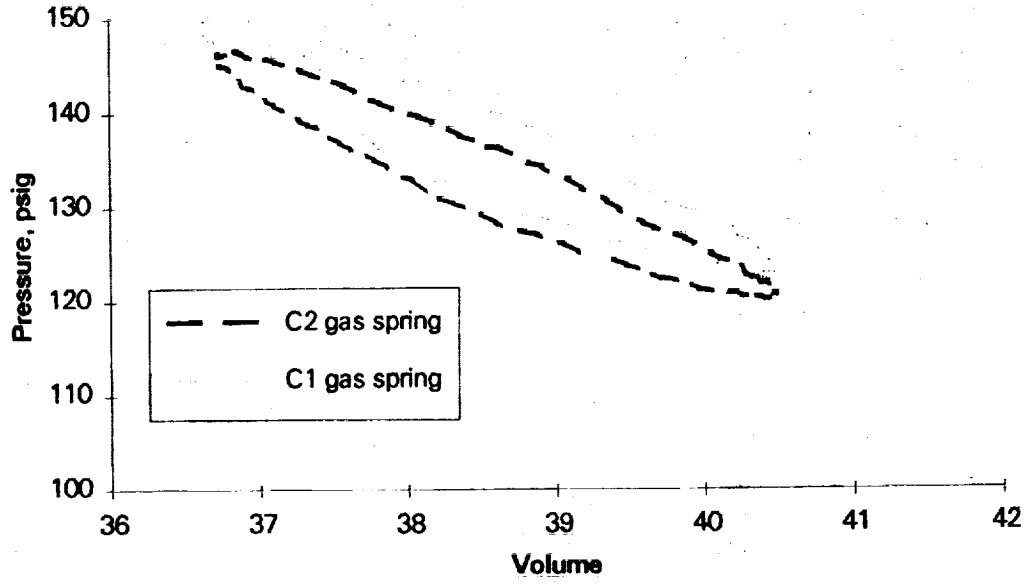

Figure 49. P - V diagram for the compressor gas springs.

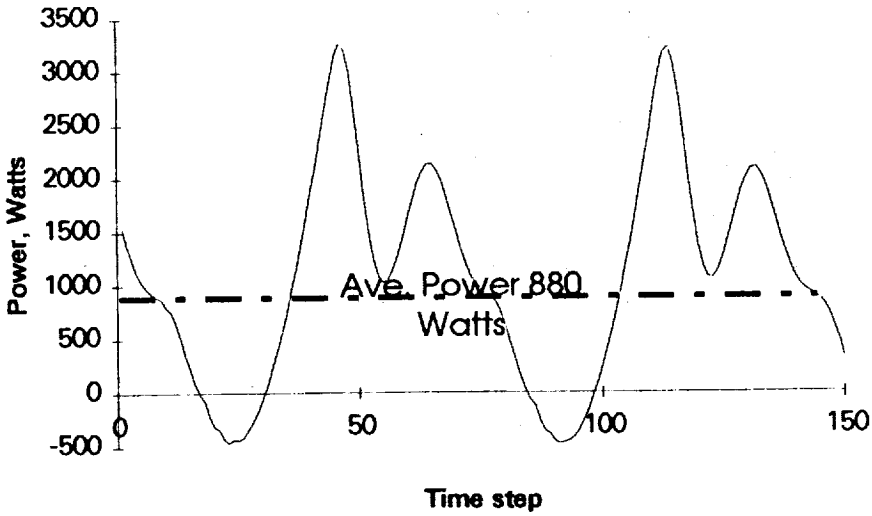

Figure 50. Instantaneous compressor power versus time.

The average power of 880 Watts is considerably less than the peak power demand. These three figures are typical results, and are from a test run at 48 Volts, 36 Hz, 130 psig (0.9 MPa) charge pressure and a stroke of 0.397" (10 mm). During this test, the lowest pulse tube temperature of 103.9 K was achieved. These results concluded the running tests of the dual compressors. The run time on the units at the end of these tests was #1 unit 605 minutes and #2 unit 550 minutes.

To further understand the compressor operation, static tests were conducted on each compressor, measuring the force versus the displacement. Figures 51 and 52 show the results for each of the compressors. Zero on the x-axis represents the geometric center of the compressor.

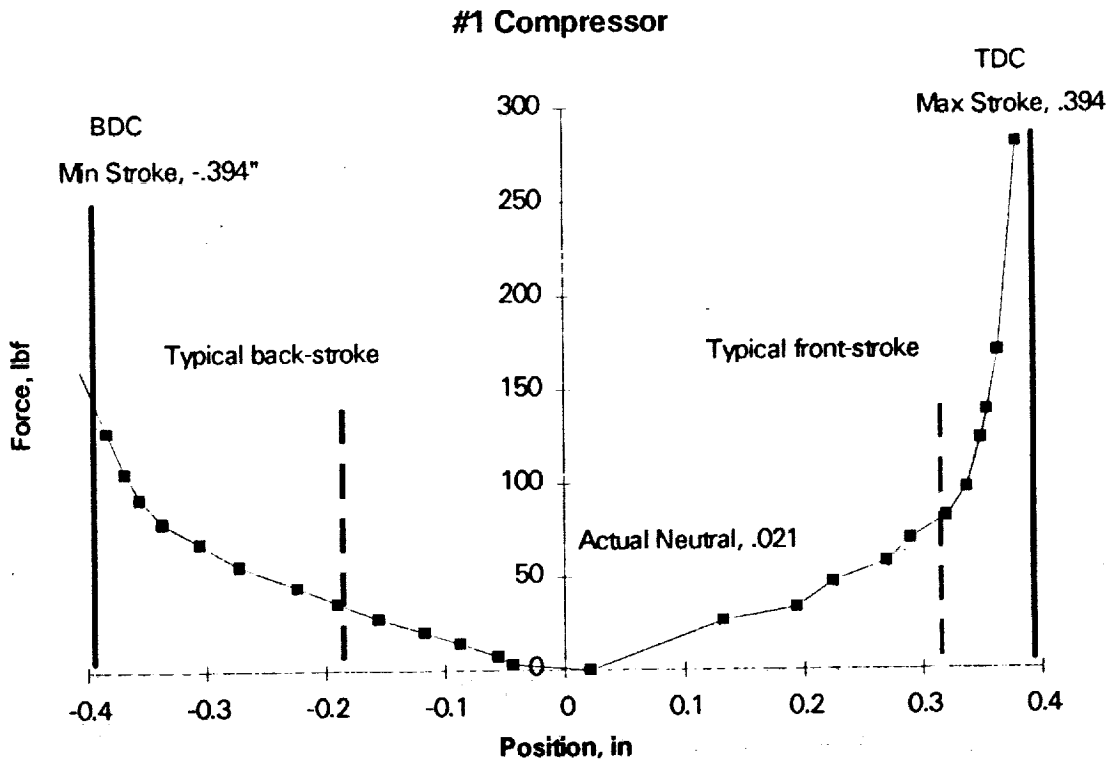

Figure 51. Force versus position for the #1 Compressor.

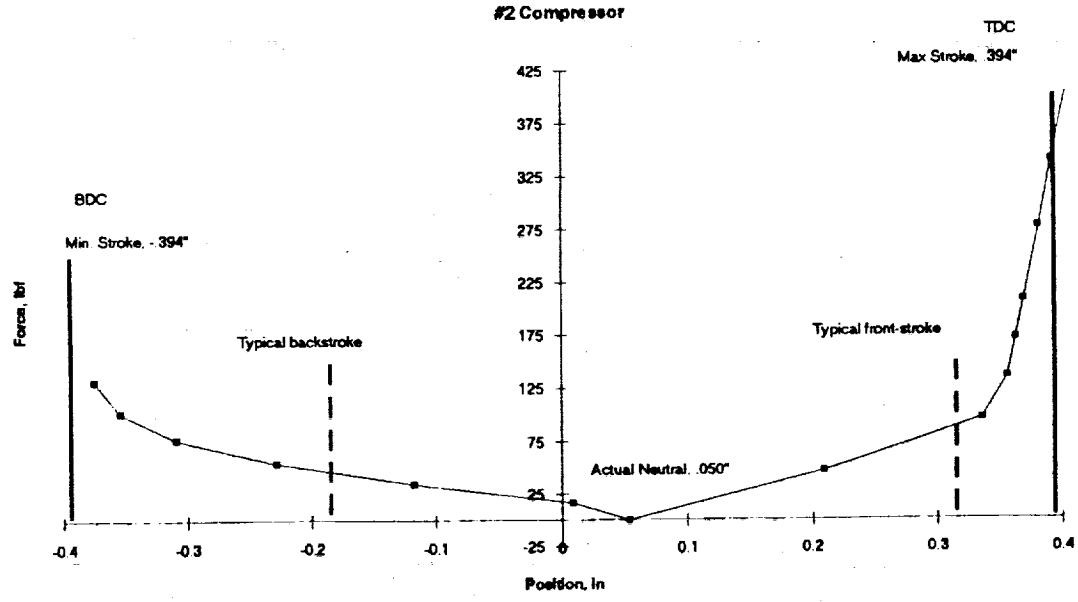

Figure 52. Force versus position for the #2 Compressor.

These two figures clearly illustrate the problems in realizing the full design stroke of the compressors. The stroke is asymmetric about the neutral position, with the forward stroke being the longest. The force needed to displace the compressor should be linear over the range of travel. However, near the end of the stroke the force increases rapidly becoming highly non-linear. This is inherent in the design of the magnet carrier and coil form, and will limit the full stroke to ± .330" (8.38 mm). A possible reason for this non-linear force is the magnetic design of the motor. At either end of the stroke the magnets line up exactly with the edge of the last winding. This forces all the lines of flux through a very small area, thereby increasing the force needed at the ends of the design stroke. The gas spring is the other possible cause of the short stroke.

Figures 53 and 54 show the clearance seal leak rate as a function of the pressure drop across the seal. The leak rate should be a linear function of the pressure drop. At very low pressures this is true, but will become non-linear at higher pressure due to gas compressibility, turbulence and loss effects. Assuming laminar, incompressible flow the momentum equation was solved to find the approximate size of the clearance seal gap, G.

$$G = \sqrt[3]{\frac{12\dot{V}\mu L}{\pi \Delta p D}}$$

where V is the volumetric leak rate, μ is the viscosity, L is the seal length, Δp is the pressure drop, and D is the cylinder diameter. The clearance seal gap was designed to be 0.0005". The #1 compressor's gaps are an order of magnitude larger than this, and the #2 compressor has gaps close to the design specifications.

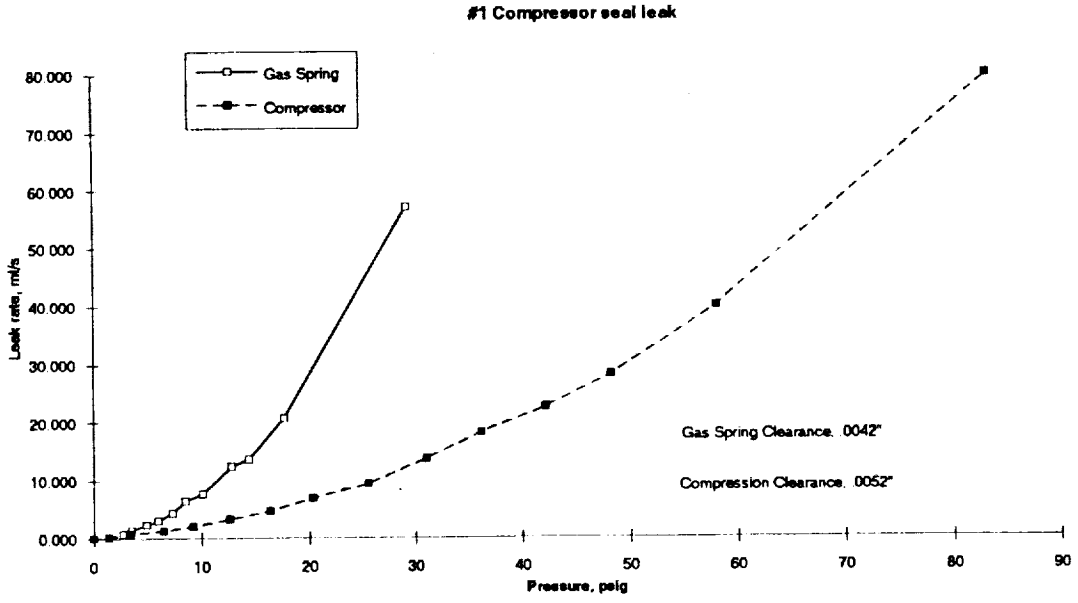

Figure 53. Compressor #1 clearance seal leakage.

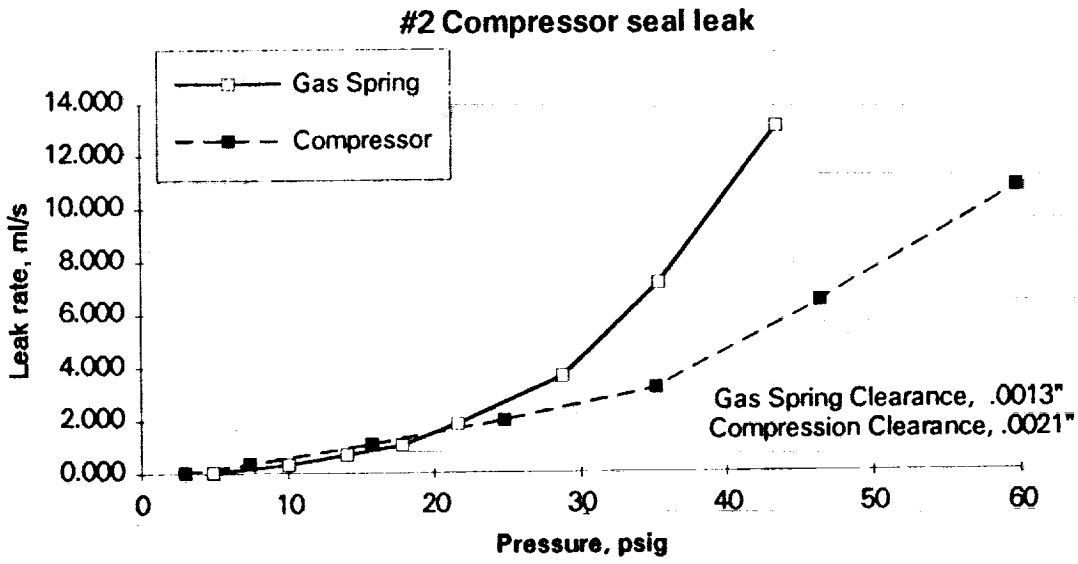

Figure 54. Compressor #2 clearance seal leakage.

A table listing a summary of all the dual compressor test data is in Appendix F.

7.0 Conclusions and Recommendations

1. The design concepts incorporated in this three-stage Stirling cycle expander driven by a dual opposed piston linear drive compressor should lead to a long-life design suitable for space craft application.

2. Analytical studies predict good efficiency for the novel third-stage regenerator that enable refrigeration at 8 K to be produced in a Stirling cycle cryocooler operating at 40 Hz.

3. The manufacturing process that was developed for the cold regenerator seems to be viable.

4. Design studies predict that 1 W at 8 K plus 2 W at 16 K plus 10 W of cooling at 60 K can be produced with an input power of 900 W and a compressor / expander weight of 68 kg.

5. More work needs to be done on the flexure bearing design to distributed the stress more uniformly in order to reduce the reciprocating mass relative to the spring rate.

6. There is an advantage in having a high ratio of stored energy in the spring mass system relative to the work output in terms of efficiency and tolerance to changes in system pressure, but compressors with moving coils which are lighter than moving magnets can still have good efficiencies.

7. It is recommended that the next generation compressor use a reciprocating coil to reduce the reciprocating mass and eliminate the gas spring.

8. Further studies are recommended for the flexure bearing to get more uniform stress distribution to reduce the reciprocating mass.

9. The linear motor coils should be about 2 mm longer in order to get a full 20 mm stroke.

10. The basic design principles are sound and justify further development.

8.0 Appendices

8.1 Appendix A: Linear Motor Size

```
'   "LMC1" LINEAR MOTOR COMPRESSOR
LPRINT "    LMC1  11/18/88          RUN 01  08/06/90"
LPRINT
LPRINT "   F-Hz     S-mm   DSI-mm  DMI-mm  DCI-mm      YC     PH-MP     QG-W    DH-mm"
LPRINT "   B-T      D-mm   DSO-mm  DMO-mm  DCO-mm      NT     PL-MP     QT-W    LH-mm"
LPRINT "   NS       V-cc   TS-mm   LM-mm   LC-mm     I-A     EF-%      URM     URS"
LPRINT "  WM-kg    WC-kg   WI-kg   WS-kg   WH-kg   WT kg  WTT-kg      UR"
'    INITIALIZE DESIGN PARAMETERS
SP = 20: DP = 43.3: QG = 250 '                  Piston S,D-mm,Power-W
F = 40: UR = 3: PI = 3.1416 '                   Freq-Hz,Energy ratio
B = .5: Y1 = .75 '                              Field in gap-T,Leakage
DSO = 175: DSI = 25: NS = 8 '                   Spring Dia-mm,#
SSM = 45000: FS = 19000000 '                    Spring-psi,psi
SHM = 20000: TH = 15 '                          Housing-psi,mm
DMO = 75: DMI = 55: LM = 70: CM = .35 '         Magnet Dim-mm
YC = .85: NT = 200: RW = .00000173# '           Coil,frac,#T,OhmCm
PH = 1.5: PL = .7 '                             Press Max,Min-MPa
RM = 8.2: RC = 8.96: RI = 7.86: RS = 8.34 '     Density-g/cc
'    CALCULATE DEPENDENT PARAMETERS
DCI = DMO + 2 * CM: DCO = (DMO ^ 2 + (DMO ^ 2 - DMI ^ 2) * Y1 / .625) ^ .5
LC = LM + 2 * SP: VC = PI * (DCO ^ 2 - DCI ^ 2) * LC / 4
VM = PI * (DMO ^ 2 - DMI ^ 2) * LM: VP = PI * DP ^ 2 * SP / 4000
AI = B * PI * DMO * LM / (2 * Y1): VI = AI * 2 * LC
QGI = QG / F: LW = NT * LM * PI * (DCO + DCI) / (2 * LC)
IM = 2 * QGI / (PI * B * LW * SP) * 1000000
RWT = RW * PI * NT ^ 2 * (DCO + DCI) * 10 / ((DCO - DCI) * YC * LC)
QT = QG + RWT * IM ^ 2: EF = 100 * QG / QT
WC = VC * RC / 1000000: WM = VM * RM / 1000000
WI = VI * RI / 1000000: WI = WC + WM + WI
UG = (PH - PL) * PI * DP ^ 2 * SP / 32000
LS = PI * (DSO + DSI) / 2: TS = LS ^ 2 * SSM / (SP * 3 * FS)
A = PI * (DSO ^ 2 - DSI ^ 2) / (4 * LS)
VS = LS * A * TS: WS = RS * VS * NS / 1000000
FSM = SP * FS * A * TS ^ 3 * .00689 / LS ^ 3: US = FSM * SP * NS / 4000
URS = (UG + US) / QGI
DIO = (2 * AI / PI + DCO ^ 2) ^ .5
DHO = DIO * (1 + 1000 * PH / (6.89 * SHM)): LH = LC + 5 * SP
VH = PI * ((DHO ^ 2 - DCO ^ 2) * LH / 4) + (PI * DHO ^ 2 * TH / 2)
WH = VH * RI / 1000000: WT = WM + WC + WI + WS + WH
UM = WM * (PI * F * SP) ^ 2 / 2000000: URM = UM / QGI
WTT = WC + WI + WH + WS * (UR * QGI - UG) / US + (WM * UR * QGI / UM)

LPRINT
LPRINT USING "####.## "; F; SP; DSI; DMI; DCI; YC; PH; QG; DHO
LPRINT USING "####.## "; B; DP; DSO; DMO; DCO; NT; PL; QT; LH
LPRINT USING "####.## "; NS; VP; TS; LM; LC; IM; EF; URM; URS
LPRINT USING "####.## "; WM; WC; WI; WS; WH; WT; WTT; UR
LPRINT : PRINT : PRINT : PRINT : PRINT : PRINT
PRINT : PRINT : PRINT : PRINT : PRINT : PRINT
END
```

8.2 Appendix B: Compressor Dynamic Model

```
'*****************************************************************
'***  SCD3 Single Stage Stirling Cooler, Dynamic Model          ****
'***  Written by R. C. Longsworth, (HP87) 11/01/91              ****
'***  Adapted to Quick Basic by J. N. Pfahler 10/15/92          ****
'*****************************************************************
```

```
OPTION BASE 0
PRINT "NASA/SCD3 RUN ON "; DATE$; " AT "; TIME$: PRINT
'***  Dimension variables and format output ********************
DIM VC(75), Vd(75), vp(75), M1(75), E(75), P(75)
'***  Initialize Variable Parameters ***************************
Ta = 300: Dc = 43.5: Sc = 20: Sd = 9.8: Po = .81: Pm = 1.1: Pl = 10: Ph = 0
n = 40: Tl = 50: Dd = 19.8: Id = 100: Dr = 24.6: Lr = 21.5: Py = .67:
va = .2: vl = .25: Eo = 180: Mp = 3.8: Ks = 185: Nt = 234: LC = 110: LM = 70
DCo = 108.1: DCi = 99.1: Bg = .7: Yc = .78: PI = 3.14178: Dw = .025
'***  T-K, D,S,L-mm, P-MPa, Q-J, q-W, n-Hz, M-kg, K-N/mm, E-V **
'***  Calculate dependent parameters   ************************
Vcs = PI * Dc ^ 2 * Sc / 4: Ap = Vcs / Sc: kss = Ks / Ap: vm = PI * n * Sc
Vvc = va * Vcs: Vdl = PI * Dd ^ 2 * Sd / 4
Vr = PI * Dr ^ 2 * Lr * Py / 4
Tr = (Ta - Tl) / LOG(Ta / Tl): Vv = vl * Vdl
Vva = Vr * Ta / Tr + Vv * Ta / Tl: Vda = Vdl * Ta / Tl
DCm = (DCo + DCi) / 2: tc = (DCo - DCi) / 2
Lw = PI * DCm * Nt: Aw = LC * tc * Yc / Nt: Lwg = Lw * LM / LC: R = .00001724# * Lw / Aw
C2 = Bg * Lwg * .000001: C3 = Bg * Lwg / (1000 * R)
'***  Calculate Volumes, Pressure & Gas Mass vs. Time   ********
PRINT
PRINT "    N        P-Mpa        Vc-mm       vp-m/s      Fg-N     Fs-N     Fe-N"
C1 = Po * (Vcs * .7 + Vvc + Vva + Vda)
a = -5: b = 65: dt = -(a / (360 * n))
VC(0) = Vcs * (1 + COS((a - b) * PI / 180)) / 2: Vd(0) = Vdl * (1 + COS(a * PI / 180)) / 2
P(0) = C1 / (VC(0) + Vvc + Vva + Vd(0) * (Ta / Tl - 1) + Vdl)
vp(0) = vm * SIN((a - b) * PI / 180): W = 1
E(0) = Eo * SIN((a - b - 5) * PI / 180) / 2 - vp(0) * C2
M1(0) = P(0) * Vd(0) * .000484 / Tl
FOR i = 1 TO 4
  Qe = 0
  FOR j = 1 TO 72
    a = a + 5: Vd(j) = Vdl * (1 + COS(a * PI / 180)) / 2
    Er = Eo * SIN((a - b - 5) * PI / 180) / 2 - vp(j - 1) * C2
    Fi = Ap * (Pm - P(j - 1)) + kss * (VC(j - 1) - Vcs / 2) + Fr * C3
    vp(j) = vp(j - 1) + Fi * dt * 1000 / Mp
    VC(j) = VC(j - 1) - dt * Ap * (vp(j) + vp(j - 1)) / 2
    IF VC(j) > 1.1 * Vcs THEN VC(j) = 1.1 * Vcs: vp(j) = 0 ELSE
    IF VC(j) < 0 THEN VC(j) = 0: vp(j) = 0 ELSE
    P(j) = C1 / (VC(j) + Vvc + Vva + Vd(j) * (Ta / Tl - 1) + Vdl)
    Er = Eo * SIN((a - b) * PI / 180) / 2 - vp(j) * C2: E(j) = Er
    Fg = Ap * (Pm - P(j)): Fs = kss * (VC(j) - Vcs / 2): Fe = Er * C3: Ff = Fg + Fs + Fe
    vp(j) = vp(j - 1) + (Fi + Ff) * dt * 500 / Mp
    VC(j) = VC(j - 1) - dt * Ap * (vp(j) + vp(j - 1)) / 2
    IF VC(j) > 1.1 * Vcs THEN VC(j) = 1.1 * Vcs: vp(j) = 0 ELSE
    IF VC(j) < 0 THEN VC(j) = 0: vp(j) = 0 ELSE
    P(j) = C1 / (VC(j) + Vvc + Vva + Vd(j) * (Ta / Tl - 1) + Vdl): W = W - 1
    M1(j) = P(j) * Vd(j) * .000484 / Tl
    Qe = Qe + ABS(Er * dt * Eo * SIN((a - b) * PI / 180) / (2 * R))
    IF W = 0 THEN PRINT ; j; P(j); VC(j); vp(j) / 1000; Fg; Fs; Fe: W = 12
    NEXT j
  VC(0) = VC(72): P(0) = P(72): E(0) = E(72): vp(0) = vp(72)
NEXT i
'***  Remember to calculate PV work   *************************
Qc = 0: Ph = 0: Pl = 100: Qdl = 0: Qi = 0: Qf = 0
FOR m = 1 TO 72
  Pav = (P(m - 1) + P(m)) / 2
  Qc = Qc + Pav * (VC(m) - VC(m - 1)) / 1000
  Qdl = Qdl + Pav * (Vd(m) - Vd(m - 1)) / 1000
  Qi = Qi + E(m) ^ 2 * dt / R
  Qf = Qf + E(m) * C3 * (VC(m) - VC(m - 1)) * .001 / Ap
  IF P(m) > Ph THEN Ph = P(m)
  IF P(m) < Pl THEN Pl = P(m)
NEXT m
'***  Remember to calculate net refrigeration rates   *********
```

```
qcs = Qc * n: qdls = Qdl * n
Eft = ((Ta - Tl) * qdls / (Tl * qcs) * 100): Efe = (Qi / Qf * 100)
'**** Output ***********************************************
PRINT
PRINT "Ta K  Dc mm  Dd mm  Dr mm  Dw mm  Ph MP  qc W  Eft %  N hz Eo V  Mp g"
PRINT "Tl K  Sc mm  Sd mm  Lr mm  Pl %  Pl MP  qdl W Efe %  b    Qc/Qf Ks N/mm"
PRINT "Eo V  Dcomm  Dcimm  LC mm  LM mm  B T  Nt  Qe W  Yc % R  Qi W"
PRINT
PRINT Ta; Dc; Dd; Dr; Dw * 1000; Ph; qcs; Eft; n; Eo; Mp * 1000
PRINT Tl; Sc; Sd; Lr; Py * 100; Pl; qdls; Efe; b; Qc / Qf; Ks
PRINT Eo; DCo; DCi; LC; LM; Bg; Nt; Qe * n; Yc * 100; R; Qi * n
PRINT
PRINT "N  P Mpa  Vc mm  Vd mm  vp m/s  Ml g  Fr V"
FOR m = 1 TO 72 STEP 9
  PRINT ; m; P(m); VC(m); Vd(m); vp(m) / 1000; Ml(m); F(m)
NEXT m
PRINT
```

SCD Run #6 11/07/90 Eo=9C Uke=3.0 Us=3.0 Mp=5.94 kg
Ks=316 I^2R=7.7% 40 Hz

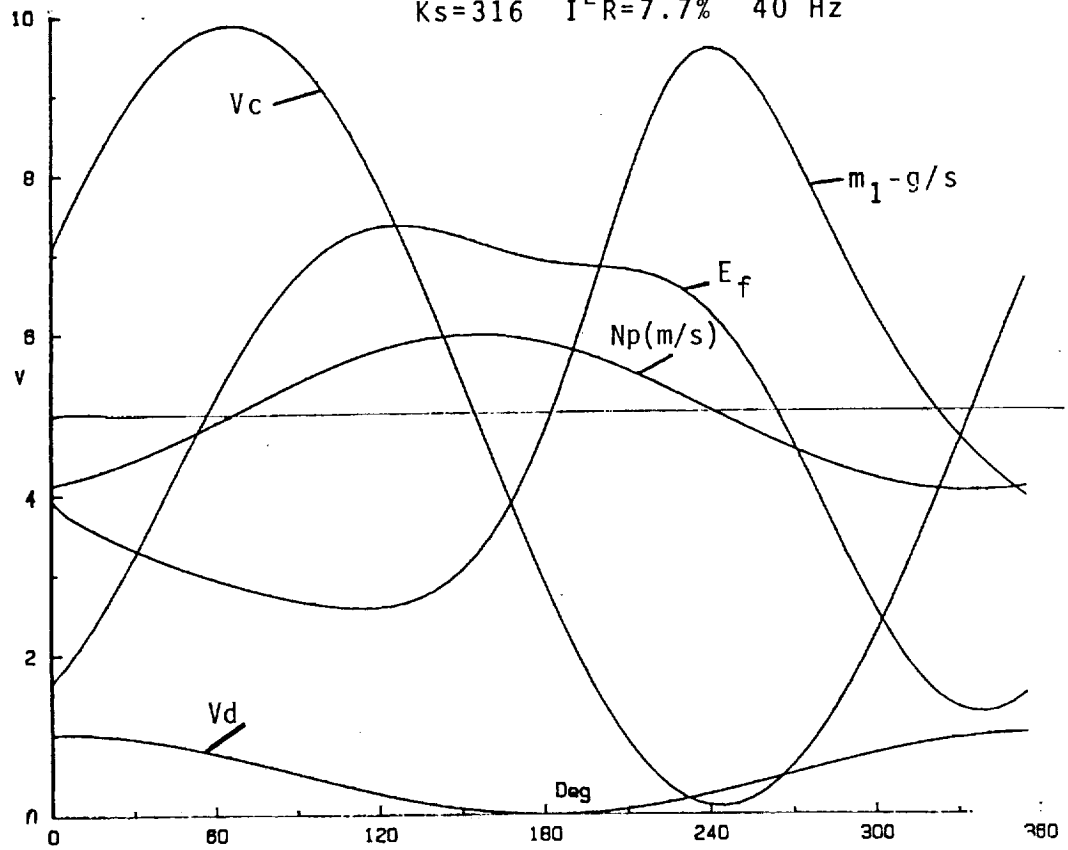

Run #6 11/07/90 n=40 Ur=3.0 Eo=90

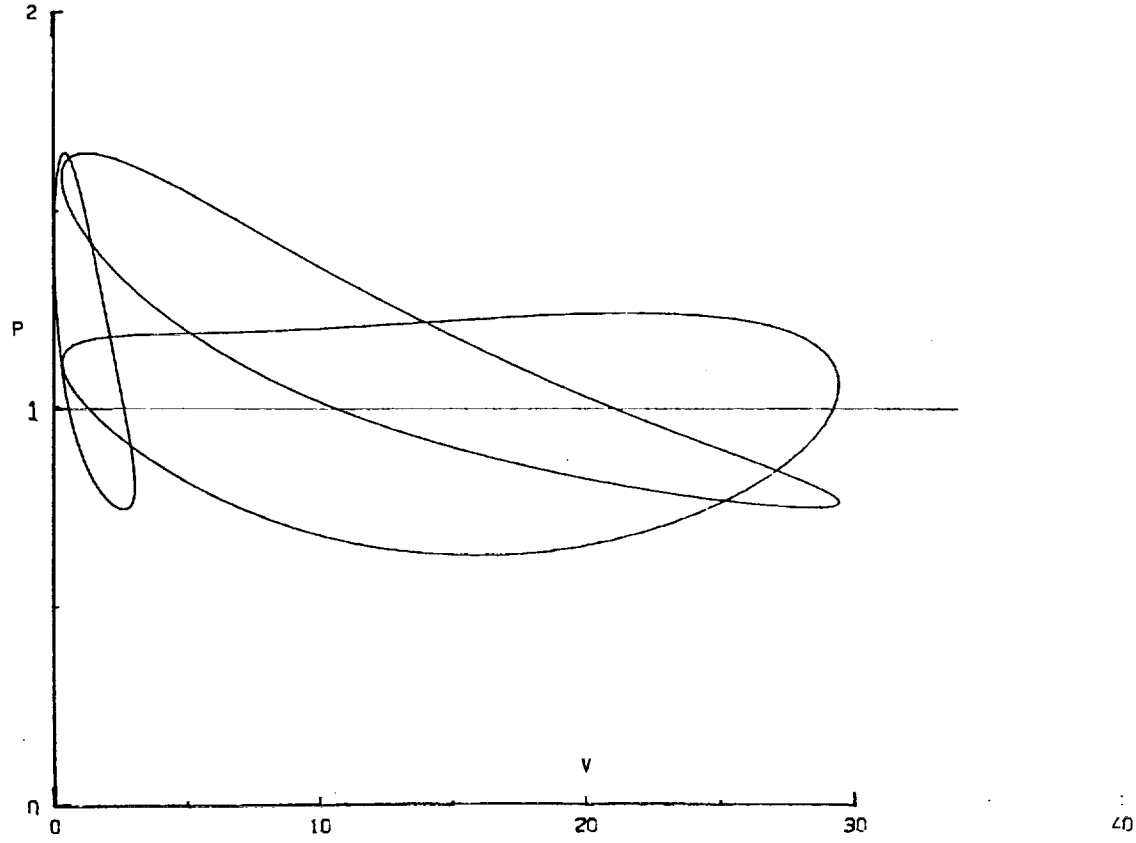

SCD Run #3 11/08/90 Eo=90 Uke=1.5 Us=1.2 Mp-2.97 kg
Ks=127 I^2R=8.5% 40 Hz

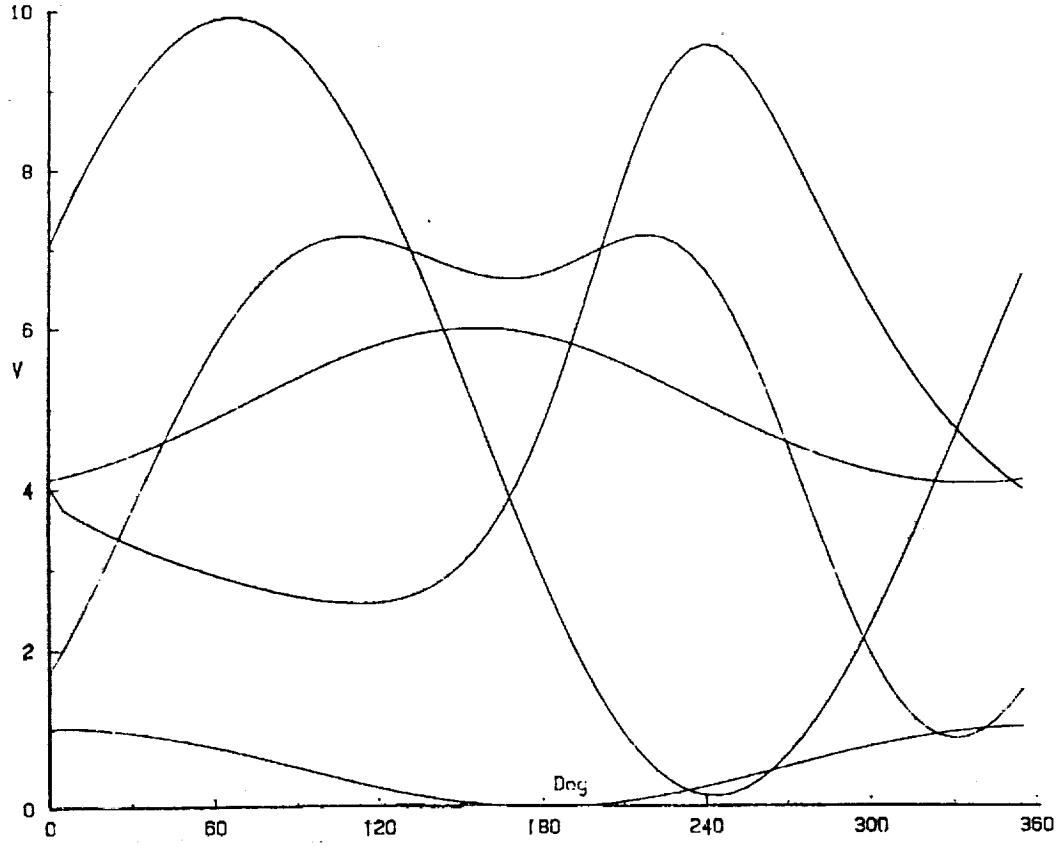

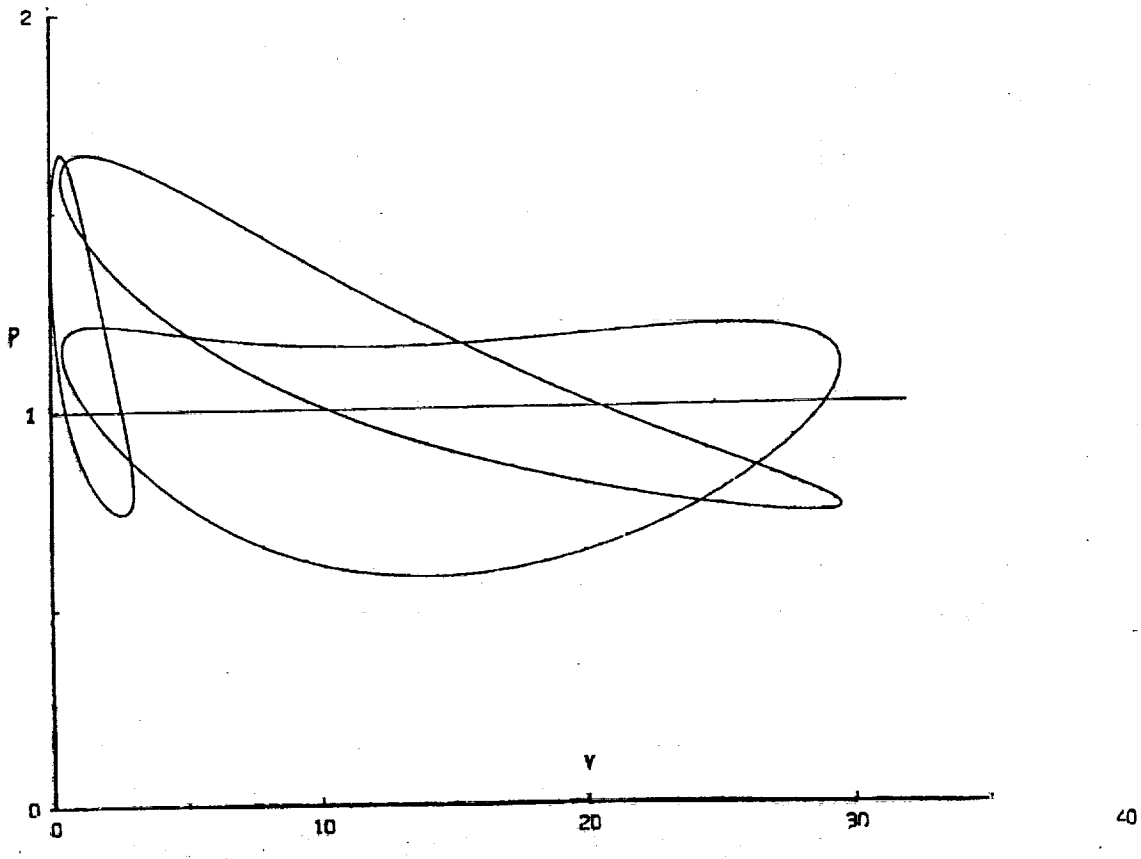

SCD Run #6 11/08/90 Eo-90 Uke=1.0 Us=.65 Mp=1.98 kg
Ks=67 I^2R=9.1 40 Hz

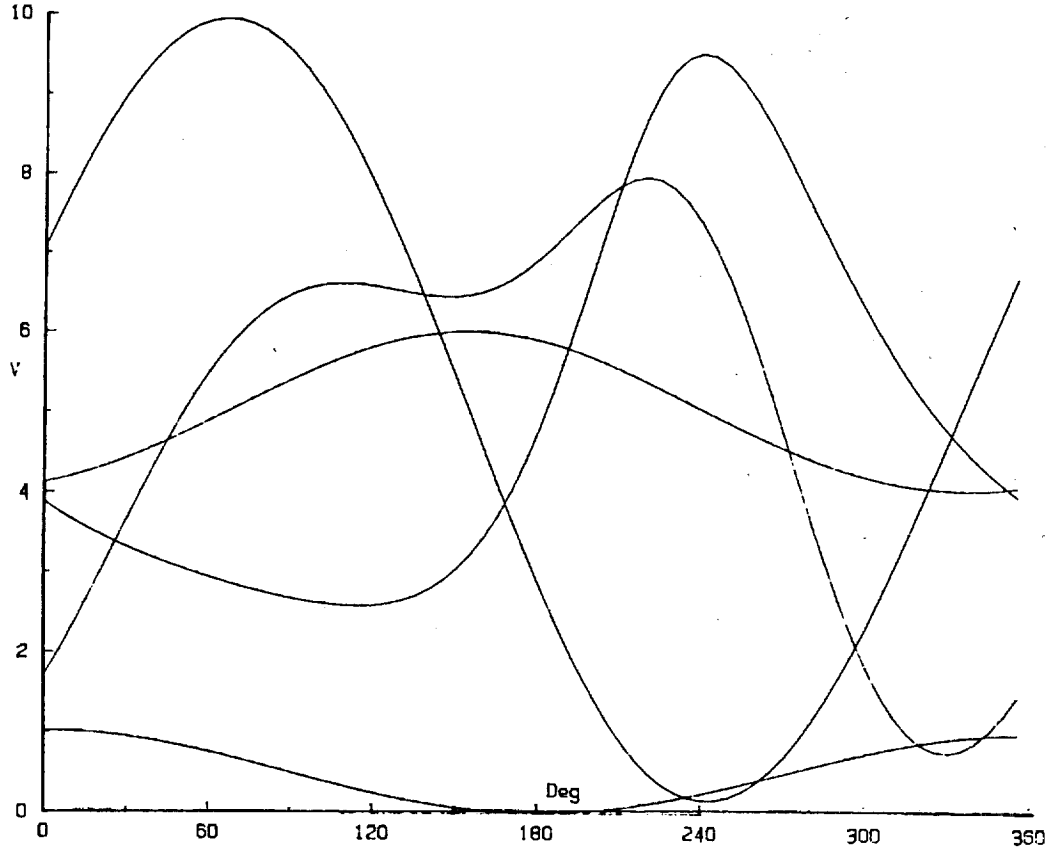

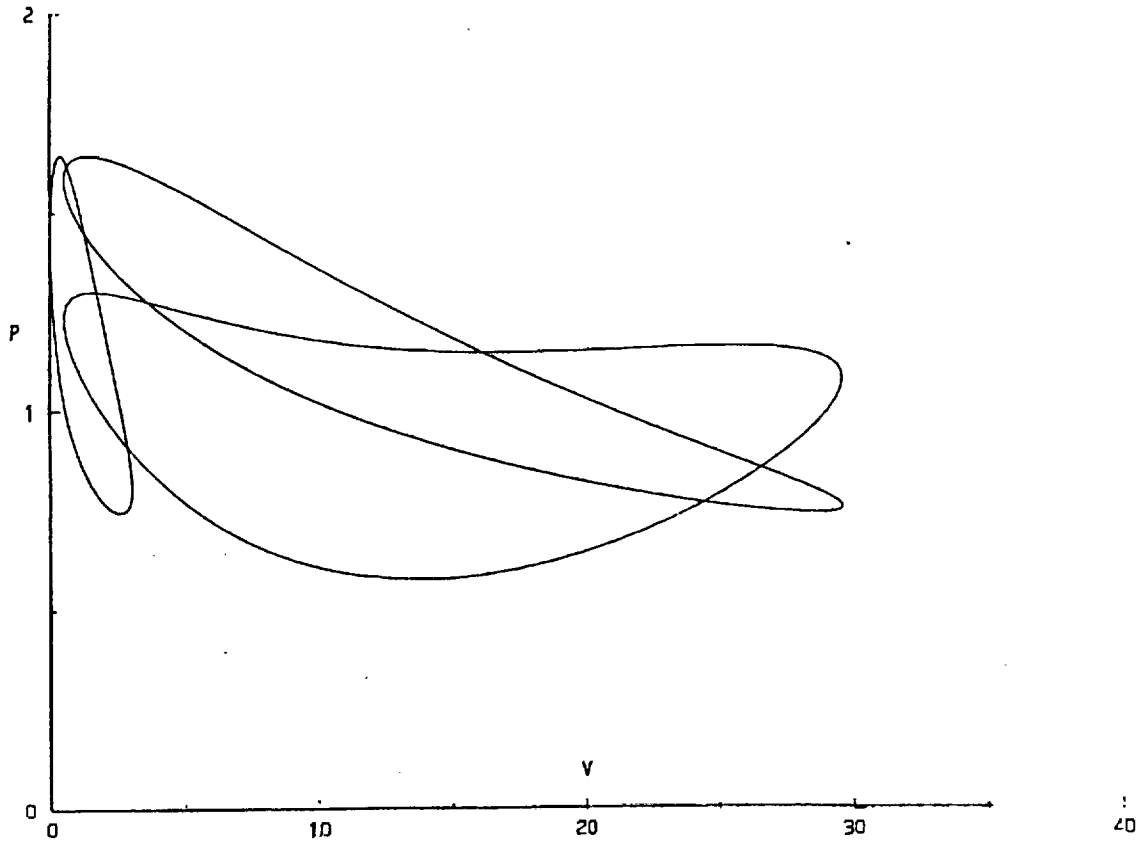

Run #11 11/08/90 Energy Ratio=.7 Mp=1.39 kg, Eo=90V
(Uke=.7), Us=.42 Ks=24 I^2R Loss=9.4%

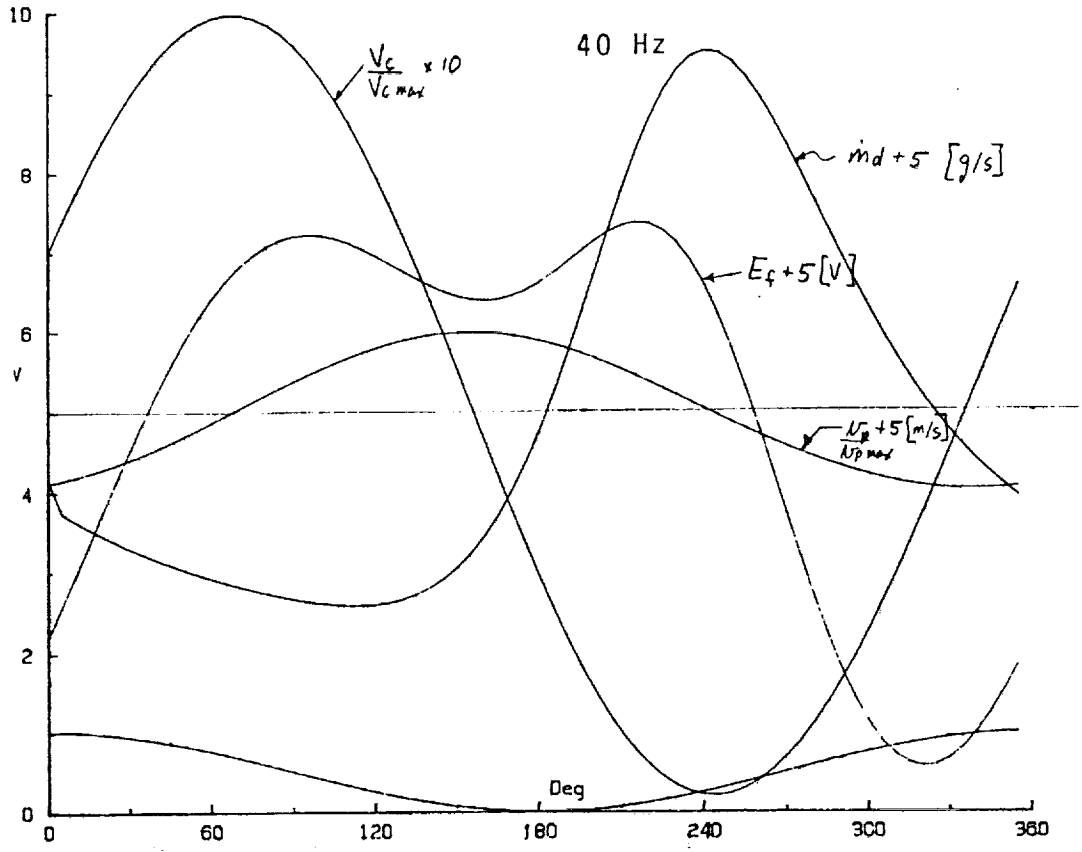

Run #11 11/08/90

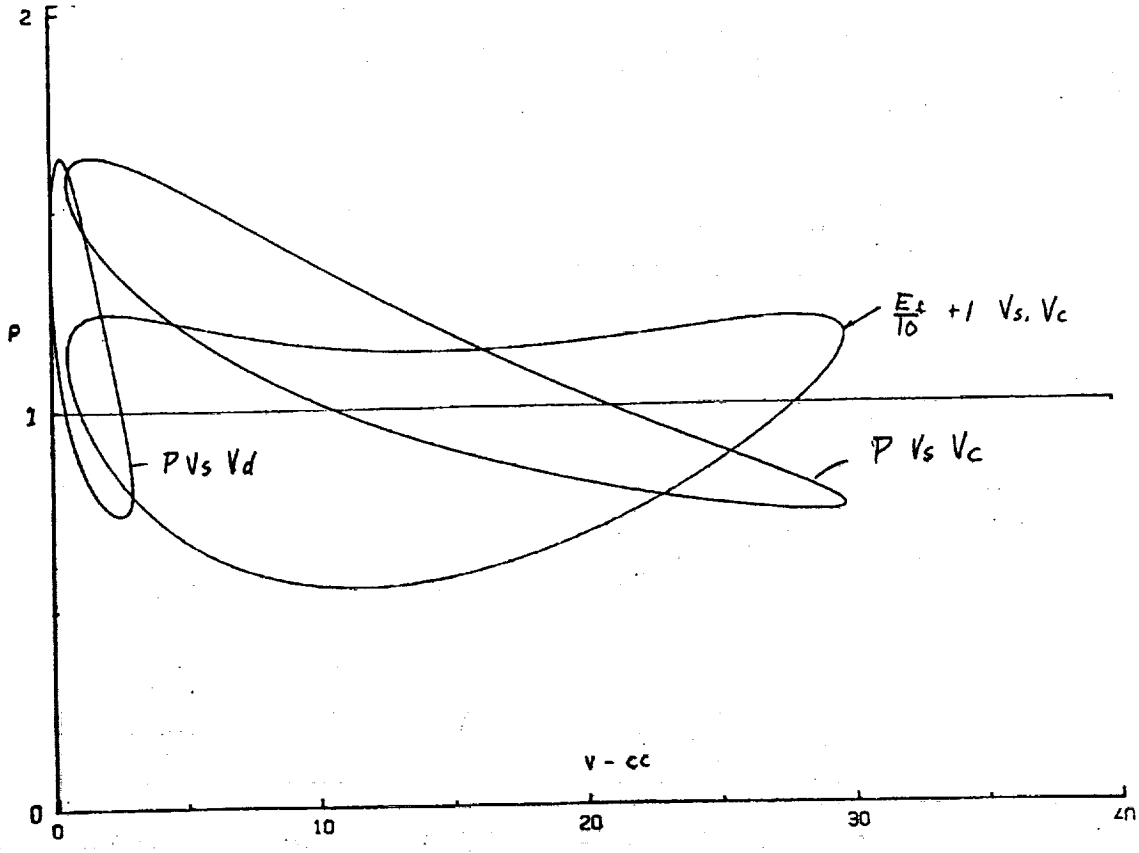

Run #15 11/08/90 Eo=82 Same as Run #11 I^2R=15.5%

35 Hz

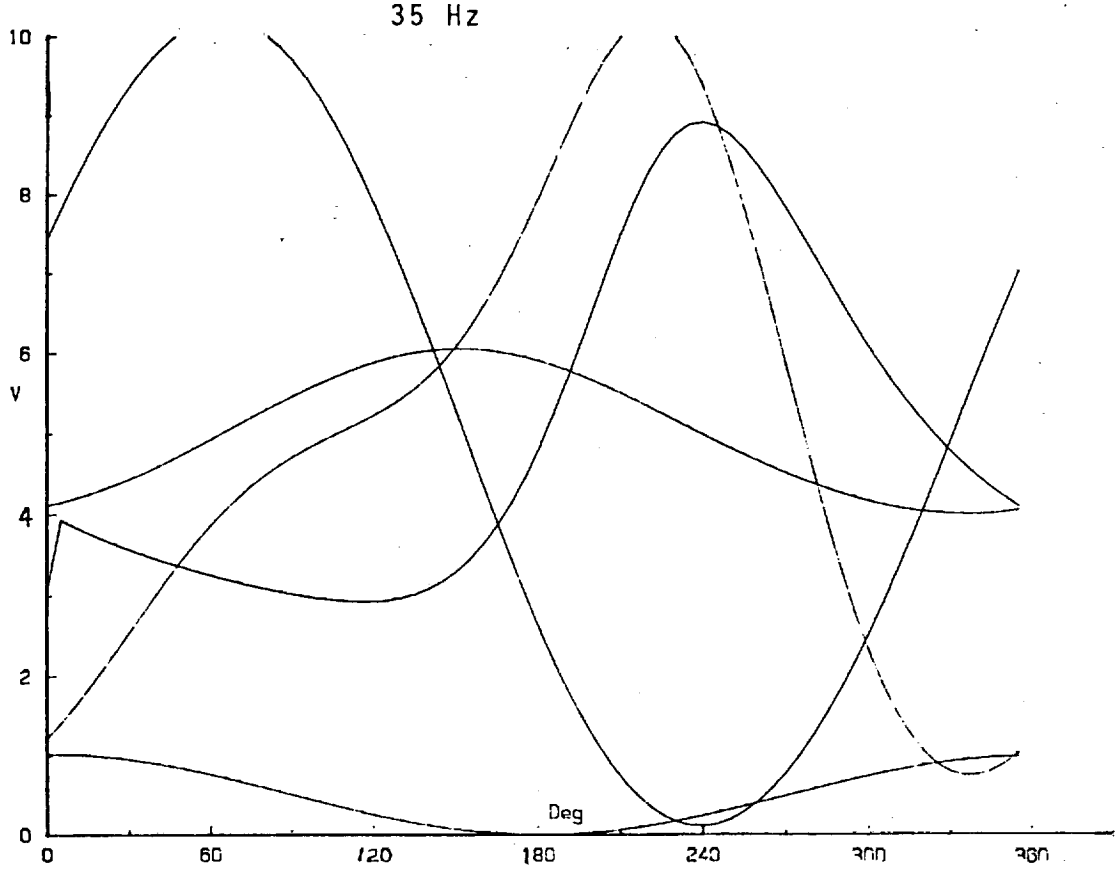

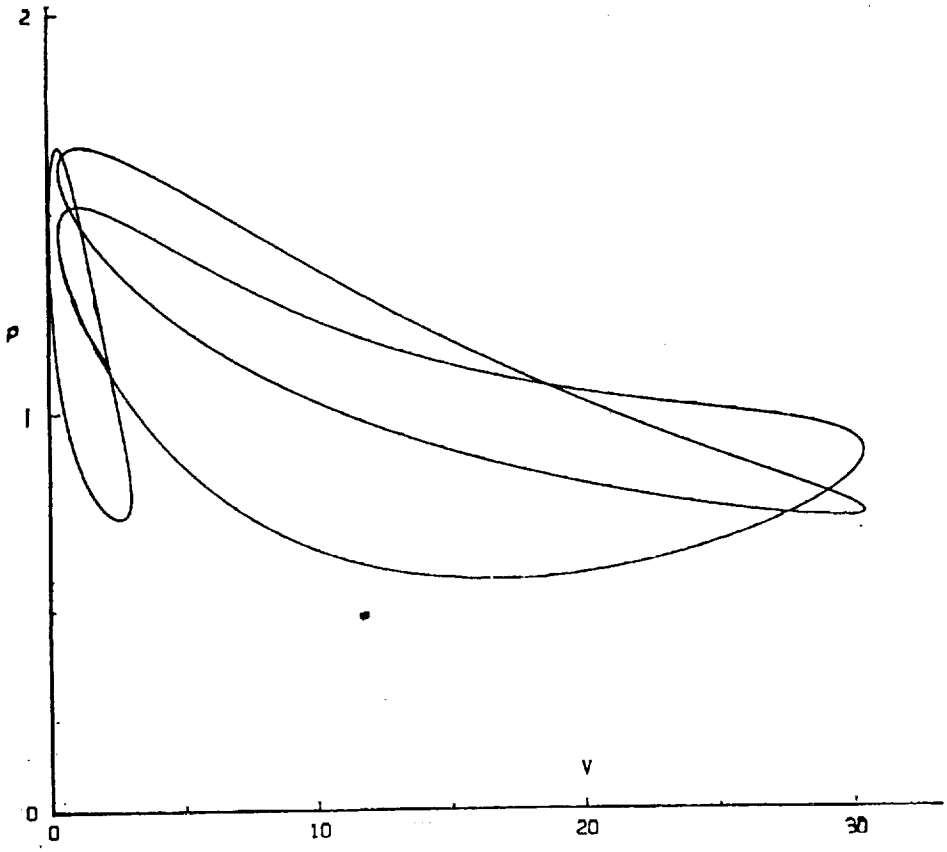

Run #16 11/08/90 Eo=96V Same as Run #11

I^2R=17.8% 45 Hz

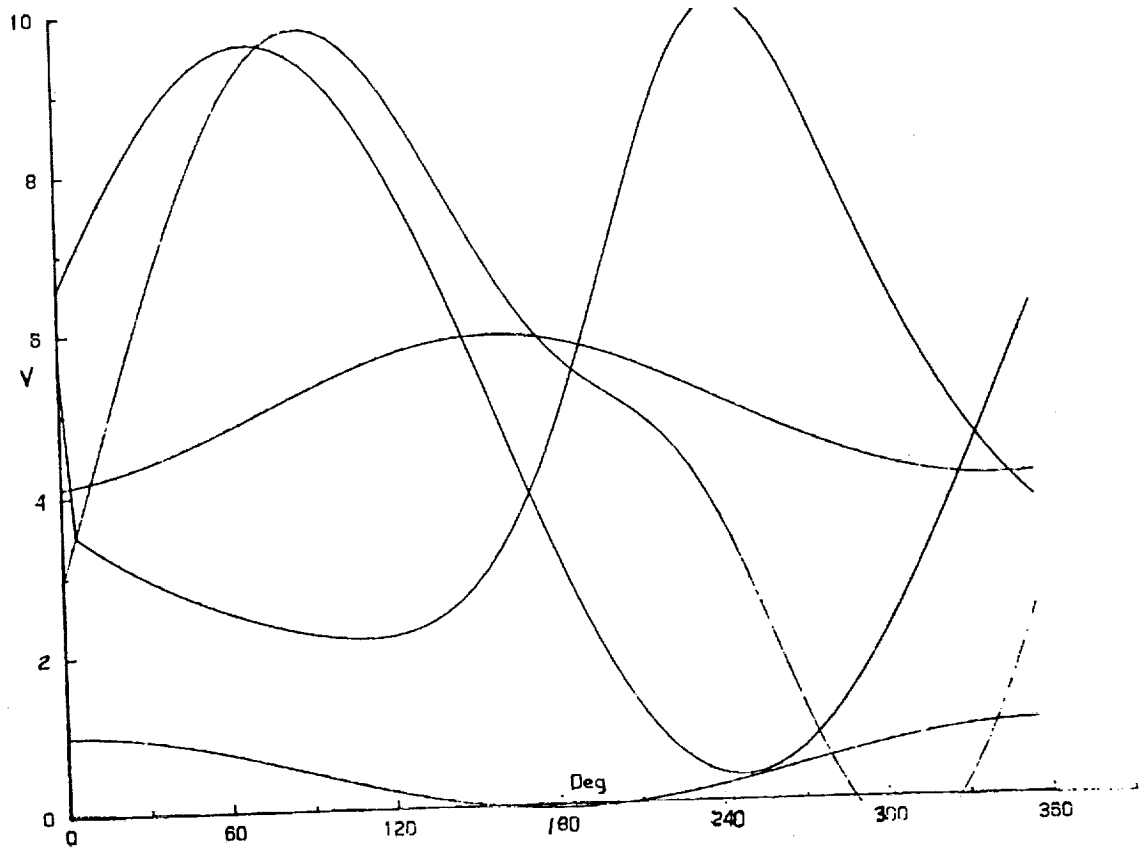

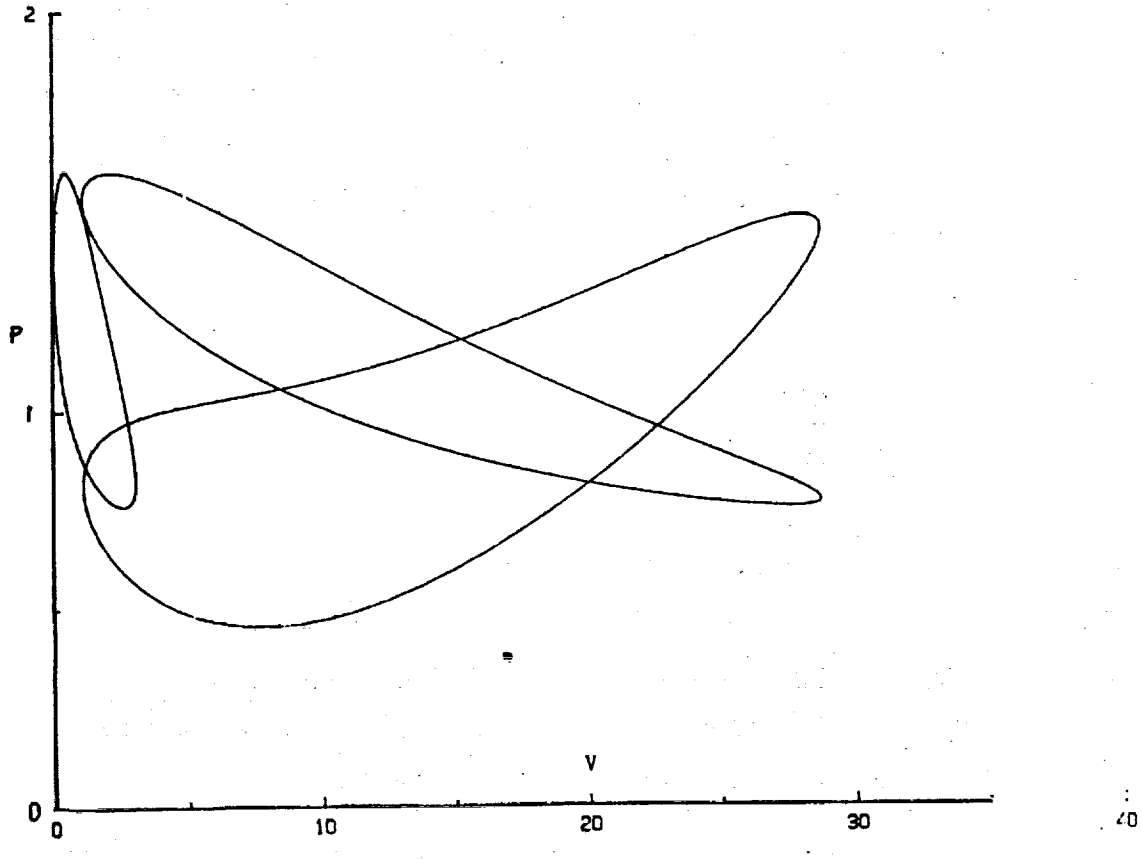

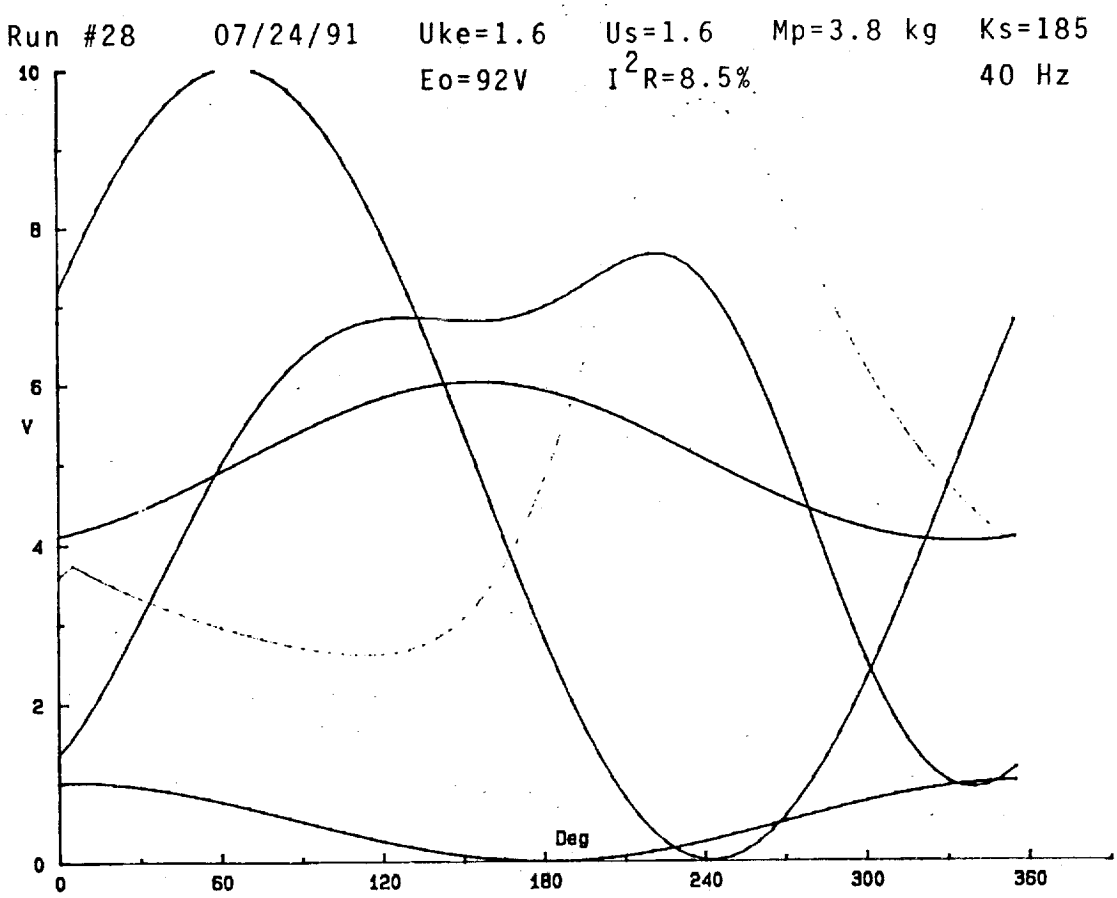
Run #28 07/24/91 Uke=1.6 Us=1.6 Mp=3.8 kg Ks=185
Eo=92V I²R=8.5% 40 Hz
10
8
6
V
4
2
0
Deg
0
60
120
180
240
300
360

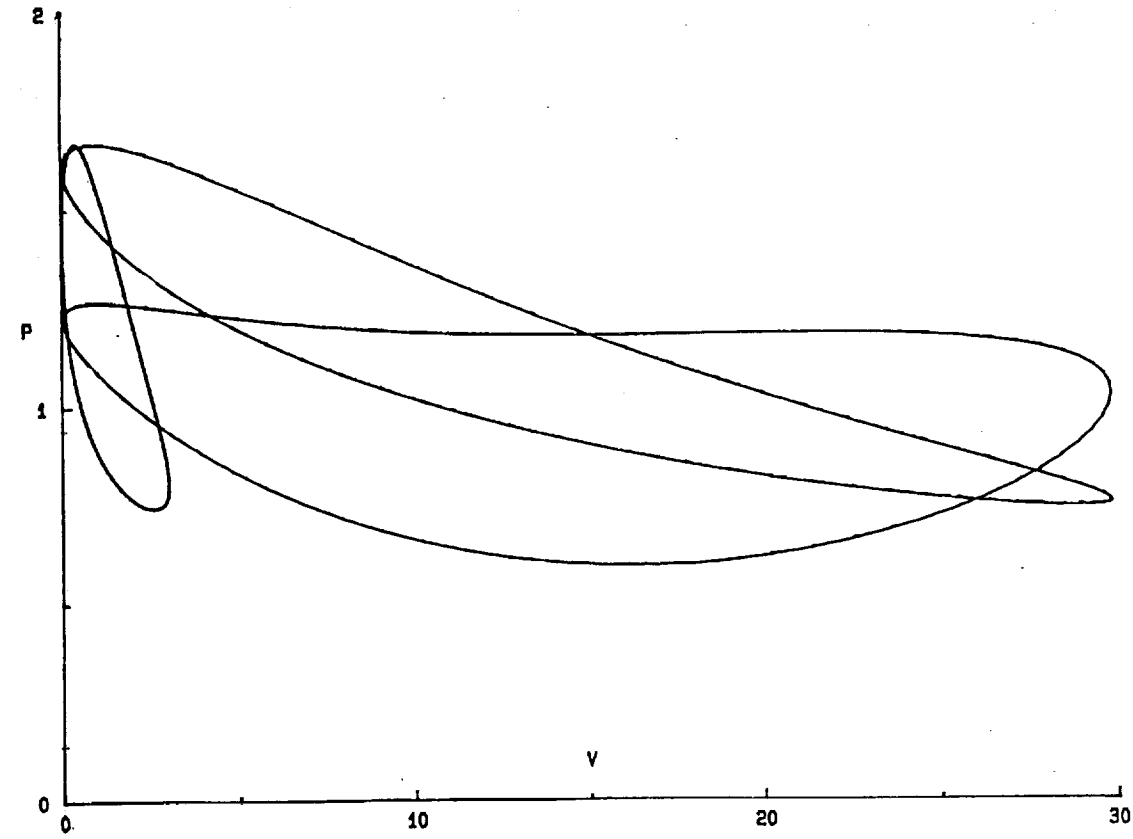
2
P
1
0
V
0
10
20
30

8.3 Appendix C: Expander Dynamic Model

```
' "SC1a.BAS" 09/29/91  3 STAGE STIRLING COOLER
' Written by R. Longsworth, modified by J. Pfahler
' Last modified 12-31-92
'                                                    Rev. 4.0
' Dimension Arrays,and Initialize Variables
'*************************************************************************
DIM T(4), DD(5), LDD(4), DR(4), LDR(4), PY(4), TR(4), SL(4), CG(4)
DIM V(4), VV(4), VVo(4), VRM(4), VR(4), VD(4), LD(4), LR(4), CL(4)
DIM VC(26), VDA(26), MA(26), MT(26), M1(26), M2(26), M3(26), P(26)
DIM MR1(26), MR2(26), MR3(26), VD1(26), VD2(26), VD3(26), VDo(26)
DIM M3T(26), M21(26), M1T(26), PAV(26), UDX(26), UD(26), P1(26), P2(26)
DIM P3(26), DM1(26), DM2(26), DM3(26), SDP1(26), SDP2(26), SDP3(26)
DIM MSL1(26), MSL2(26), MSL3(26), IEH1(26), IEH2(26), IEH3(26), Jqdpp3(26)
DIM JqdP1(26), JqdP2(26), JqdP3(26), Jqdpp1B(26), Jqdpp1S(26), Jqdpp2(26)
T(0) = 300: DD(1) = 28: LDD(1) = 4.5: DR(1) = 31.5: LDR(1) = .62: PY(1) = .686
T(1) = 60:  DD(2) = 12: LDD(2) = 4: DR(2) = 17: LDR(2) = .655:  PY(2) = .41
T(2) = 16:  DD(3) = 6:  LDD(3) = 6: DR(3) = 16: LDR(3) = 1.3
T(3) = 8:   DD(4) = 0:
V(0) = .1:  MAH = 0: MAL = 100: Qqd1 = 0: qd1 = 0: qr1 = 0: QdP1 = 0: qqr1 = 0
V(1) = .1:  M1H = 0: M1L = 100: Qqd2 = 0: qd2 = 0: qr2 = 0: QdP2 = 0: qqr2 = 0
V(2) = .1:  M2H = 0: M2L = 100: Qqd3 = 0: qd3 = 0: qr3 = 0: QdP3 = 0: qqr3 = 0
V(3) = .1:  M3H = 0: M3L = 100
M2TH = 0:   M2TL = 100
M3TH = 0:   M3TL = 100
Qc = 0: PH = 0: PL = 100: CPb = .8: CTp = .8
DC = 66: SDC = .26: SDD = .18: Po = .85: N = 40: DG = 0: PI = 3.1416
DW = .025: DS = .0445:      NT = 17: DT = .02: QJT = 0
DH1 = DW * PY(1) / (1 - PY(1))
DH2 = DS * .667 * PY(2) / (1 - PY(2))
DH3 = DT / 2
FOR I = 1 TO NT
        DG = DG + DR(3) * (2 * I - 1) / (2 * NT)
NEXT I
PY(3) = 4 * DG * DT / DR(3) ^ 2
U1 = .000016: U2 = .0000061: U3 = .0000024'       Avg Viscosity He    Pa.s
KG1 = .125: KG2 = .047: KG3 = .018'               Avg Therm Cond He   W/mK
KI1 = 2.86: KI2 = .188: KI3 = .0066'              Therm Cond Int SS   W/mm
CG1 = 5.2: CG2 = 5.3: CG3 = 7'                    Cp He               J/gK
CW = .32: CS = .049: CT = .042'                   Cp                  J/gK
'******** Values for Seal Leakage Calculations*****************************
musl1 = 1.863E-11
musl2 = 6.45E-12  '*************He viscosity MPa-s, at 275, 55 and 14K******
musl3 = 2.63E-12
SL(1) = 28: SL(2) = 12: SL(3) = 12  '******************Seal length***********
CG(1) = .0026: CG(2) = .0025: CG(3) = .00135'*********Clearance gap*********
CP1 = 5.2: CP2 = 5.2: CP3 = 5.36 '********************Cp He   J/gK**********
'*************************************************************************
'   Calculate DEPENDENT PARAMETERS, All angles are in radians
'   CPb IS Pb FRACTION, CTp IS THERMAL PENETRATION FRACTION
'*************************************************************************
SD = DD(1) * SDD: VC = PI * DC ^ 3 * SDC / 4: SC = DC * SDC: Z = N / 1000
VVC = V(0) * VC:  VVA = 0: VDA = 0: VD(0) = PI * DD(1) ^ 2 * SD / 4
FOR L = 1 TO 3:
        VD(L) = PI * (DD(L) ^ 2 - DD(L + 1) ^ 2) * SD / 4
        VR(L) = PI * DR(L) ^ 3 * LDR(L) * PY(L) / 4
        VRM(L) = VR(L) * (1 - PY(L)) / PY(L)
        CL(L) = .1 + .002 * DD(L)
        LD(L) = LDD(L) * DD(L)
        LR(L) = LDR(L) * DR(L)
        TR(L) = (T(L - 1) - T(L)) / LOG(T(L - 1) / T(L))'******Natural Log
        VDA = VD(L) * T(0) / T(L) + VDA
NEXT L
```

```
MRW = VRM(1) * .00896: MRS = VRM(2) * .0114: MRT = VRM(3) * .0114 * CPb * CTp
'********************Piping Sizes*************************************************
DP1B = 2.1:     DP1S = 2.1:     DP2 = 1.25:     DP3 = 1!'******Diameter of piping
LP1B = 56: LP1S = SQR(97 ^ 2 + (LD(2) - LR(2)) ^ 2)'******Length of piping
LP2 = 28: LP3 = 26 + (DR(3) - 10)
VV(1) = PI / 4 * (DP1B ^ 2 * LP1B + DP1S ^ 2 * LP1S)
VV(2) = PI / 4 * (DP2 ^ 2 * LP2): VV(3) = PI / 4 * (DP3 ^ 2 * LP3)
FOR L = 1 TO 3
'**********************          VV(L) = V(L) * VD(L)
        VVo(L) = VR(L) * T(0) / TR(L) + VV(L) * T(0) / T(L)
        VVA = VVA + VVo(L)
NEXT L
'*******************************************************************************
'  CALCULATE VOLUMES,PRESSURE & GAS MASS Vs TIME
'*******************************************************************************
VDA = VDA + VD(3) * .4 * T(0) / T(3) + VD(2) * .05 * T(0) / T(2)
VVA = VVA + VV(3) * .4 * T(0) / T(3) + VR(3) * .14 * T(0) / TR(3)
C1 = Po * (VC / 2 + VVC + VVA + VDA)
A = -.2618: B = 1.0472 '**********************.2618 radians=15 degrees*******
FOR I = 1 TO 25
        A = A + .2618
        VC(I) = (1 + SIN(A)) * (VC / 2)
        X = (1 + SIN(A + B)) / 2
        UDX(I) = (1 - X) * SD'**************displacer position, 0 is TDC
        VDA(I) = X * VDA
        VDo(I) = VD(0) * (1 - X)
        P(I) = C1 / (VC(I) + VVC + VDA(I) + VVA + VDo(I))
        VD1(I) = VD(1) * X:     VD2(I) = VD(2) * X:     VD3(I) = VD(3) * X
        MA(I) = P(I) * (VC(I) + VVC + VDo(I)) * .000484 / T(0)
        M3(I) = P(I) * (VD3(I) + VV(3)) * .000484 * (1.81 - .391 * P(I)) / T(3)
        M3T(I) = P(I) * VR(3) * .000484 * 1.14 / TR(3) + M3(I)
        M2(I) = P(I) * (VD2(I) + VV(2)) * .000484 * 1.05 / T(2) + M3T(I)
        M2T(I) = M2(I) + P(I) * VR(2) * .000484 / TR(2)
        M1(I) = P(I) * (VD1(I) + VV(1)) * .000484 / T(1) + M2T(I)
        M1T(I) = M1(I) + P(I) * VR(1) * .000484 / TR(1)
        MT(I) = MA(I) + M1T(I)
NEXT I
'*******************************************************************************
'  Calculate PV work of compressor and displacer, Regenerator mass flow rates
'*******************************************************************************
FOR m = 2 TO 25
        PAV(m) = (P(m - 1) + P(m)) / 2
        Qc = Qc + PAV(m) * (VC(m) - VC(m - 1))
        Qqd1 = Qqd1 + PAV(m) * (VD1(m) - VD1(m - 1))
        Qqd2 = Qqd2 + PAV(m) * (VD2(m) - VD2(m - 1))
        Qqd3 = Qqd3 + PAV(m) * (VD3(m) - VD3(m - 1))
        UD(m) = (UDX(m) - UDX(m - 1)) * N * 24'**********displacer velocity***
        IF P(m) > PH THEN PH = P(m)
        IF P(m) < PL THEN PL = P(m)
        IF M1T(m) > MAH THEN MAH = M1T(m)
        IF M1T(m) < MAL THEN MAL = M1T(m)
        IF M1(m) > M1H THEN M1H = M1(m)
        IF M1(m) < M1L THEN M1L = M1(m)
        IF M2(m) > M2H THEN M2H = M2(m)
        IF M2(m) < M2L THEN M2L = M2(m)
        IF M2T(m) > M2TH THEN M2TH = M2T(m)
        IF M2T(m) < M2TL THEN M2TL = M2T(m)
        IF M3(m) > M3H THEN M3H = M3(m)
        IF M3(m) < M3L THEN M3L = M3(m)
        IF M3T(m) > M3TH THEN M3TH = M3T(m)
        IF M3T(m) < M3TL THEN M3TL = M3T(m)
        MR1(m) = (M1T(m) - M1T(m - 1) + M1(m) - M1(m - 1)) / 2
        MR2(m) = (M2T(m) - M2T(m - 1) + M2(m) - M2(m - 1)) / 2
        MR3(m) = (M3T(m) - M3T(m - 1) + M3(m) - M3(m - 1)) / 2
'*******************************************************************************
```

```
' First Regenerator:  fanning friction factor, Reynolds and Stanton numbers,
'       pressure drop MPa, heat transfer inefficiency, and regenerator loss.
'*************************************************************************
        MR = MR1(m) * N * 24
        GR = MR * 4 / (PI * DR(1) ^ 2 * PY(1))
        NRE = ABS(GR * DH1 / U1)
        IF NRE < 32 THEN
                F = 40 / NRE
                GOTO 435
        END IF
        F = 4.637 / NRE ^ .3783
435     DP = F * LR(1) * GR ^ 2 * (T(0) + T(1)) / (DH1 * PAV(m) * 484)
        P1(m) = PAV(m) - DP
        IF GR < 0! THEN P1(m) = PAV(m) + DP
        NRE1 = NRE
        JqdP1(m) = DP * (VD1(m) - VD1(m - 1)) * Z
        QdP1 = ABS(DP * (VD1(m) - VD1(m - 1))) + QdP1
        NST = .78 / NRE ^ .4
        IEH1(m) = DH1 / (NST * LR(1) * 2):  IEH1 = IEH1(m) + IEH1
        qr1 = qr1 + ABS(MR1(m) * IEH1(m))
'***************Second Regenerator*****************************************
        MR = MR2(m) * N * 24
        GR = MR * 4 / (PI * DR(2) ^ 2 * PY(2))
        NRE = ABS(GR * DH2 / U2)
        IF NRE < 32 THEN
                F = 13 / NRE ^ .514
                GOTO 470
        END IF
        F = 1.42 / NRE ^ .144
470     DP = F * LR(2) * GR ^ 2 * (T(1) + T(2)) / (DH2 * PAV(m) * 484)
        P2(m) = P1(m) - DP
        IF GR < 0! THEN P2(m) = P1(m) + DP
        NRE2 = NRE
        JqdP2(m) = DP * (VD2(m) - VD2(m - 1)) * Z
        QdP2 = ABS(DP * (VD2(m) - VD2(m - 1))) + QdP2
        NST = .3 / NRE ^ .3
        IEH2(m) = DH2 / (NST * LR(2) * 2):  IEH2 = IEH2 + IEH2(m)
        qr2 = qr2 + ABS(MR2(m) * IEH2(m))
        HJT = 96.01 - 6.313 * PAV(m)
        QJT = QJT + HJT * (M3T(m - 1) - M3T(m))'****JT REFRIGERATION @ 16 K**
'*****************Third Regenerator*****************************************
        MR = MR3(m) * N * 24
        GR = MR * 4 / (PI * DR(3) ^ 2 * PY(3))
        NRE = ABS(GR * DH3 / U3)
        IF NRE < 200 THEN
                F = 24 / NRE
                GOTO 515
        END IF
        F = .0906 / NRE ^ .266
        NST = .0064 / NRE ^ .087
515     DP = F * LR(3) * GR ^ 2 * (T(2) + T(3)) / (DH3 * PAV(m) * 484)
        P3(m) = P2(m) - DP
        IF GR < 0! THEN P3(m) = P2(m) + DP
        NRE3 = NRE
        NST = 6.6 / NRE
        JqdP3(m) = DP * (VD3(m) - VD3(m - 1)) * Z
        QdP3 = ABS(DP * (VD3(m) - VD3(m - 1))) + QdP3
        IEH3(m) = DH3 / (NST * LR(3) * 2):        IEH3 = IEH3 + IEH3(m)
        qr3 = qr3 + ABS(MR3(m) * IEH3(m))
'*************************************************************************
'         Do seal leakage calculations
'*************************************************************************
        DM1(m) = UD(m) * CG(1) / 2
        DM2(m) = UD(m) * CG(2) / 2
        DM3(m) = UD(m) * CG(3) / 2
```

```
        SDP1(m) = (2 / (3 * SL(1) * musl1)) * (CG(1) / 2) ^ 3 * (PAV(m)   P1(m))
        SDP2(m) = (2 / (3 * SL(2) * musl2)) * (CG(2) / 2) ^ 3 * (P1(m)   P2(m))
        SDP3(m) = (2 / (3 * SL(3) * musl3)) * (CG(3) / 2) ^ 3 * (P2(m)   P3(m))
MSL1(m) = PI * DD(1) * (PAV(m) + P1(m)) * .000484 * (DM1(m)   SDP1(m)) / (T(0) + T(1))
MSL2(m) = PI * DD(2) * (P2(m) + P1(m)) * .000484 * (DM2(m)   SDP2(m)) / (T(2) + T(1))
MSL3(m) = PI * DD(3) * (P3(m) + P2(m)) * .000484 * (DM3(m)   SDP3(m)) / (T(3) + T(2))
        MSLT1 = MSLT1 + MSL1(m)
        MSLT2 = MSLT2 + MSL2(m)
        MSLT3 = MSLT3 + MSL3(m)
'*************************************************************************
'*****         Calculate the losses in the piping                        ***
'*************************************************************************
        MP1B = (M1(m)   M1(m   1)   (M2T(m)   M2T(m   1))) * N * 24'***Piping
        MP1S = (M2T(m)   M2T(m   1)) * N * 24           '*****to first Regen.
        GRPB = MP1B * 4 / (PI * DP1B ^ 2): GRPS = MP1S * 4 / (PI * DP1S ^ 2)
        NREPB = ABS(GRPB * DP1B / U1):     NREPS = ABS(GRPS * DP1S / U1)
        FPB = 16 / NREPB: FPS = 16 / NREPS
        IF NREPB > 2000 THEN
                FPB = .046 / NREPB ^ .2
        END IF
        IF NREPS > 2000 THEN
                FPS = .046 / NREPS ^ .2
        END IF
        DPPB = FPB * LP1B * GRPB ^ 2 * 2 * T(1) / (DP1B * P1(m) * 484)
        DPPS = FPS * LP1S * GRPS ^ 2 * 2 * T(1) / (DP1S * P1(m) * 484)
        Jqdpp1B(m) = DPPB * (VD1(m)   VD1(m   1)) * Z
        QdPP1B = ABS(DPPB * (VD1(m)   VD1(m   1)))
        Big = Big + QdPP1B
        Jqdpp1S(m) = DPPS * (VD2(m)   VD2(m   1)) * Z
        QdPP1S = ABS(DPPS * (VD2(m)   VD2(m   1)))
        Small = Small + QdPP1S
        QdPP1 = QdPP1 + QdPP1B + QdPP1S
'************Piping to second Regen*************************************
        MP2 = (M2(m)   M2(m   1)) * N * 24
        GRP = MP2 * 4 / (PI * DP2 ^ 2)
        NREP = ABS(GRP * DP2 / U2)
        FP = 16 / NREP
        IF NREP > 2000 THEN
                FP = .046 / NREP ^ .2
        END IF
        DPP = FP * LP2 * GRP ^ 2 * 2 * T(2) / (DP2 * P2(m) * 484)
        Jqdpp2(m) = DPP * (VD2(m)   VD2(m   1)) * Z
        QdPP2 = QdPP2 + ABS(DPP * (VD2(m)   VD2(m   1)))
'***************Piping to third Regen.*************************************
        MP3 = (M3(m)   M3(m   1)) * N * 24
        GRP = MP3 * 4 / (PI * DP3 ^ 2)
        NREP = ABS(GRP * DP3 / U3)
        FP = 16 / NREP
        IF NREP > 2000 THEN
                FP = .046 / NREP ^ .2
        END IF
        DPP = FP * LP3 * GRP ^ 2 * 2 * T(3) / (DP3 * P3(m) * 484)
        Jqdpp3(m) = DPP * (VD3(m)   VD3(m   1)) * Z
        QdPP3 = QdPP3 + ABS(DPP * (VD3(m)   VD3(m   1)))
NEXT m
'********************************** ***************************************
'   Calculate ave. IEH, regenerator capacity ratio, Capacity Iec, & Heat Loss
'
'*************************************************************************
IEH1 = IEH1 / 24
IEH2 = IEH2 / 24
IEH3 = IEH3 / 24
MRG1 = (MAH   MAL + M1H   M1L) / 2
MRG2 = (M2TH   M2TL + M2H   M2L) / 2
MRG3 = (M3TH   M3TL + M3H   M3L) / 2
```

```
CR1 = MRW * CW / (MRG1 * CG1): IEC1 = .036 / CR1
CR2 = MRS * CS / (MRG2 * CG2): IEC2 = .036 / CR2
CR3 = MRT * CT / (MRG3 * CG3): IEC3 = .036 / CR3
'***************First Regenerator*****************************************
qrc = MRG1 * N * (T(0) - T(1)) * CG1 * IEC1
qr = qr1 * N * (T(0) - T(1)) * CG1 + qrc
qra = MRG1 * N * (T(0) - T(1)) * CG1 * .008
IE1 = qr / qra
IF qr < qra THEN qr = qra
qqr1 = qr
'*****************Second Regenerator*****************************************
qrc = MRG2 * N * (T(1) - T(2)) * CG2 * IEC2
qr = qr2 * N * (T(1) - T(2)) * CG2 + qrc
qra = MRG2 * N * (T(1) - T(2)) * CG2 * .016
IE2 = qr / qra
IF qr < qra THEN qr = qra
qqr2 = qr
'******************Third Regenerator*****************************************
qrc = MRG3 * N * (T(2) - T(3)) * CG3 * IEC3
qr = qr3 * N * (T(2) - T(3)) * CG3 + qrc
qra = MRG3 * N * (T(2) - T(3)) * CG3 * .024
IE3 = qr / qra
IF qr < qra THEN qr = qra
qqr3 = qr
'***********CALCULATE SEAL LEAKAGE LOSSES*************************************
qs11 = ABS(MSLT1 * CP1 * 240) '*****Heat loss in W
qs12 = ABS(MSLT2 * CP2 * 44)
qs13 = ABS(MSLT3 * CP3 * 8)
'***********CALCULATE CONDUCTION LOSS*****************************************
qk1 = PI * KI1 * (.55 / LDR(1) + 1 / (LD(1) - SL(1)))
qk2 = PI * KI2 * (.55 / LDR(2) + 1 / (LD(2) - SL(2)))
qk3 = PI * KI3 * (.55 / LDR(3) + 1 / (LD(3) - SL(3)) + DR(3) ^ 2 / (4 * (1 - CPb) *
LR(3)))
'***********CALCULATE SHUTTLE LOSSES******************************************
qs1 = PI * KG1 * DD(1) * SD ^ 2 * (T(0) - T(1)) / ((LD(1) - SL(1)) * CL(1) * 8000)
qs2 = PI * KG2 * DD(2) * SD ^ 2 * (T(1) - T(2)) / ((LD(2) - SL(2)) * CL(2) * 8000)
qs3 = PI * KG3 * DD(3) * SD ^ 2 * (T(2) - T(3)) / ((LD(3) - SL(3)) * CL(3) * 8000)
'*************************************************************************
'              CALCULATE NET REFRIGERATION RATES
'*************************************************************************
qqc = Qc * Z
qqJT = QJT * Z
qqdPP1 = QdPP1 * Z:   qqdPP2 = QdPP2 * Z + qqdPP1 * (VD(2) / VD(1)):
qqdPP3 = QdPP3 * Z + qqdPP2 * (VD(3) / VD(2))
qd1 = Qqd1 * Z: qqdP1 = QdP1 * Z:              qp1 = qd1 - qqdP1 - qqdPP1
qd2 = Qqd2 * Z: qqdP2 = QdP2 * Z + qqdP1 * (VD(2) / VD(1))
qp2 = qd2 - qqdP2 - qqdPP2
qd3 = Qqd3 * Z: qqdP3 = QdP3 * Z + qqdP2 * (VD(3) / VD(2))
qp3 = qd3 - qqdP3 - qqdPP3
qn3 = qp3 - qqr3 - qs3 - qk3 - qs13 + qqJT
qn2 = qp2 - qqr2 - qs2 - qk2 - qs12 + qs13 + qqr3 + qs3 + qk3 - qqJT
qn1 = qp1 - qqr1 - qs1 - qk1 - qs11 + qs12 + qqr2 + qs2 + qk2
qcn = qqc + qp1 + qp2 + qp3
EFF = (qn1 * 4 + qn2 * 17.75 + qn3 * 36.5) / (-qcn)
'*************************************************************************
'                    OUTPUT
'*************************************************************************
LPRINT "NASA/SC3 RUN ON "; DATE$; " AT "; TIME$: LPRINT
LPRINT
LPRINT "   TA-K  DC-mm  SC-mm  SD-mm   N-Hz PH-MPa P1-MPa  Eff-%  "
LPRINT "   T1-K DD1-mm DR1-mm DW1-um   P1-%   "
LPRINT "   T2-K DD2-mm DR2-mm DW2-um   P2-%   "
LPRINT "   T3-K DD3-mm DR3-mm DW3-um   P3-%   "
LPRINT USING "####.##"; T(0); DC; SC; SD; N; PH; PL; EFF * 100
LPRINT USING "####.##"; T(1); DD(1); DR(1); DW * 1000; PY(1) * 100
```

```
LPRINT USING "####.##"; T(2); DD(2); DR(2); DS * 1000; PY(2) * 100
LPRINT USING "####.##"; T(3); DD(3); DR(3); DT * 1000; PY(3) * 100
LPRINT : LPRINT :  LPRINT "            Losses, W                          Pipe Sizes, mm"
LPRINT "   Shuttle  Conduction Seal   Piping    DP1B    DP1S     DP2      DP3"
LPRINT USING "####.####"; qs1; qk1; qsl1; qqdPP1; DP1B; DP1S; DP2; DP3
LPRINT USING "####.####"; qs2; qk2; qsl2; qqdPP2
LPRINT USING "####.####"; qs3; qk3; qsl3; qqdPP3
LPRINT
LPRINT "      I      P-MPa     VC-mL     VD-mL      MA-g      M1-g      MT-g"
FOR I = 1 TO 23 STEP 6
LPRINT USING "#####.###"; I; P(I); VC(I) / 1000; VD1(I) / 1000; MA(I); M1(I); MT(I)
NEXT I
LPRINT
LPRINT "     Nre       Cl       Cr    Ieh %    Iec %     Ie %"
LPRINT USING "####.###"; NRE1; CL(1) * 100; CR1; IEH1 * 100; IEC1 * 100; IE1 * .8
LPRINT USING "####.###"; NRE2; CL(2) * 100; CR2; IEH2 * 100; IEC2 * 100; IE2 * 1.6
LPRINT USING "####.###"; NRE3; CL(3) * 100; CR3; IEH3 * 100; IEC3 * 100; IE3 * 2.4
LPRINT
LPRINT "   qd-W  QdP*Z-W   qdP-W    qp-W    qr-W    qn-W"
LPRINT USING "####.###"; qd1; QdP1 * Z; qqdP1; qp1; qqr1; qn1' "1st stage"
LPRINT USING "####.###"; qd2; QdP2 * Z; qqdP2; qp2; qqr2; qn2' "2nd stage"
LPRINT USING "####.###"; qd3; QdP3 * Z; qqdP3; qp3; qqr3; qn3' "3rd stage"
LPRINT
LPRINT "      MH       M1      MRG       LD       LR"
LPRINT USING "####.###"; MAH; MAL; MAH - MAL
LPRINT USING "####.###"; M1H; M1L; MRG1; LD(1); LR(1)' "1st stage"
LPRINT USING "####.###"; M2H; M2L; MRG2; LD(2); LR(2)' "2nd stage"
LPRINT USING "####.###"; M3H; M3L; MRG3; LD(3); LR(3)' "3rd stage"
LPRINT
LPRINT "     NT         B Deg        CPb       CTp     qJT-W     qc-W      qcn-W"
LPRINT USING "######.###"; NT; B * 180 / PI; CPb; CTp; -qqJT; -qqc; -qcn
'*************************************************************************
'      Open and write to file of comma separated values for spreadsheet.
'*************************************************************************
'OPEN "c:\jnp\output.csv" FOR APPEND AS #3
'WRITE #3,
'***WRITE #3, DR(1), LR(1), DR(2), LR(2), DR(3), LR(3), DS * 1000, DT * 1000, N, qn1, qn2,
qn3, -qqc, EFF * 100
'FOR j = 2 TO 25
'        Iregen = JqdP1(j) + JqdP2(j) + JqdP3(j)
'        Lpipe = Jqdpp1B(j) + Jqdpp1S(j) + Jqdpp2(j) + Jqdpp3(j)
'        WRITE #3, PAV(j), UD(j), P1(j), P2(j), P3(j), Iregen, Lpipe, UDX(j)
'***WRITE #3, MR1(j), MR2(j), MR3(j)
'***WRITE #3, MSL1(j), MSL2(j), MSL3(j), PAV(j), P1(j), P2(j), P3(j)
'NEXT j
'CLOSE #3
END
```

8.4 Appendix D: Expander Gas Spring Design

```
' "SCDD-2"  STIRLING CYCLE DYNAMIC DISPLACER ANALYSIS"
LPRINT "    SCDD-2 1/8/92  RUN ON  "; DATE$; " AT "; TIME$
' DIMENSION VARIABLES AND FORMAT OUTPUT
DIM VC(75), VD(75), vP(75), P(75), PS1(75), PS2(75), MA(75), M1(75)
TA = 300: DC = 61.2: SC = 20: SD = 5.04: PO = .68: PM = 1.1: F = 40: PI = 3.1416
TI = 35.8: DD = 28: LD = 100: DR = 24.6: LR = 28: PY = .67: DW = .023
VO = .2: V1 = .25: MD = .25: KS = 6.9: DS = 3.4: DP = 13.5
CO = 4.45: XP = CO * SD: U = .000016' Pa.s
'CALCULATE DEPENDENT PARAMETERS
AP1 = PI * DP ^ 2 / 4: AD = PI * DD ^ 2 / 4: ASt = PI * DS ^ 2 / 4
AP2 = AP1 - ASt: AR1 = AP1 / AD: AR2 = AP2 / AD
VCM = PI * DC ^ 2 * SC / 4: VDM = PI * DD ^ 2 * SD / 4: K = 1000
SK = KS / AD: VO = VO * VCM: VS = AP1 * XP
```

```
VR = PI * DR ^ 2 * LR * PY / 4
TR = (TA - T1) / LOG(TA / T1): DH = DW * PY / (1 - PY)
VV = V1 * VDM * TA / T1 + VR * TA / TR + V0
C1 = P0 * (VCM * .7 + VV + VDM * TA / T1)
C2 = PM * (VS + AR1 * VDM / 2): LPRINT
'CALCULATE RESONANT FREQUENCY
dPR = 1 + .5 / CO - ((CO + .5) / (CO + 1))
PEg = dPR * PM * PI * DP ^ 2 * SD / 16000
PEs = KS * SD ^ 2 / 8000
fr = ((PEg + PEs) * 1000000 / (.5 * MD * PI ^ 2 * SD ^ 2)) ^ .5
LPRINT "   TA-K  DC-mm  SC-mm  SD-mm   N-Hz PO-MPa PEg-mJ"
LPRINT "   T1 K  DR-mm  LR-mm  DW-mm   P1-% PM-MPa PEk-mJ  Nf-Hz"
LPRINT "KS-N/mm  DD-mm  LD-mm  DS-mm  DP-mm  XP-mm   MD-g "
LPRINT USING "####.# "; TA; DC; SC; SD; F; P0; PEg * 1000
LPRINT USING "####.# "; T1; DR; LR; DW; PY; PM; PEs * 1000; fr
LPRINT USING "####.# "; KS; DD; LD; DS; DP; XP; MD * 1000: LPRINT
LPRINT "   A-Deg    P-MPa    VC-cc    VD-cc  vP-cm/s  PS1-MPa  dPR-KPa "
'CALCULATE INITIAL VALUES
VS1 = VS: VS2 = VS + AR2 * VDM
PS1(1) = C2 / VS1: PS2(1) = C2 / VS2
A = .5: B = 60: dt = .5 / (360 * F)): N = 1
VC(N) = VCM * (1 + COS((A - B) * PI / 180)) / 2
VD(N) = VDM * (1 + COS(A * PI / 180)) / 2
P(N) = C1 / (VC(N) + VV + VD(N) + (TA / T1 - 1) + VDM)
MA(N) = P(N) * (VC(N) + V0 + VDM - VD(N)) * .000484 / TA
M1(N) = P(N) * (VD(N) + V1 * VDM) * .000484 / T1
vP(1) = -.05: dPR = .03: W = 1: Sn = 1
'CALCULATE CYCLE DYNAMICS
FOR I = 1 TO 2:  QdP = 0: Qst = 0
FOR N = 2 TO 73
A = A + 5: VC(N) = VCM * (1 + COS((A - B) * PI / 180)) / 2
'*** FIRST ITERATION ***
Fi = PS1(N - 1) * AP1 - PS2(N - 1) * AP2  '          Force on gas spring piston
Fi = Fi + P(N - 1) * (AD - ASt) - (P(N - 1) + dPR * Sn) * AD 'Force on displ'
Fi = Fi + SK * (VD(N - 1)  VDM / 2) '                          Spring force
vP(N) = vP(N - 1) + Fi * dt * 1000 / MD
VD(N) = VD(N - 1) - dt * AD * (vP(N) + vP(N - 1)) / 2
'VD(N) = VDM * (1 + COS(A * PI / 180)) / 2
IF VD(N) > 1.01 * VDM THEN 100 ELSE 102
100 VD(N) = 1.01 * VDM: vP(N) = 0
102 IF VD(N) < 0 THEN 104 ELSE 106
104 VD(N) = 0: vP(N) = 0
106 P(N) = C1 / (VC(N) + VV + VD(N) + (TA / T1 - 1) + VDM)
PAV = (P(N) + P(N - 1)) / 2
MA(N) = P(N) * (VC(N) + V0 + VDM - VD(N)) * .000484 / TA
M1(N) = P(N) * (VD(N) + V1 * VDM) * .000484 / T1
MR = (MA(N) - MA(N - 1) + M1(N - 1) - M1(N)) / 2
MR = MR * F * 24: GR = MR * 4 / (PI * DR ^ 2 * PY): NRE = ABS(GR * DH / U)
IF NRE < 32 THEN FF = 40 / NRE: GOTO 108
FF = 4.637 / NRE ^ .3783
108 dPR = FF * LR * GR ^ 2 * (TA + T1) / (DH * PAV * 484)
VS1 = VS + AR1 * (VDM - VD(N)): VS2 = VS + AR2 * VD(N)
PS1(N) = C2 / VS1: PS2(N) = C2 / VS2
IF GR > 0 THEN Sn = 1 ELSE Sn = -1
'*** SECOND ITERATION ***
Fs = PS1(N) * AP1 - PS2(N) * AP2
Fs = Fs + P(N - 1) * (AD - ASt) - (P(N - 1) + dPR * Sn) * AD
Fs = Fs + SK * (VD(N) - VDM / 2)
Fi = (Fi + Fs) / 2
vP(N) = vP(N - 1) + Fi * dt * 1000 / MD
VD(N) = VD(N - 1) - dt * AD * (vP(N) + vP(N - 1)) / 2
'VD(N) = VDM * (1 + COS(A * PI / 180)) / 2
IF VD(N) > 1.01 * VDM THEN 110 ELSE 112
110 VD(N) = 1.01 * VDM: vP(N) = 0: LPRINT ; " HIT TOP AT "; N * 5: PRINT N * 5
112 IF VD(N) < 0 THEN 114 ELSE 116
```

```
114 VD(N) = 0: vP(N) = 0: LPRINT : " HIT BOTTOM  AT "; N * 5: PRINT N * 5
116 P(N) = C1 / (VC(N) + VV + VD(N) + (TA / T1 - 1) * VDM)
PAV = (P(N) + P(N - 1)) / 2
MA(N) = P(N) * (VC(N) + V0 + VDM - VD(N)) * .000484 / TA
M1(N) = P(N) * (VD(N) + V1 * VDM) * .000484 / T1
MR = (MA(N) - MA(N - 1) + M1(N - 1) - M1(N)) / 2
MR = MR * F * 24: GR = MR * 4 / (PI * DR ^ 2 * PY): NRE = ABS(GR * DH / U)
IF NRE < 32 THEN FF = 40 / NRE: GOTO 118
FF = 4.637 / NRE ^ .3783
118 dPR = FF * LR * GR ^ 2 * (TA + T1) / (DH * PAV * 484)
QdP = ABS(dPR * (VD(N) - VD(N - 1))) + QdP
Qst = Fi * (VD(N) - VD(N - 1)) / AD + Qst
VS1 = VS + AR1 * (VDM - VD(N)): VS2 = VS + AR2 * VD(N)
PS1(N) = C2 / VS1: PS2(N) = C2 / VS2: W = W - 1
IF GR > 0 THEN Sn = 1 ELSE Sn = -1
IF W = 0 THEN 120 ELSE 122
120 PRINT USING "#####.## "; A; P(N); VC(N) / K; VD(N) / K; vP(N) / K; PS1(N); dPR * 1000
* Sn
LPRINT USING "#####.## "; A; P(N); VC(N) / K; VD(N) / K; vP(N) / K; PS1(N); dPR * 1000 *
Sn
W = 3
122 NEXT N
P(1) = P(73): VD(1) = VD(73): vP(1) = vP(73): PS1(1) = PS1(73): PS2(1) = PS2(73)
MA(1) = MA(73): M1(1) = M1(73)
LPRINT "  qdP= "; QdP * N / 1000; " W  "; " qst= "; Qst * N / 1000; "  W"
A = -5: NEXT I
'OPEN "A:\SCDD1.CSV" FOR APPEND AS #3
'WRITE #3,
'FOR J = 1 TO 73
'WRITE #3, J, P(J), VC(J), VD(J), vP(J)
'NEXT J
'CLOSE #3
PRINT : fr; " Hz  "; QdP * N / 1000; " W   "; Qst * N / 1000
END
```

8.5 Appendix E: Pulse Tube Program

```
' "SPT-1"  STIRLING PULSE TUBE ,SINE MOTION"
LPRINT "    SPT-1 1/28/92  RUN ON  "; DATE$; " AT "; TIME$
' DIMENSION VARIABLES AND FORMAT OUTPUT
DIM VC(75), VD(75), P(75), MA(75), M1(75)
TA = 300: DC = 61.2: SC = 20: SD = 20: PO = .83: PM = 1.1: F = 40: PI = 3.1416
T1 = 35.8: DD = 9: LD = 100: DR = 24.6: LR = 28: PY = .67: DW = .023
V0 = .1: V1 = .25: K = 1000
C0 = 4.45:  U = .000016' Pa.s
'CALCULATE DEPENDENT PARAMETERS
AD = PI * DD ^ 2 / 4
VT = PI * LD * DD ^ 2 / 4
VCM = PI * DC ^ 2 * SC / 4
VDM = PI * DD ^ 2 * SD / 4
V0 = V0 * VCM
VR = PI * DR ^ 2 * LR * PY / 4
TR = (TA - T1) / LOG(TA / T1)
DH = DW * PY / (1 - PY)
VV = V1 * VDM * TA / T1 + (VR + VT) * TA / TR + V0
C1 = PO * (VCM * .7 + VV + VDM): LPRINT
LPRINT "   TA-K  DC-mm  SC-mm  SD-mm   N-Hz PO-MPa "
LPRINT "   T1-K  DR-mm  LR-mm  DW-mm   P1-% PM-MPa "
LPRINT "  DD-mm  LD-mm   "
LPRINT USING "####.# "; TA; DC; SC; SD; F; PO
LPRINT USING "####.# "; T1; DR; LR; DW; PY; PM
LPRINT USING "####.# "; DD; LD:  LPRINT
LPRINT "   A-Deg    P-MPa    VC-cc    VD-cc   "
```

```
'CALCULATE INITIAL VALUES
A = -5: B = 60: dL = (A / (360 * F)): N = 1
VC(N) = VCM * (1 + COS((A - B) * PI / 180)) / 2
VD(N) = VDM * (1 + COS(A * PI / 180)) / 2
P(N) = C1 / (VC(N) + VV + VD(N))
MA(N) = P(N) * (VC(N) + V0) * .000484 / TA
M1(N) = P(N) * (VD(N) / TA + VT / TR + V1 * VDM / T1) * .000484
W = 1: Sn = 1
'CALCULATE CYCLE PARAMETERS
FOR I = 1 TO 1:  QdP = 0: QP = 0
FOR N = 2 TO 73
A = A + 5: VC(N) = VCM * (1 + COS((A - B) * PI / 180)) / 2
VD(N) = VDM * (1 + COS(A * PI / 180)) / 2
P(N) = C1 / (VC(N) + VV + VD(N))
PAV = (P(N) + P(N - 1)) / 2
MA(N) = P(N) * (VC(N) + V0) * .000484 / TA
M1(N) = P(N) * (VD(N) / TA + VT / TR + V1 * VDM / T1) * .000484
MR = (MA(N) - MA(N - 1) + M1(N - 1) - M1(N)) / 2
MR = MR * F * 24
GR = MR * 4 / (PI * DR ^ 2 * PY)
NRE = ABS(GR * DH / U)
IF NRE < 32 THEN FF = 40 / NRE: GOTO 108
FF = 4.637 / NRE ^ .3783
108 dPR = FF * LR * GR ^ 2 * (TA + T1) / (DH * PAV * 484)
QdP = ABS(dPR * (VD(N) - VD(N - 1))) + QdP
QP = PAV * (VD(N) - VD(N - 1)) + QP
W = W - 1
IF W = 0 THEN 120 ELSE 122
120 PRINT USING "#####.## "; A; P(N); VC(N) / K; VD(N) / K; dPR * 1000 * Sn
LPRINT USING "#####.## "; A; P(N); VC(N) / K; VD(N) / K; dPR * 1000 * Sn
W = 6
122 NEXT N
P(1) = P(73): VD(1) = VD(73)
MA(1) = MA(73): M1(1) = M1(73)
LPRINT "  qdP= "; QdP * N / K; " W  "; " qP= "; QP * N / K; "  W"
A = -5: NEXT I
'OPEN "A:\SCDD1.CSV" FOR APPEND AS #3
'WRITE #3,
'FOR J = 1 TO 73
'WRITE #3, J, P(J), VC(J), VD(J), vP(J)
'NEXT J
'CLOSE #3
PRINT : fr; " Hz  "; QdP * N / K; " W  "; QP * N / K
END
```

8.6 Appendix F: Dual Compressor Test Data

Date	Voltage RMS	Frequency	Charge Pressure	Total Current RMS	Total Power	#1 Stroke	#2 Stroke	Ave. Comb. Stroke	Pressure Ratio	Gas Spring	Bypass valve	Pulse Tube Valve
	Volts	Hz	psig	Amps	Watts	in	in	in				
10/28/92	56	40	125	32.76	1834	0.494	0.477	0.485	2.34	soft	closed	closed
10/28/92	54	43	125	32.25	1741	0.513	0.422	0.468	2.27	soft	closed	closed
10/28/92	54	41	125	31.07	1678	0.504	0.455	0.480	2.24	soft	closed	closed
10/28/92	54	41	125	31.00	1674	0.537	0.448	0.493	2.46	soft	open	closed

10/28/92	41	48	125	32.60	1337	0.337	0.341	0.339	1.85	soft	**open**	closed
10/28/92	41	48	125	32.61	1337	0.351	0.347	0.349	1.81	soft	closed	closed
10/28/92	54	45	140	31.25	1687	0.468	0.485	0.477	2.24	soft	closed	closed
10/28/92	51	40	140	32.53	1659	0.341	0.342	0.342	1.73	soft	closed	closed
10/28/92	55	40	140	33.35	1834	0.453	0.408	0.431	2.12	soft	closed	closed
10/28/92	57	42	140	33.86	1930	0.485	0.430	0.457	2.11	soft	closed	closed
10/28/92	57	44	140	33.38	1903	0.467	0.449	0.458	2.06	soft	closed	closed
10/28/92	54	39	140	33.50	1809	0.444	0.395	0.420	2.04	soft	closed	closed
10/30/92	54	40	125	31.36	1693	0.532	0.450	0.491	2.55	soft	closed	closed
10/30/92	54	45	125	32.99	1781	0.504	0.498	0.501	2.55	soft	closed	closed
10/30/92	54	39	125	32.85	1774	0.458	0.431	0.445	2.30	soft	closed	closed
10/30/92	54	38	125	33.46	1807	0.458	0.421	0.440	2.18	soft	closed	closed
10/30/92	36	29	125	30.29	1090	0.305	0.286	0.296	1.68	soft	closed	closed
10/30/92	36	32	125	25.29	911	0.336	0.317	0.326	1.71	soft	closed	closed
10/30/92	36	35	125	22.96	826	0.348	0.331	0.340	1.76	soft	closed	closed
10/30/92	36	38	125	20.45	736	0.364	0.345	0.354	1.80	soft	closed	closed
10/30/92	36	41	125	20.20	727	0.387	0.364	0.376	1.87	soft	closed	closed
10/30/92	36	44	125	23.24	837	0.379	0.376	0.378	1.90	soft	closed	closed
10/30/92	54	39	125	33.43	1805	0.501	0.381	0.441	2.25	hard	closed	closed
10/30/92	54	40	125	32.16	1737	0.505	0.386	0.445	2.38	hard	closed	closed
10/30/92	54	41	125	31.35	1693	0.507	0.390	0.449	2.19	hard	closed	closed
10/30/92	54	41	125	30.66	1656	0.506	0.425	0.466	2.14	hard	**open**	closed
10/30/92	54	45	125	30.94	1671	0.510	0.432	0.471	2.36	hard	closed	closed
10/30/92	57	42	125	32.34	1844	0.524	0.418	0.471	2.39	hard	closed	closed
10/30/92	36	29	125	30.30	1091	0.296	0.267	0.282	BAD	hard	closed	closed
10/30/92	36	32	125	28.80	1037	0.284	0.268	0.276	1.64	hard	closed	closed
10/30/92	36	35	125	25.81	929	0.313	0.296	0.304	1.72	hard	closed	closed
10/30/92	36	38	125	22.17	798	0.329	0.311	0.320	1.78	hard	closed	closed
10/30/92	36	41	125	19.52	703	0.354	0.329	0.341	1.91	hard	closed	closed

C-2

10/30/92	36	44	125	19.44	700	0.372	0.353	0.362	1.92	hard	closed	closed
10/30/92	50	38	125	30.21	1510	0.438	0.405	0.421	2.04	hard	closed	closed
10/30/92	50	39	125	32.17	1609	0.499	0.302	0.400	2.04	hard	closed	**Open**
10/30/92	50	39	125	30.54	1527	0.486	0.375	0.430	2.06	hard	closed	open
10/30/92	52	40	125	31.10	1617	0.496	0.386	0.441	2.12	hard	closed	open
10/30/92	52	38	125	31.60	1643	0.454	0.390	0.422	2.18	hard	closed	open
10/30/92	54	39	125	32.79	1771	0.471	0.392	0.431	2.10	hard	closed	open
10/30/92	54	38	125	33.44	1806	BAD	0.391	N/A	2.05	hard	closed	open
11/3/92	46	40	125	30.77	1415	0.388	0.330	0.359	1.84	Soft	No valve	closed
11/3/92	48	40	125	32.22	1546	0.395	0.330	0.363	1.84	Soft	No valve	closed
11/3/92	48	41	125	32.38	1554	0.395	0.323	0.359	1.84	Soft	No valve	closed
11/3/92	48	39	125	32.73	1571	0.393	0.317	0.355	1.88	Soft	No valve	closed
11/3/92	48	40	125	32.90	1579	0.388	0.308	0.348	1.79	Soft	No valve	**Open**
11/3/92	45	42	125	31.47	1416	0.359	0.292	0.325	1.71	Soft	No valve	Open
11/3/92	48	41	125	34.29	1646	0.377	0.300	0.338	1.71	Soft	No valve	Open
11/3/92	45	40	125	31.21	1404	0.370	0.296	0.333	1.73	Soft	No valve	Open
11/3/92	45	39	125	31.40	1413	0.374	0.296	0.335	1.72	Soft	No valve	Open
11/3/92	48	39	125	34.00	1632	0.387	0.307	0.347	1.73	Soft	No valve	Open
11/3/92	42	32	125	32.64	1371	0.350	0.296	0.323	1.64	Soft	No valve	Open
11/3/92	42	35	125	31.37	1318	0.353	0.297	0.325	1.61	Soft	No valve	Open
11/3/92	42	38	125	30.11	1265	0.364	0.291	0.328	1.67	Soft	No valve	Open
11/4/92	48	40	125	31.43	1509	0.386	0.350	0.368	1.91	Soft	Open	Closed
11/4/92	48	40	125	28.73	1379	0.449	0.412	0.431	2.07	Soft	Closed	Closed
11/4/92	48	40	125	29.80	1431	0.425	0.387	0.406	2.09	Soft	Closed	Open
11/4/92	48	41	125	30.72	1475	0.426	0.379	0.402	1.96	Soft	Closed	Open
11/4/92	48	39	125	30.76	1477	0.417	0.365	0.391	2.10	Soft	Closed	Open
11/4/92	48	39	125	30.84	1480	0.419	0.359	0.389	1.86	Soft	Closed	Open
11/4/92	48	40	125	34.28	1646	0.351	0.305	0.328	1.64	Soft	Open	Open
11/4/92	48	39	125	34.21	1642	0.350	0.298	0.324	1.60	Soft	Open	Open
11/4/92	42	37	125	30.69	1289	0.330	0.290	0.310	1.58	Soft	Open	Open
11/4/92	42	37	125	27.02	1135	0.401	0.358	0.379	1.76	Soft	**Closed**	Open
11/4/92	43	35	125	28.81	1239	0.399	0.364	0.382	1.82	Soft	Closed	Open

11/4/92	43	34	125	29.21	1256	0.394	0.360	0.377	1.85	Soft	Closed	Open
11/4/92	42	32	125	29.75	1249	0.383	0.351	0.367	1.71	Soft	Closed	Open
11/4/92	39	32	125	29.92	1167	0.309	0.278	0.294	1.56	Soft	**Open**	Open
11/4/92	42	32	125	32.17	1351	0.321	0.286	0.303	1.52	Soft	**Open**	Open
11/4/92	45	32	125	31.93	1437	0.416	0.376	0.396	1.74	Soft	**Closed**	Open
11/5/92	54	40	125	32.53	1757	0.528	0.426	0.477	2.32	Soft	Closed	Closed
11/5/92	52	39	125	31.78	1652	0.502	0.410	0.456	2.24	Soft	Closed	Closed
11/5/92	52	39	125	32.57	1694	0.475	0.380	0.428	2.06	Soft	Closed	**Open**
11/5/92	50	39	125	32.56	1628	0.450	0.361	0.405	1.95	Soft	Closed	**Open**
11/5/92	50	39	125	32.61	1631	0.450	0.357	0.404	1.95	Soft	Closed	**Partial**
11/5/92	50	39	125	32.53	1626	0.463	0.356	0.409	1.86	Soft	Closed	**Partial**
11/5/92	50	39	125	32.72	1636	0.459	0.356	0.407	2.02	Soft	Closed	**Partial**
11/11/92	50	40	125	29.39	1469	0.485	0.440	0.462	2.24	Soft	Closed	Closed
11/11/92	50	40	125	30.53	1527	0.463	0.403	0.433	2.12	Soft	Closed	Open
11/11/92	50	40	125	34.62	1731	0.367	0.320	0.343	1.66	Soft	**Open**	Open
11/11/92	50	40	125	32.04	1602	0.446	0.383	0.414	1.94	Soft	**Closed**	Partial, outlet throttled
11/11/92	50	40	125	32.11	1606	0.451	0.370	0.410	1.90	Soft	**Closed**	Partial, inlet throttled
11/11/92	48	38	125	31.34	1504	0.442	0.355	0.398	1.88	Soft	Closed	Open
11/11/92	47	37	125	31.07	1460	0.437	0.346	0.391	1.85	Soft	Closed	Open

9.0 References

Shigley, J. E., and Mitchell, L. D., 1983, Mechanical Engineering Design, Mcgraw-Hill, New York.

Kittel, P., "Eddy Current Heating in Magnetic Refrigerators", NASA-Ames

Young, W. C., 1989, Roark's Formulas for Stress & Strain, Mcgraw-Hill, New York.

REPORT DOCUMENTATION PAGE

Form Approved
OMB No. 0704-0188

Public reporting burden for this collection of information is estimated to average 1 hour per response, including the time for reviewing instructions, searching existing data sources, gathering and maintaining the data needed, and completing and reviewing the collection of information. Send comments regarding this burden estimate or any other aspect of this collection of information, including suggestions for reducing this burden, to Washington Headquarters Services, Directorate for information Operations and Reports, 1215 Jefferson Davis Highway, Suite 1204, Arlington, VA 22202-4302, and to the Office of Management and Budget, Paperwork Reduction Project (0704-0188), Washington, DC 20503.

1. AGENCY USE ONLY *(Leave blank)*	2. REPORT DATE	3. REPORT TYPE AND DATES COVERED
	August 1993	Contractor Report

4. TITLE AND SUBTITLE

Three-Stage Linear, Split-Stirling Cryocooler for 1 to 2K Magnetic Cold Stage

5. FUNDING NUMBERS

NAS2-13180

6. AUTHOR(S)

R. C. Longsworth

7. PERFORMING ORGANIZATION NAME(S) AND ADDRESS(ES)

APD Cryogenics
1833 Vultee Street
Allentown, PA 18103

8. PERFORMING ORGANIZATION REPORT NUMBER

A-93105

9. SPONSORING/MONITORING AGENCY NAME(S) AND ADDRESS(ES)

National Aeronautics and Space Administration
Washington, DC 20546-0001

10. SPONSORING/MONITORING AGENCY REPORT NUMBER

NASA CR-4538

11. SUPPLEMENTARY NOTES

Point of Contact: Peter Kittel, Ames Research Center, MS 244-10, Moffett Field, CA 94035-1000; (415) 604-4297

12a. DISTRIBUTION/AVAILABILITY STATEMENT

Unclassified — Unlimited
Subject Category 70

12b. DISTRIBUTION CODE

13. ABSTRACT *(Maximum 200 words)*

A long-life, linear, high efficiency 8K split Stirling cycle cryocooler has been designed, built, and tested. The refrigerator is designed for cooling a 50 mW, 1.5K magnetic cold stage. Dual opposed piston compressors are driven by moving-coil linear motors. The three stage expander, although not completed, is also driven by a linear motor and is designed to produce 15W at 60K, 4W at 16K, and 1.2W at 8K. The cold regenerator employs a parallel gap construction for high efficiency. The key technology areas addressed include warm and cold flexible suspension bearings and a new cold regenerator geometry for high efficiency at 8K.

14. SUBJECT TERMS

Cryogenics, Liquid helium, Cryocoolers

15. NUMBER OF PAGES

103

16. PRICE CODE

A06

17. SECURITY CLASSIFICATION OF REPORT	18. SECURITY CLASSIFICATION OF THIS PAGE	19. SECURITY CLASSIFICATION OF ABSTRACT	20. LIMITATION OF ABSTRACT
Unclassified	Unclassified		